***Carnets Geol.* 22 (13)**

E-ISSN 1634-0744
DOI 10.2110/carnets.2022.2213

Tithonian-Hauterivian chronostratigraphy (latest Jurassic-Early Cretaceous), Mediterranean-Caucasian Subrealm and southern Andes: A stratigraphic experiment and Time Scale

Robert W. SCOTT [1]

Abstract: New radioisotopic dates of Tithonian-Hauterivian strata in the Neuquén Basin significantly recalibrate Early Cretaceous numerical ages. In order to evaluate the implications of these revised ages, a graphic correlation experiment of twenty-three Andean Tithonian to Hauterivian sections integrated the ranges of 254 species, sequence boundaries, polarity chrons, and radioisotopic ages that compose the ANDESCS DB. This database accurately reproduces the order of Andean ammonite zones and places them in a relative metric scale of a composite reference section. The ranges in the ANDESCS DB were correlated with the LOK2016 DB that comprises Tithonian-Albian ammonites, calpionellids, nannofossils, and polarity chrons in Mediterranean-Caucasian Subrealm stage reference sections. In 2017 these ranges were calibrated to GTS2016 mega-annums (MA). Although most Andean ammonoids were endemic to the Indo-Pacific Subrealm, nannofossils, calpionellids and polarity chrons were present in both areas.

This stratigraphic experiment correlates base Berriasian as defined in France within the *Substeueroceras koeneni* Zone. In Andean sections this boundary is correlated with the *Crassicolaria/Calpionella* zone boundary dated at about 141 Ma. The base of the Valanginian defined by *Calpionellites darderi* correlates with the *Neocomites wichmanni* Zone of the Neuquén Basin (NB) recalibrated at 139.50 Ma, which is confirmed by multiple dates in Argentina, Mexico, Tibet, and elsewhere. The base Hauterivian correlates with base of *Holcoptychites neuquensis* Zone in the NB recalibrated at 131 Ma. Top of Hauterivian is in the *Sabaudiella riverorum* Zone in the NB and is dated at 127 Ma below an unconformity.

Previous cyclostratigraphic astrochronologic cycles are averaged and calibrate the duration of the Tithonian at 5.67 myr, the Berriasian at 5.27 myr, the Valanginian at 5.30 myr, and the Hauterivian at 5.60 myr. The age of each stage is recalibrated by adding revised durations to the most common age of base Valanginian of 139.5 Ma. These ages revise the Berriasian to Hauterivian stages time scale, and the ages of stage boundaries are on average 2.8 myr longer than proposed by the new Neuquén Basin radioisotopic dates.

Keywords:

- Early Cretaceous numerical dates;
- Tithonian;
- Berriasian;
- Valanginian;
- Hauterivian;
- biostratigraphy;
- Indo-Pacific Subrealm

Citation: SCOTT R.W. (2022).- Tithonian-Hauterivian chronostratigraphy (latest Jurassic-Early Cretaceous), Mediterranean-Caucasian Subrealm and southern Andes: A stratigraphic experiment and Time Scale.- *Carnets Geol.*, Madrid, vol. 22, no. 13, p. 619-660.

Highlights:

- Indo-Pacific Subrealm new high quality radioisotopic ages of the Tithonian-Hauterivian stages in the Neuquén Basin, Indo-Pacific Subrealm, propose significant changes to the Early Cretaceous numerical time scale.
- A chronostratigraphic database of of ammonites, calpionellids, nannofossils, dinoflagellates, and polarity chrons spans uppermost Tithonian to Albian stages from outcrops and drill cores on five continents, the LOK2016 DB, serves as a chronostratigraphic reference data set.

[1] *Precision Stratigraphy Associates, 149 West Ridge Road, Cleveland Oklahoma 74040 (U.S.A.)*
rwscott@cimtel.net

Published online in final form (pdf) on August 1, 2022
[Editor: Bruno R.C. GRANIER]

• Stratigraphic range data of Andean taxa and polarity chrons, the ANDESCS DB, integrates stratigraphic events into a common metric scale.
• Correlation of Andean ammonite zones with the global database projects European stage boundaries into Andean sections about as predicted.
• The new U/Pd zircon dates would shorten the durations of stages, ammonite zones and depositional cycles.
• New radioisotopic dates together with stage durations measured in Tethys sections suggest that age of base Valanginian is close to 139.5 Ma and ages of other stage boundaries may be calibrated by cyclostratigraphy.

Résumé : *Chronostratigraphie du Tithonien-Hauterivien (Jurassique terminal-Crétacé inférieur), sous-domaine méditerranéen-caucasien et Andes méridionales : Un exercice stratigraphique et l'échelle des temps.-* De nouvelles datations radio-isotopiques des strates de l'intervalle Tithonien-Hauterivien du Bassin de Neuquén contribuent à significativement recalibrer les âges numériques du Crétacé inférieur. Afin d'évaluer les implications de la révision de ces âges, un exercice de corrélation graphique incluant vingt-trois coupes andines de l'intervalle Tithonien-Hauterivien a été réalisé. Il intègre les distributions de 254 espèces, les limites de séquence, les chrons de polarité et les âges radio-isotopiques qui composent la base de données ANDESCS. Cette base de données reproduit fidèlement l'ordre des zones d'ammonites andines et les replace sur l'échelle métrique relative d'une coupe composite de référence. Les éléments de la base de données ANDESCS ont été corrélés avec la base de données LOK2016 qui restitue les distributions des ammonites, calpionelles et nannofossiles ainsi que des chrons de polarité pour l'intervalle Tithonien-Albien pour des coupes de référence d'étages du sous-domaine méditerranéo-caucasien. En 2017, ces distributions furent calibrées sur les millions d'années de la GTS2016. Bien que la plupart des ammonoïdes andins soient endémiques du sous-domaine indo-pacifique, des zones de nannofossiles et de calpionelles ainsi que des chrons de polarité ont été reconnus dans les deux sous-domaines.
Cet exercice stratigraphique permet de placer la base du Berriasien telle que définie en France au sein de la Zone à *Substeueroceras koeneni*. Dans les coupes andines, cette limite est corrélée avec celle des zones à *Crassicolaria* et à *Calpionella* datée d'environ 141 Ma. La base du Valanginien définie par *Calpionellites darderi* se corrèle avec la Zone à *Neocomites wichmanni* du Bassin de Neuquén recalibrée à 139,50 Ma, ce qui est confirmé par de multiples datations en Argentine, au Mexique, au Tibet et en d'autres régions. La base de l'Hauterivien est corrélée avec la base de la Zone à *Holcoptychites neuquensis* du Bassin de Neuquén recalibrée à 131 Ma. Le sommet de l'Hauterivien se trouve dans la Zone à *Sabaudiella riverorum* du Bassin de Neuquén et est daté de 127 Ma sous une discordance.
Les cycles astrochronologiques cyclostratigraphiques précédents ont fait l'objet de calculs de moyennes qui attribuent au Tithonien une durée de 5,67 myr, 5,27 myr au Berriasien, 5,30 myr au Valanginien, et 5,60 myr à l'Hauterivien. L'âge de chaque étage est alors recalculé en soustrayant ou ajoutant les durées révisées à l'âge le plus couramment attribué à la base du Valanginien soit 139,5 Ma. Ces âges constituent une révision de l'échelle de temps des étages Berriasien à Hauterivien. Les âges des limites des étages sont ainsi en moyenne 2,8 myr plus longs que ceux proposés suite aux dernières datations radio-isotopiques du Bassin de Neuquén.

Mots-clefs :

• datations numériques du Crétacé inférieur ;
• Tithonien ;
• Berriasien ;
• Valanginien ;
• Hauterivien ;
• biostratigraphie ;
• sous-domaine indo-pacifique

1. Introduction

Numerical-age calibration of the Cretaceous Period has evolved over more than sixty years as radioisotopic measurements have been acquired and revised. Numerical ages were first estimated by radioisotopic ages, then by rates of sea-floor spreading and most recently by astrochronology and strontium isotopes. In 1959 numerical ages of the beginning and end of the Cretaceous Period were dated from 135±5 to 70±2 Ma (HOLMES in HINTE, 1976) (Table 1). Since 1976 this time scale has been revised at least nineteen times. Beginning in 1995 a series of frequent updates adjusted the Cretaceous time scale as new data and methods were acquired (OGG *et al.*, 2004, 2012, 2016; HUANG, 2018; WALKER *et al.*, 2018; GALE *et al.*, 2020; COHEN *et al.*, 2021). The most recent update, GTS2020 (GALE *et al.*, 2020), resulted in more precise dates based on improved isotopic procedures and techniques. The development of cyclostratigraphy and astrochronology provide more accurate stage durations. In addition, biostratigraphic correlation of stages in the Mediterranean-Caucasian Subrealm of the Tethys Realm, where most type localities lie, with other provinces has become reliably demonstrated.

Table 1. Evolution of Cretaceous Period time scale. Ages from HINTE (1976), GRADSTEIN *et al.* (1995), REMANE *et al.* (2002), OGG *et al.* (2004, 2012, 2016), and GALE *et al.* (2020). Andean ages as recalibrated from radioisotopic dates herein.

Evolution of the Cretaceous Time Scale - Ma of Bases								
AGES	**1976**	**1995**	**2002**	**2004**	**2012**	**2016**	**2020**	**2021-ICS**	**Andean**
Paleogene	65	65	65.5	65.5	66	66	66.04	66	
Maastrichtian	70	71.3	71.3	70.6	72.1	72.1	72.17	72.1 ±0.2	
Campanian	78	83.5	83.5	83.5	83.6	89.2	83.65	83.6 ±0.2	
Santonian	82	85.8	85.8	85.8	86.3	86.5	85.7	86.3 ±0.5	
Coniacian	86	89	89	89.3	89.8	89.8	89.39	89.8 ±0.3	
Turonian	92	93.5	93.5	93.5	93.9	93.9	93.9	93.9	
Cenomanian	100	98.9	98.9	99.6	100.5	100.5	100.5	100.5	
Albian	108	112.2	112.2	112	113	113.1	113.7	~113	
Aptian	115	121	121	125	126.3	126.3	121.4	~125	
Barremian	121	127	127	130	130.8	130.8	126.5	~ 129.4	127
Hauterivian	126	132	132	136.4	133.9	134.7	132.6	~ 132.6	131
Valanginian	131	137	136.5	140.2	139.4	139.4	137.7	~ 139.8	139
Berriasian	135	144.2	142	145.5	145	145	143.1	~145	141

The use of "absolute" as an adjective for geological ages carries the connotation that the date will never change, is complete, is true, or is unlimited. A review of the Cretaceous time scale demonstrates that numerical ages of stage boundaries have changed as new data and technical methods have evolved and been applied (Table 1).

Along the eastern Pacific convergent margin of South America Upper Jurassic and Lower Cretaceous strata extend from Chile to southern Argentina. Andean retroarc basins were deformed during Middle Jurassic-Early Cretaceous time (NAIPAUER *et al.*, 2012; HORTON *et al.*, 2016; KIETZMANN *et al.*, 2020, 2021a). This thick succession was deposited in a series of basins from the Abanico and Cura-Mallin basins in central Chile to the Neuquén Basin in west-central Argentina. The Lower Cretaceous strata are an essential source of chronostratigraphic data that enable correlation between the Tethys-Caucasian-Himalayan Province (sensu PAGE 2008 for the Tithonian) and the Andean area of the Indo-Pacific Subrealm.

New high-quality radioisotopic dates of the Tithonian-Hauterivian stages in the Neuquén Basin of the Indo-Pacific Subrealm propose important changes to the numerical age calibration of that time interval (Table 2) (VENNARI *et al.*, 2014; AGUIRRE-URRETA *et al.*, 2017, 2019; LENA *et al.*, 2019). These measurements would shift the age of the base Berriasian by 2-4 million years and less so the bases of the Valanginian, Hauterivian and Barremian. The result would be major recalibration of the ages of all the Tithonian-Hauterivian biozones (OGG *et al.*, 2016; AGUIRRE-URRETA *et al.*, 2017; REBOULET *et al.*, 2018; GALE *et al.*, 2020; KIETZMANN *et al.*, 2020) and potentially affects ages and durations of subjacent and suprajacent stages.

In order to evaluate the effects of these recent numerical dates, a stratigraphic experiment was conducted to integrate new Andean biostratigraphic taxa into a relative metric numerical database. From among the many well documented outcrop stratigraphic sections twenty-three were selected to represent the Andean Tithonian-Hauterivian stages (Fig. 1). The second objective was to correlate the Andean zonal database with fossil zones in the Mediterranean Tethys in order to correlate the positions of stage boundaries with Andean zones. The Tethys and Andean range databases were combined and then the new radioisotope dates were projected into the database. The relative ages of first and last occurrences of nearly 250 stratigraphic events were recalibrated to new dates. These Andean stage ages are compared with GTS2020 ages. The recalibration of numerical ages of Andean stratigraphic markers has significant implications on durations of stages and zones as well as sedimentary rates and durations. Ages of Berriasian-Hauterivian stage boundaries recalibrated by different methods are compared.

Table 2. Important radioisotopic dates of uppermost Jurassic-Lower Cretaceous strata.

Early Cretaceous radioisotopic dates								
Authors	**Method**	**Location**	**Biostratigraphy**	**Stage**	**ANDESCS Dates Mu**	**Radioisotope Dates (Ma)**	**GTS2016 FAD taxa**	**LOK2016DB FAD taxa**
Bralower *et al.*, 1990	Tuff, zircon, U/Pb	Grindstone Creek, California	*Grantarhabdus meddii*	Valanginian		137.1±0.6		139
Wan *et al.*, 2011	SHRIMP of rhyolite	Gyangze, southern Tibet	*Calcicalathina oblongata*	Valanginian		136±3	139.4	139.6
Lopez-Martínez *et al.*, 2017	Tuff, zircon, U/Pb	Tlatlauquitepec, Puebla	*Calpionellites major* Zone	Valanginian		134.0 ± 0.5		139.4
Lopez-Martínez *et al.*, 2017	LAMC-ICPMS 87Sr86	Tlatlauquitepec, Puebla	*Calpionellites darderi* Zone	Valanginian		139.85	139.4	139.5
Lopez-Martínez *et al.*, 2015	Zircon LA-ICPMS U/Pb	Tamazunchale, San Luis Potosí	*Calpionella elliptica* overlies tuff above *Crassicolaria*	upper Berriasian		139.1±2.6	NA	139.2 LAD 139.8 LAD
Lena *et al.*, 2019	Zircon TIMS U/Pb	Puebla State, Mexico	*N. steinmanni minor*	Berriasian		140.51±0.03	145.5	145.9
Lena *et al.*, 2019	Sediment rate	Puebla State, Mexico	*N. steinmanni minor*	Berriasian		140.7	145.5	145.9
Lena *et al.*, 2019	Sediment rate	Puebla State, Mexico	*Calpionella alpina*	upper Tithonian		140.9	145.7	146.9
Liu *et al.*, 2013	Zircon SIM U/Pb	Nagarze, southern Tibet	*Manivitella pemmatoidea*	Berriasian		141-140		146.2
Aguirre-Urreta *et al.*, 2019	Zircon TIMS U/Pb	El Portón, Argentina	*S. riverorum*	Upper Hauterivian	1290 Mu	126.97±0.15		131,3
Aguirre-Urreta *et al.*, 2015	Zircon TIMS U/Pb	Neuquén Basin Argentina	*P. groeberi*	Upper Hauterivian	1281 Mu	127.42±0.15	NA	131,8
Aguirre-Urreta *et al.*, 2015	Zircon TIMS U/Pb	Mina San Eduardo, Argentina	*S. riccardii*	Upper Hauterivian	1085 Mu	129.09±0.16	NA	132.9
Aguirre-Urreta *et al.*, 2008	Zircon SHRIMP U/Pb	Caepe Malal, Argentina	*S. riccardii*	Upper Hauterivian		132.5±1.3	NA	132.9
Aguirre-Urreta *et al.*, 2017, 2019	Zircon LA-ICPMS U/Pb	El Portón, Argentina	*H. agrioensis*	Lower Hauterivian	810 Mu	130.39±0.16	NA	134.5
Schwartz *et al.*, 2016	Zircon SHRIMP U/Pb	Neuquén Basin Argentina	*H. neuquenensis*	Lower Hauterivian		130.0±0.80	NA	134.7
Vennari *et al.*, 2014	Zircon TIMS	Las Loicas, Argentina	*A. noduliferum*	Berriasian	160 Mu	139.55±0.18	NA	143.9
Lena *et al.*, 2019, Fig. 2	Zircon TIMS U/Pb	Las Loicas, Argentina	*A. noduliferum*	Berriasian	153 Mu	139.24±0.05	NA	143.9
Lena *et al.*, 2019	Zircon TIMS U/Pb	Las Loicas, Argentina	*A. noduliferum*	Berriasian	130 Mu	139.96±0.06	NA	143.9
Lena *et al.*, 2019	Bayesian age-depth	Las Loicas, Argentina	*N. winteri*	Berriasian		140.22±0.13	145.5	145.9
Lena *et al.*, 2019	Zircon TIMS U/Pb	Las Loicas, Argentina	*R. asper*	Tithonian	112 Mu	140.34±0.08	145.5	145.9
Lena *et al.*, 2019	Bayesian age-depth	Las Loicas, Argentina	*R. asper*	Tithonian		140.54±0.34	145.5	145.9
Lena *et al.*, 2019	Bayesian age-depth	Las Loicas, Argentina	*R. asper*	Tithonian		140.6±0.4	145.5	145.9
Lena *et al.*, 2019	Bayesian age-depth	Las Loicas, Argentina	*U. granulosa*	Tithonian		141.31±0.56		
Lena *et al.*, 2019	Zircon TIMS U/Pb	Las Loicas, Argentina	Crassicolaria Zone	Tithonian	60 Mu	142.04±0.06		147.7
Aguirre-Urreta *et al.*, 2014; Lena *et al.*, 2019	Zircon CA-ID-TIMS	La Yesera, Argentina	Tordillo Fm. 1.5m below *V. andesensis*	Tithonian		147.11±0.08		
Naipauer *et al.*, 2015b	Zircon LA-ICPMS U/Pb	Las Loicas, Argentina	Tordillo Formation	Tithonian		144		
Horton *et al.*, 2016	Zircon LA-ICPMS U/Pb	Neuquén Basin, Argentina	Tordillo Formation	Tithonian		143.0±1.0 - 149.5±1.2		
Naipauer *et al.*, 2015c			Tordillo Formation	Tithonian		144		
Lena *et al.*, 2019			Tordillo Formation	Kimmeridgian		147.11±0.078		
Naipauer *et al.*, 2012	Zircon U/Pb		Tordillo Formation	Kimmeridgian		152		

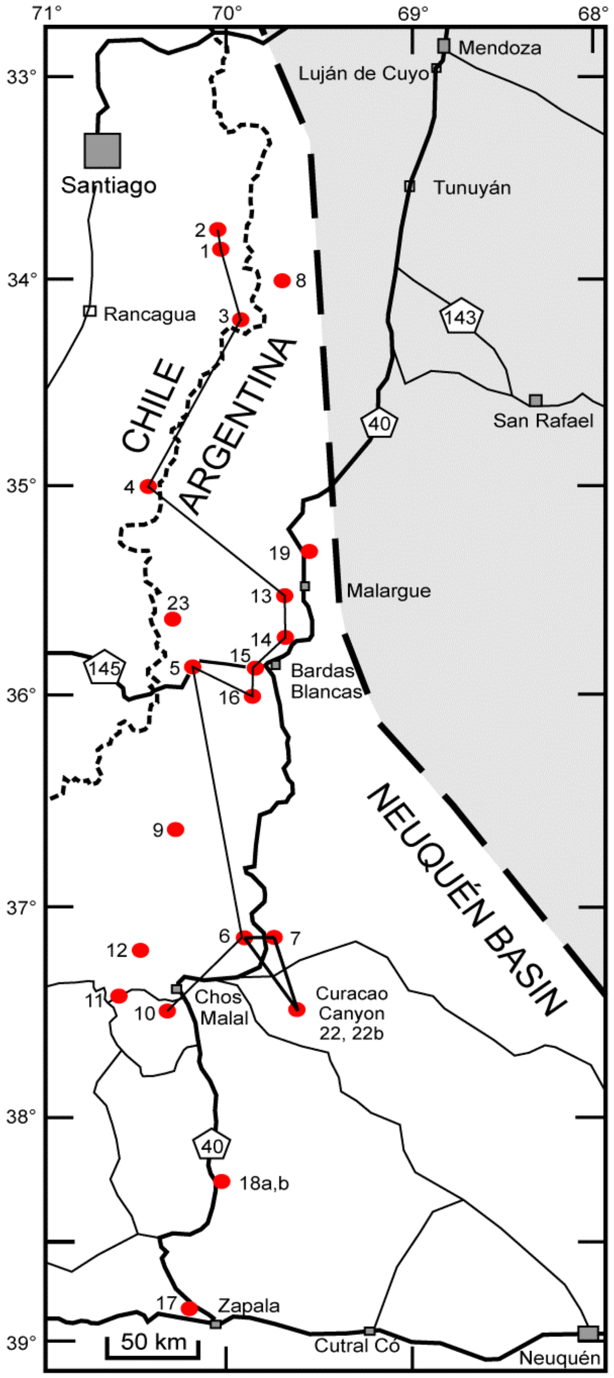

Figure 1: Location of outcrop measured sections of upper Tithonian-Hauterivan stages in Chile and Argentina that compose the ANDESCS Database. 1-Lo Valdés, Chile; 2-Cajón del Morado, Chile; 3-Cruz de Piedra, Chile; 4-Rio Maitenes, Chile; and Argentinian sections 5-Las Loicas; 6-Pampa Tril; 7-El Portón; 8-Real de las Coloradas; 9-Cerro Domuyo; 10-Mina San Eduardo; 11-Arroyo Truquico; 12-Cerro La Parva; 13-Arroyo Loncoche; 14-Cuesta del Chihuido; 15-Bardas Blancas; 16-Arroyo Rahue; 17-Los Catuto; 18a Bajada Viejo; 18b Bajada del Agrio; 19 Arroyo Cieneguita; 22b Puerta Curaco Section; and 23 Las Tapaderas Section. The composited section of Pampa Tril (6), Puerta Curaco (22b) and El Portón (7) is indicated by the triangle.

2. Material and methods

Abbreviations: CA-ID-TIMS - Chemical Abrasion Isotope-Dilution Thermal Ionization Mass Spectrometry; CLS - correlation line of synchroneity; DB - database; FO/LO - first and last occurrence datums in a given section; FAD/LAD - first and last appearance datums in all database sections; GSSP - global stratotype section and point; Ma - mega-annums; MU - metric units; myr - million years duration; RS - reference section; SAR - sediment accumulation rate; U-Pb - uranium-lead.

A comprehensive chronostratigraphic database of the first and last appearance datums (FAD/LAD) of ammonites, calpionellids, nannofossils, dinoflagellates, and polarity chrons in uppermost Tithonian to Maastrichtian stages from numerous public documents of outcrops and drill cores on five continents was compiled (Scott, 2014, 2019a). A subset of this database is composed of 70 Lower Cretaceous reference sections in France, Spain, Italy, Eastern Europe, North Africa, Iran, Tibet, the Atlantic basin, North and South America (Appendix 1). Included are GSSP or candidate reference sections of Berriasian to Barremian stages. This data set also includes polarity chrons M16n through M20r from nine sections in Spain, Italy and Poland and DSDP 534 core in the western Atlantic. Beginning in 2017 fossil ranges were integrated into a single database, LOK16CS DB, scaled to what then was the most recent time scale GTS2016 (Ogg *et al.*, 2016) using the graphic correlation technique (Carney & Pierce, 1995) and the GraphCor software (Hood, 1995) (Appendix 2). GTS2020 (Gale *et al.*, 2020) was published after this project was completed.

Bioevents and polarity chrons in the Mediterranean-Caucasian (Westernman, 2000) sections in meters/feet were cross-plotted on the Y-axis with the GTS2016 geologic time scale in mega-annums on the X-axis to create hypotheses of synchroneity between section pairs. The correlation line of synchroneity (CLS) extended the first and last species occurrences in each section (FOs, LOs) relative to ranges in other sections combining ranges in all sections, in which each taxon was present. The composited range extensions in all sections approximated first and last appearance datums (FADs, LADs) calibrated to numerical ages (Ma) (Table 3) of the 2016 Geologic Time Scale (Ogg *et al.*, 2016). This stratigraphic experiment placed the calpionellid, nannofossil, dinoflagellate, and ammonite FADs in the predicted order relative to polarity chrons M16n through M22r (Wimbledon, 2017; Reboulet *et al.*, 2018). The numeric ages of all taxa calibrated by this method are within less than 0.1% of the ages predicted by GTS2016.

Table 3. Numerical mega-annum ages calibrated to GTS2016/2020 of Tethys ammonites, calpionellids and calcareous nannofossils correlated with Andean ammonites and polarity chrons.

Age Ma GTS2016	Stage	Substage	Tethys Ammonites	FAD Ma GTS2016	FAD Ma LOK2016	Calpionellid Events Lakova & Petrova, 2012	Radioisotopic Ages	FAD Ma LOK2016 DB	Tethys Calcareous Nannofossils GTS 2016	FAD Ma LOK2016 DB	Top Polarity Chrons	GTS2016	LOK2016DB
130,8	Hauterivian	Late	*Pseudothurmannia ohmi*	131.5	131.2				LAD *Calcicalathina oblongata*	130.6	CM5R	130.9	131.7
			Balearites balearis	132.4	131.4				FAD *Rucinolith. terebrodent.*	132.6	CM6R	131.7	131.9
			Pleisiospitidiscus ligatus	132.9	132				LAD *Speetonia colligata*	131.3	CM8R	132.6	132.5
			Subsayanella sayni	133.4	132.2				LAD *Lithraphidites bollii*	130.4	CM9R	133	133.5
		Early	*Lyticoceras nodosplicatus*	133.9	133.6				LAD *Cruciellipsis cuvillieri*	131.6	CM10	133.5	133.9
			Crioceratites loryi	134.3	134.3				FAD *Lithraphidites bollii*	133.9			
			Acanthodiscus radiatus	134.7	134.7						CM10N	134.2	134.3
134,7	Valanginian	Late	*Criosarasinella furcilliata*	135.4	135.4				FAD *Eiffellithus striatus*	135.3	M11r	135.3	136.1
			Neocomites peregrinus	136.8	136.4				Common *Tubodiscus verenae*	NA			
			Saynoceras verrucosum	137.6	137	LAD *Calpionellites*		133.6			M12n	136.9	136.9
		Early	*Karakaschiceras biasalense*	138.3	138						M13n	138.3	138.3
			Neocomites neocomiensiformis	138.3	138.6	*Calpionellites major*	134.0±05	139.4	FAD *Eiffellithus windi*	139.3			
			"*Thurmaniceras*" *pertransiens*	139.4	139.4	*Calpionellites darderi*	136±3 139.85	139.5	FAD *Calcicalathina oblongata*	139.6	M14n	138.6	138.6
139,4	Berriasian	Late	*Tirnovella alpillensis*		141,6	*Praecalpionellites murgeanui*		139.97			M15n M16n	139.5 140.4	139.4 140.4
			Fauriella boissieri	142	141.7	*Calpionellopsis oblonga* *C. simplex*		143.3 143.4			M17n	142.2	142.2
		Middle	*Subthumannia occitanica*	143.5	143.4	*Calpionella elliptica*	139.1±2.6	144.9	FAD *Retacapsa angustiforata*	138			
		Early	"*Berriasella*" *jacobi*			FAD *Remaniella* spp.		145.2	FAD *Nannoconus kamptneri*/ FAD *N. steinmannii*	144.4 145.3	M18n	144	143.3
											M19n M19n.1n M19n.1r M19n.2n	144.6 145.0 145.1 145.3	144.6 145.0 145.1 145.3
145	Tithonian	Late		146	145.8	LAD *Calpionella elliptalpina*		146.5					
			Protacanthoceras andraeai			*Calpionella grandalpina*		146.5			M20n	146.5	146.1
						Tintinnopsella remanei		147.6					
				146,5	146.1	*Praetintinnopsella andrusovi*		147.3					
			Micracanthoceras microcanthum	147.7	147.6								
		Early	*Micracanth. ponti / B. peroni*	148	NA	*Dobenilla [Chitinoidella] dobeni*		147.8			M21n	148.5	147.8
			Semiformiceras fallauxi	149.9	NA						M21r	149.3	148.4
											M22n	150	148.8
			Semiformiceras semiforme	150.5	NA						M22r	151	150
			Semiformiceras darwini	150.9	NA								
			Hybonoticeras hybonotum	15.1	NA								

In order to construct a quantitative database of Andean Tithonian-Hauterivian biostratigraphy twenty-three stratigraphic outcrop sections were selected from among the many excellent published data. Experienced professional geologists have measured, described, sampled, and analyzed these sections for ammonites, and where possible calpionellids, dinoflagellates, nannofossils, and polarity chrons (Appendix 3). The Andes Chronostratigraphic Database, ANDESCS DB, comprises bioevent data scaled to metric units (MUs) of the Chos Malal composite reference section (Table 4).

Because no single stratigraphic section is known in the Andes that spans the upper Tithonian-Hauterivian stages, a composited reference section was necessary in order to scale taxon ranges relative to each other. The Chos Malal reference section represents the Mendoza Group in the Neuquén Basin and was assembled by combining the Pampa Tril section at the base (PARENT *et al.*, 2015) with the overlying Puerta Curaco section (SCHWARZ *et al.*, 2006; KEITZMANN *et al.*, 2021a) at the contact of the Vaca Muerta and Mulichinco formations; then the El Portón section was added above at the base of the Agrio Formation (AGUIRRE-URRETA *et al.*, 2015, 2017) (Fig. 2). These sections are within 50 km of each other, two of which were studied by the same team and the third by a most experienced team. The Pampa Tri section exposes the Vaca Muerta shale with diverse ammonites (PARENT *et al.*, 2015; VENNARI, 2016). The Puerta Curaco section spans the Vaca Muerta-Quintuco and Mulinchinco formations. The nearby El Portón section spans the upper Valanginian-upper Hauterivian Agrio Formation, which yields ammonites, nannofossils and a succession of radioisotope ages (AGUIRRE-URRETA *et al.*, 2017, 2019). These three sections document detailed biostratigraphy that correlates with Tethys stages (AGUIRRE-URRETA & RAWSON, 2010).

As successive sections were plotted to the reference section the metric positions of FO/LOs were extended by the correlation line of synchroneity (CLS), which was positioned by the stratigraphic interpreter to align with known bioevents (Fig. 3.A-B). For example, the Las Loicas section was plotted to the Andes database and the CLS was constrained by ammonite and nannofossil bioevents (Fig. 3.A). The offset in the lower part of section is an artifact of stacking separately measured sections, the lower Tithonian section (VENNARI *et al.*, 2016) with the upper Tithonian-Berriasian interval (VENNARI *et al.*, 2014). The FOs of many other nannofossils were previously calibrated in the Agrio Formation and they range lower in the Vaca Muerta Formation and their ranges were extended and recalibrated at lower metric positions. Several LOs (plus signs) are left of the CLS and were extended higher-younger in

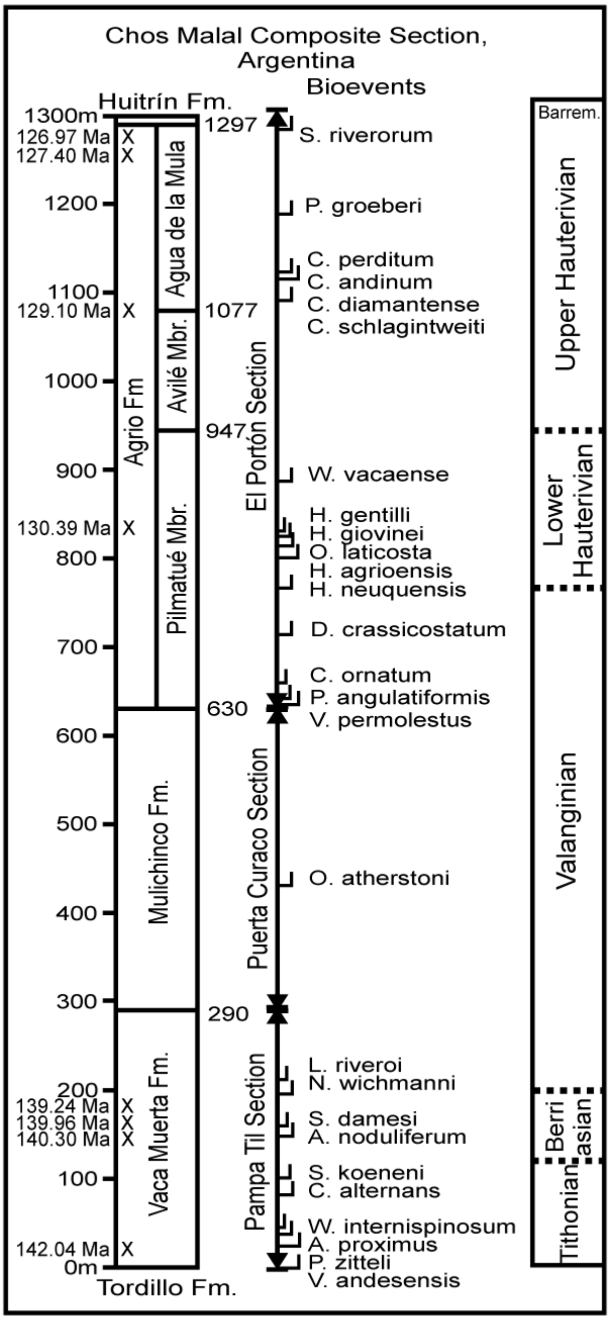

Figure 2: Chos Malal composite section composed of three stratigraphic sections stacked at common lithostratigraphic contacts: Vaca Muerta/Mulichinco and Mulichinco/Agrio formations to form a single reference section calibrated in meters.

the database. The calpionellid bioevents and zones were integrated from the nearby Las Loicas outcrop (Fig. 3.B) (Kietzmann *et al.*, 2021b) and the Arroyo Loncoche and Cuesta del Chihuido sections (Kietzmann *et al.*, 2020). The composited ranges compose the ANDESCS Database (Table 4). The stage boundaries previously have been correlated by ammonites and nannofossils (Aguirre-Urreta *et al.*, 2005, 2017, 2019; Vennari *et al.*, 2014). The vertical spacing and scaling of the zones are in meters of the thickness of the reference section (MUs) and do not measure zone durations.

3. Data

Stratigraphy of the Mediterranean-Caucasian Subrealms. The uppermost Jurassic Tithonian Stage and the Berriasian, Valanginian and Hauterivian stages of the Lower Cretaceous System time scale were initially defined in southern France, and as of this writing only the Hauterivian at La Charce, Drôme, southern France, has been designated a Global Section Stratotype Points (GSSP) (Ogg *et al.*, 2016; Gale *et al.*, 2020; Mutterlose *et al.*, 2020). Reference sections of Tithonian-Hauterivian stages, substages, ammonite, calpionellid, and nannofossil zones were calibrated to GTS2016 mega-annums in the LOK2016 DB (Table 3). Tithonian-Berriasian polarity chrons were correlated with biostratigraphic zones in 23 European sections (Grabowski & Pszczółkowski, 2006; Grabowski, 2011; Grabowski *et al.*, 2018), nine of which are in our database.

The upper Tithonian Stage is represented in part by the LOK2016 DB by the FADs of *Micracanthoceras microcanthum* at 147.6 Ma, *Protacanthoceras andraeai* at 146.1 Ma and "*Berriasella" jacobi* at 145.8 Ma. Two Tithonian chitinodellid calpionellid species are *Dobinella [Chitinoidella] dobeni* at 147.83 Ma and *Bonetilla [Chitinoidella] boneti* at 147.73 Ma (systematics revised by Benzaggagh, 2021). Calcareous nannofossil events span the Tithonian-Berriasian boundary as documented by Casellato and Erba (2021). The absence of lower Tithonian ammonite zones in the LOK2016 DB indicates that this interval of the database is incomplete, because no older sections are in the DB.

The Berriasian Stage is represented in southeastern France by marine carbonates and siliciclastics with ammonite, calpionellid and calcareous nannofossil zones (Wimbledon, 2017; Reboulet *et al.*, 2018; Wimbledon *et al.*, 2020). The base of the Berriasian has been defined by the base of the *Calpionella* Zone, which was defined as the "…abrupt increase in the abundance of *Calpionella alpina* … (and) … becomes the predominate element of the fauna" (Alleman *et al.*, 1971). Wimbledon *et al.* defined the *C. alpina* Zone more precisely as the "…the turnover from *Crassicollaria* and large *Calpionella* to small orbicular *Calpionella alpina* (together with *Crassicollaria parvula* and *Tintinopsella carpathica*…" (2017, p. 182). These definitions differ from the FAD of *Calpionella alpina* (Gale *et al.*, 2020, p. 1025), which is diachronous (Scott, 2019a). This transition is in polarity Chron M19n.2n. The commonly used ammonite species, "*Berriasella" jacobi*, has been revised, most of its records challenged, and the species reassigned to *Strambergella* (Frau *et al.*, 2016). These authors rejected use of the "Jacobi" Zone to define base Berriasian. The most recent revision of late Tithonian-early Berriasian ammonite biostratigraphy in the Mediterranean region replaced the former "Jacobi" Zone with a refined zonation (Szives &

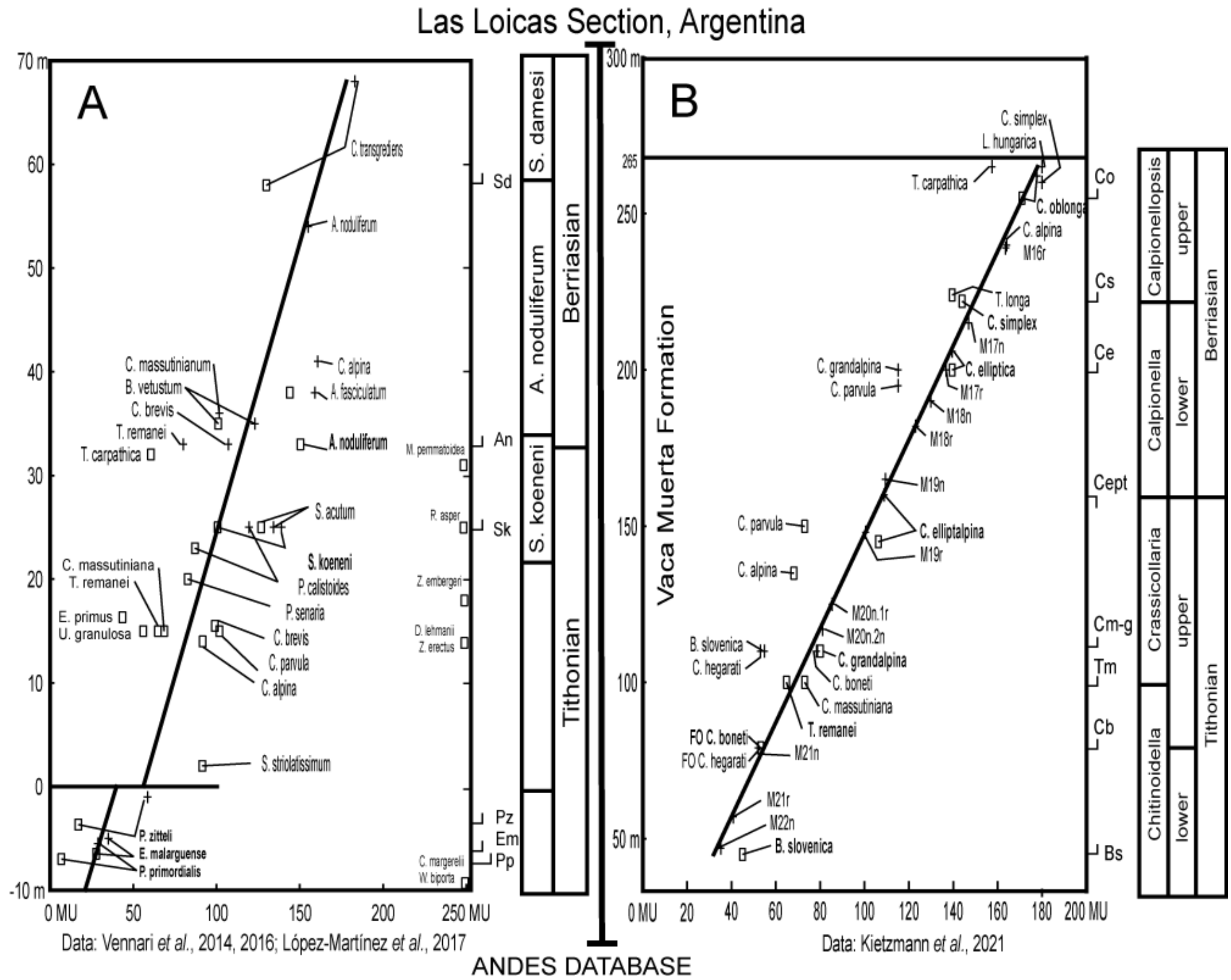

Figure 3: Stratigraphic correlation plots of two data sets of the Las Loicas section with the ANDESCS DB based on the Chos Malal Composite reference section (SRS) (□ signs are FOs, + signs are LOs). Sloping correlation lines (CLS) are constrained by ammonite and nannofossil bioevents. A. Nannofossil FO bioevents right of the CLS in the Agrio Formation will be extended into the Vaca Muerta Formation and their ranges will be recalibrated in meters of the reference section. B. Calpionellid and polarity chrons tightly constrain the CLS.

Főzy, 2022). Most ammonite species used to subdivide the stage are endemic to the Mediterranean region so that global substage correlation is problematic (Wimbledon, 2017). Calcareous nannofossils define effective secondary biomarkers. Candidate GSSP sections considered by the former Berriasian Working Group (BWG) at Tré Maroua and Le Chouet in France, and Puerto Escaño and Rio Argos in Spain are in LOK2016 DB. Definition of the Berriasian Stage as base of Cretaceous is reviewed by Énay (2020) and Granier *et al.* (2020), who proposed to define base Cretaceous at base Valanginian following Oppel. A new BWG II is discussing the issue and will officially propose the base of the Berriasian Stage, its GSSP and its role in defining (or not) the J/K boundary.

The Valanginian Stage as first defined in southern France is subdivided by ammonite zones (Bulot *et al.*, 1993; Reboulet & Atrops, 1999; Reboulet *et al.*, 2018 and references therein; Kenjo *et al.*, 2021). The FAD of the ammonite *"Thurmaniceras" pertransiens* defines base Valanginian (Martinez *et al.*, 2013; Reboulet *et al.*, 2018; Kenjo *et al.*, 2021; Szives & Főzy, 2022). Closely associated is the FAD of the calpionellid *Calpionellites darderi*, which is proposed as the primary marker (Ogg *et al.*, 2016; Gale *et al.*, 2020). The Rio Argos reference section, Caravaca, Spain, yields calpionellids, ammonites, planktic foraminifera, dinoflagellates, and polarity chrons (Hoedemaker & Leereveld, 1995; Hoedemaker *et al.*, 2016). Other reference sections in France are the Barret-le-Bas and the Angles sections with ammonites, calpionellids and cycles (Ogg *et al.*, 2016). Marker species in each of these sections are incorporated in LOK2016 DB. Detailed ammonite and nannofossil biostratigraphy of the Vergol section, France, is proposed as the candidate GSSP (Kenjo *et al.*, 2021).

Table 4. Chronostratigraphic classification of ammonite zones and polarity chrons in the ANDESCS DB. Scale is metric units (MUs) in the Chos Malal composite section (SRS). Early-middle Tithonian zones after VENNARI (2016); late Tithonian to Berriasian zones after KIETZMANN *et al.* (2018); Valanginian-Hauterivian zones after AGUIRRE-URRETA *et al.* (2015, 2017, 2019); central Chilean zones after SALAZAR *et al.* (2020).

Age Ma GTS2020	Stage	Substage	Tethys Ammonites Reboulet *et al.*, 2018	FAD Ma LOK2016	Andean Ammonites Aguirre-Urreta *et al.*, 2019a, 2019b	FAD Ma LOK2016	Calpionellid Events Lakova & Petrova, 2012	FAD Ma LOK2016	Tethys/Neuquén Calcareous Nannofossils Aguirre-Urreta *et al.*, 2019a, 2019b	FAD Ma LOK2016	Top Polarity Chrons	Ma LOK2016
126.5	Hauterivian	Late	*Pseudothumannia ohmi*		*Sabaudiella riverorum* *Paraspiticeras groeberi*	130.2 131					CM5N	
				131.2					LAD *Calcicalathina oblongata*	130.6	CM5R	131.7
			Balearites balearis	131.4	*Crioceratites diamantense*	131.5			FAD *Rucinolith. terebrodent.*	132.6	CM6R	131.9
			Pleisiospit scus ligatus	132	*Crioceratites schlagintweiti*	131.7			LAD *Speetonia colligata*	131.3	CM8R	132.5
			Subsayanella sayni	132,2	*Spiti discus riccardii*	131.8			LAD *Lithraphidites bollii*	130.2	CM9R	133.5
		Early	*Lyticoceras nodosplicatus*	133.6	*Weavericeras vacaense*	133.4			LAD *Cruciellipsis cuvillieri*	131.6	CM10	133.9
			Crioceratites loryi	134.3	*Hoplytocrioceris gentilli*	133.8			FAD *Lithraphidites bollii*	133.9		
			Acanthodiscus radiatus	134.7	*Holcoptychites neuquensis*	134.3					CM10N	134.3
132.6	Valanginian	Late	*Criosarasinella furcilliata*	135.4	*Pseudofavrella angulatiformis*	135.4			FAD *Eiffellithus striatus*	135.3		
			Neocomites peregrinus	136.4					Common *Tubodiscus verenae*	NA	M11r	136.1
			Saynoceras verrucosum	137	*Olcostephanus atherstoni*	137.2	LAD Calpionellites	133.6			M12n	136.9
		Early	*Karakaschiceras biasalense*	138								
			Neocomites neocomiensiformis	138,6			*Calpionellites major*	139.4	FAD *Eiffellithus windi*	139.3	M13n	138.3
			"*Thurmaniceras*" *pertransiens*	139.4	*Lissonia riveroi* *Neocomites wichmanni*	139.3 139.4	*Calpionellites darderi*	139.5	FAD *Calcicalathina oblongata*	139.6	M14n	138.6
137.7	Berriasian	Late	*Tirnovella alpillensis*	141.6			*Praecalpionellites murgeanui*	139.97			M15n M16n	139.4 140.4
			Fauriella boissieri	141.7			*Calpionellopsis oblonga* *C. simplex*	143.3 144.5				
		Middle	*Subthumannia occitanica*	143.4	*Spiticeras damesi*	142.1	*Calpionella elliptica*	144.9	FAD *Retacapsa angustiforata*	145.2	M17n	142.2
		Early	"*Berriasella*" *jacobi*		*Argentiniceras noduliferum*	144.5	FAD *Remaniella* spp.	145.2	FAD *Nann. kampt. minor*/ FAD *N. steinmannii*	145.1 145.3	M18n	143.3
143.1	Tithonian	Late		145.8	*Substeueroceras koeneni*	145.8	LAD *Calpionella elliptalpina*	146.5			M19n M19n.1n M19n.1r M19n.2n	144.6 145.0 145.1 145.3
			Protacanthoceras andreaei				*Calp. grandalpina* *Calp. alpina*	146.7 146.9			M20n M20n.1n M20n.1r M20n.2n	146.1 146.2 146.4 146.5
				146.1	*Corongoceras alternans*	146.5	*Tintinnopsella remanei*	147.6	*Nannoconus wintereri*	146,3		
			Micracanthoceras microcanthum	147.6			*Praetintinnopsella andrusovi*	147.3	*Umbria granulosa*	147,4		
		Early	*Micracanth. ponti / B. peroni*	148*	*Windhauseniceras internispinosum*	148.3	*Dobenilla* [*Chitinoidella*] *dobeni*	147.8	*Rhagodiscus asper*	148	M20r	147.2
			Semiformiceras fallauxi	149.7*	*Aulacosphinctes proximus*	148.7			*Eiffellithus primus*	148.1	M21n	147.5
					Pseudolissoceras zitteli	149.9			*Polycostella senaria*	148.7	M21r	148.4
			Semiformiceras semiforme	150.4*					*Hexalithus noelae*	148.9		
					Virgatosphinctes andesensis	151			*Polycostella beckmannii*	149.4	M22n M22r	148.8 150
			Semiformiceras darwini	150.9*								
			Hybonoti ceras hybonotum	152.1*								

The Hauterivian Stage GSSP is in southeastern France where the FO of the ammonite *Acanthodiscus radiatus* is used as the primary marker (OGG *et al.*, 2004, 2016; GALE *et al.*, 2020). The La Charce outcrop section is accepted as the GSSP with detailed ammonite zones, carbon isotope chemozones and depositional cycles (BULOT *et al.*, 1993; GALE *et al.*, 2020; MUTTERLOSE *et al.*, 2020). The base of the Barremian is defined by the FAD of the ammonite *Taveraidiscus hughi* in the basinal Rio Argos section (OGG *et al.*, 2004, 2016; GALE *et al.*, 2020). Each of these sections is in LOK2016 DB. On the carbonate shelf the Barremian is represented by benthic foraminifers and calcareous algae (CLAVEL *et al.*, 2010, in the HA-BA set of sections in LOK2016 DB).

Andean Lithostratigraphy: Uppermost Jurassic and Lower Cretaceous Mendoza Group of the Neuquén Basin is composed of the lower Tithonian-Valanginian-Hauterivian Vaca Muerta, Quintuco, Mulichinco or Chachao, and Agrio formations (AGUIRRE-URRETA, 2001; LEANZA *et al.*, 2011; SCHWARZ *et al.*, 2006; KIETZMANN *et al.*, 2020, 2021a). At its base the non-marine clastic Tordillo Formation disconformably overlies older Jurassic strata and conformably underlies the Tithonian-Valanginian Vaca Muerta Formation (SCHWARZ *et al.*, 2006; NAIPAUER *et al.*, 2015a, 2015b; HORTON *et al.*, 2016) (Fig. 4). Lower but not lowermost Tithonian ammonites are in the basal part of the Vaca Muerta (VENNARI, 2014, 2016; KIETZMANN *et al.*, 2021a). This stratigraphic succession comprises three long-term cycles of paralic sandstone to flooding organic-rich marine shale to shoaling-up marl, limestone, and sandstone (SCHWARZ *et al.*, 2006; KIETZMANN *et al.*, 2015, 2020).

In central Chile the Tithonian-Hauterivian Lo Valdés Formation correlates with the Mendoza Group. At its type locality near the village of Lo Valdés, Chile, the Lo Valdés overlies Jurassic andesite and is composed of four lithological subunits, a lower interval of andesite overlain by a lower sandstone interval 73 m thick, a middle siltstone interval 214 m thick, and an upper limestone interval 252 m thick (SALAZAR SOTO, 2012; SALAZAR & STINNESBECK, 2015, 2016; SALAZAR *et al.*, 2020). The top of the Lo Valdés is unconformably overlain by volcanic breccia with limestone clasts. It is laterally equivalent in part with the marine Baños del Flaco Formation, which overlies Kimmeridgian continental strata (Fig. 4).

A 600 km north-south stratigraphic correlation cross section depicts the lithostratigraphic relations among the various formations (Fig. 4). This transect is approximately subparallel with the north-south Malargüe and Agrio fold and thrust belts (HORTON *et al.*, 2016; LENA *et al.*, 2019),

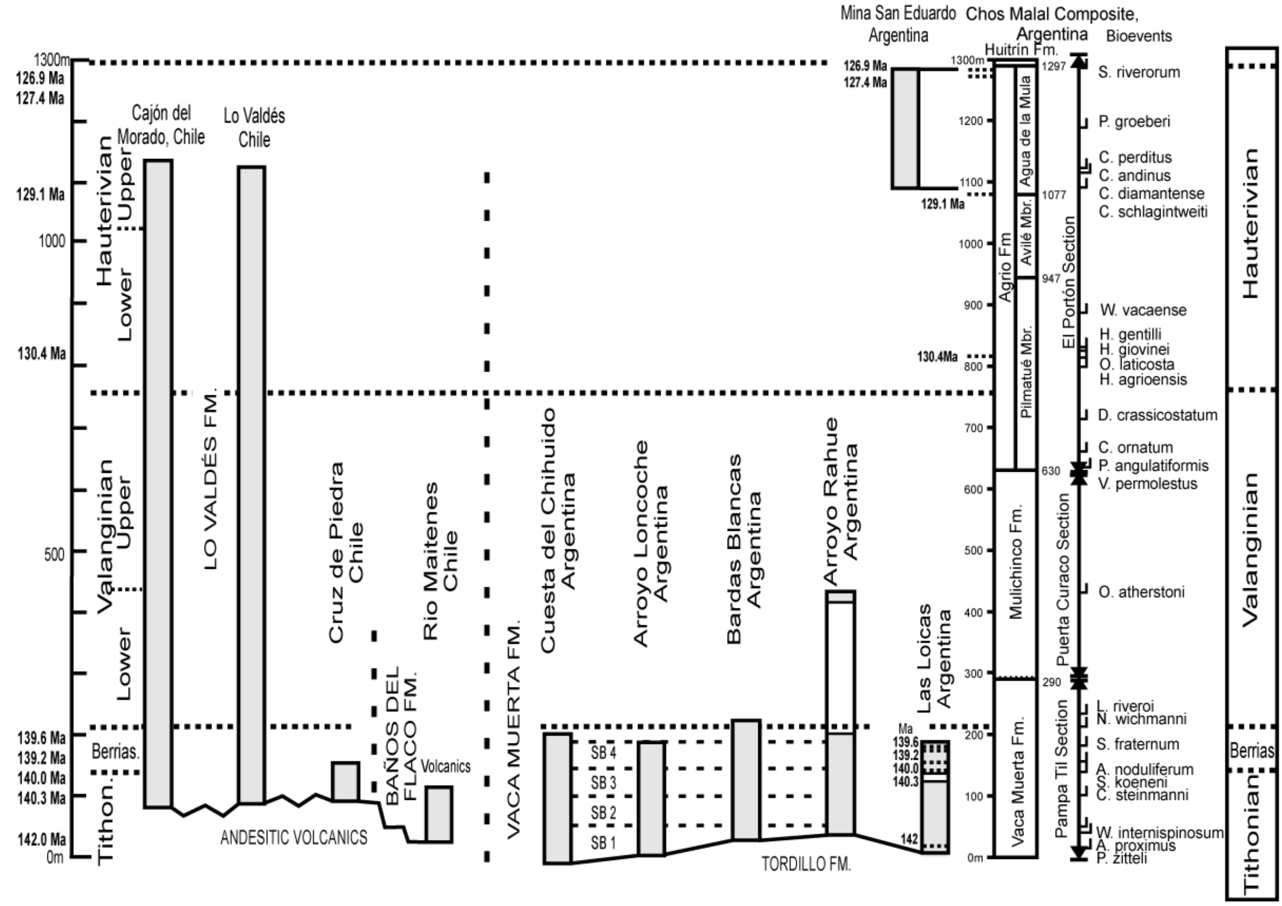

Figure 4: Stratigraphic cross section of Andean sections. Biozone numeric scale in metric units (MUs) of the Chos Malal composite section. Sequence contacts (SB) in KIETZMANN *et al.* (2018); dated ash beds in Las Loicas and El Portón sections (dotted lines) from VENNARI *et al.* (2014) and AGUIRRE-URRETA *et al.* (2017). Stratigraphic data from AGUIRRE-URRETA *et al.*, 2005, 2007, 2015, 2017; SALAZAR, 2012; VENNARI *et al.*, 2014, 2016; SALAZAR and STINNESBECK, 2015; PARENT *et al.*, 2015; KIETZMANN *et al.*, 2018; KOHAN MARTÍNEZ *et al.*, 2018.

which is the trend of the eastern proto-Pacific Ocean shoreline.

The Tithonian to upper Berriasian Vaca Muerta Formation is composed of bituminous shale, calcareous shale, and sandstone (LEANZA *et al.*, 2011; PARENT *et al.*, 2011, 2015, 2017). Its thickness ranges from 100 to 1200 m. Regularly interbedded limestone and marlstone cycles approximate 21 ky, 90-120 ky and 400 ky frequencies (KIETZMANN *et al.*, 2018, 2020). Cyclostratigraphy and biostratigraphy suggest that the Tithonian duration was 5.67 myr and the Berriasian duration was 5.27 myr (KIETZMANN *et al.*, 2018). Four transgressive-regressive composite depositional sequences are composed of bundles of limestone and marlstone bounded by sequence boundaries SB 1-4. A basin-to-ramp succession extends from Cuesta del Chihuido, Arroyo Loncoche, Bardas Blancas, and Arroyo Rahue (Fig. 4) (KIETZMANN *et al.*, 2018, 2020). The 280 m-thick Arroyo Loncoche section integrates ammonite biostratigraphy and polarity chrons (IGLESIA LLANOS & KIETZMANN, 2020). At the Pampa Tril section farther south, the Vaca Muerta contains diverse ammonite faunas and is subdivided into ammonite zones, subzones and biohorizons (PARENT *et al.*, 2015; KIETZMANN *et al.*, 2016; VENNARI, 2016).

The Berriasian-lower Valanginian Quintuco Formation gradationally overlies the Vaca Muerta Formation and is up to 300 m-thick marine claystone, sandstone and limestone comprising several transgressive-regressive sequences (SCHWARZ *et al.*, 2006; LEANZA *et al.*, 2011; KIETZMANN *et al.*, 2016; GARRIDO & PARENT, 2017). It is overlain conformably to disconformably by the Valanginian Mulichinco Formation, which is composed mainly of paralic terrigenous clastic units and the upper member is composed of mixed siliciclastic-carbonate transgressive-regressive sequences (SCHWARZ *et al.*, 2006, 2013; GARRIDO & PARENT, 2017).

The Mulichinco is overlain conformably by the upper Valanginian to Hauterivian Agrio Formation. The Agrio is up to 540 m thick and is disconformably overlain by the regressive Barremian Huitrín Formation. The Agrio is composed of three members from lower to upper: the Pilmatué, Avilé and Agua de la Mula members (AGUIRRE-URRETA *et al.*, 2017). The Pilmatué was deposited in a mixed siliciclastic-carbonate ramp setting and is composed of limestone/marl cycles suggestive of climatic control (KIETZMANN & PAULIN, 2019). The Avilé is a regressive-transgressive sandstone 25 to 40 m thick that disconformably overlies marine shale and grades up into a marine unit (Schwarz *et al.*, 2016).

Andean Biostratigraphy: Andean assemblage and interval biozones are based on ammonites, calpionellids, calcareous nannofossils, and calcareous dinoflagellates that are correlated with Tithonian-upper Hauterivian stages in the Mediterranean-Caucasian Subrealm (Table 3) (Aguirre-Urreta *et al.*, 2005, 2007, 2015, 2017, 2019; Kietzmann *et al.*, 2011, 2015; Lazo *et al.*, 2009; Soto, 2012; Vennari *et al.*, 2014, 2017; Parent *et al.*, 2015, 2017; Salazar & Stinnesbeck, 2015, 2016; Vennari, 2016; Ivanova & Kietzmann, 2017; Kietzmann, 2017; Salazar *et al.*, 2020; Iglesia Llanos and Kietzmann, 2020). In this stratigraphic experiment zones are defined by the FO of nominal species rather than basing zones on genera or assemblages.

In the Neuquén Basin five ammonite FO events in the Pampa Tril and Arroyo Loncoche sections and six other sections are correlated with the Tethys Tithonian Stage (Vennari, 2016; Parent *et al.*, 2017; Kietzmann *et al.*, 2018). Different correlation hypotheses correlate base Berriasian in the Mediterranean sections with the Vaca Muerta Formation. One interpretation correlates base of the *Substeueroceras koeneni* Zone at 101 MU with base Berriasian (Salazar & Stinnesbeck, 2016; Iglesia Llanos & Kietzmann, 2020). Alternative correlations of base Berriasian are either within the *S. koeneni* Zone (Vennari *et al.*, 2014; Kietzmann *et al.*, 2020, 2021a) or with the base of the *Argentiniceras noduliferum* Zone (Parent *et al.*, 2015) at 115 Mu. The basal part of the Vaca Muerta Formation records polarity chrons M22r to M15r (Iglesia Llanos *et al.*, 2017; Kohan Martinez *et al.*, 2018). The top of polarity chron M19n at 112 MU in the ANDESCS DB is correlated above the Tithonian-Berriasian boundary and the FO of *Calpionella alpina* below at 81 Mu (Table 3). The FADs of several calcareous nannofossils that span the Tithonian-Berriasian boundary (Casellato & Erba, 2021) are slightly above the FAD of *S. koeneni*.

The FO of *Neocomites wichmanni* at 180 MU is correlated with base Valanginian (Aguirre-Urreta, 2001; Parent *et al.*, 2015; Riccardi, 2015). It occurs together with *Calpionellites darderi* in the Cuesta del Chihuido and Puerta Curaco sections (Kietzmann *et al.*, 2020). The early-late Valanginian boundary is correlated within the *Olcostephanus atherstoni* Zone (Aguirre-Urreta, 2001), which spans 429-472 MU (Table 4).

Base Hauterivian is correlated with the FO of *Holcoptychites neuquensis* at MU 772 in the Bajada Viejo section (Aguirre-Urreta *et al.*, 2015, 2017), which is slightly above the FO of the nannofossil *Retacapsa surirella* at 765 MU in the El Portón section. The lower-upper boundary is at the base of the *Spitidiscus riccardii* Zone (Lazo *et al.*, 2009; Aguirre-Urreta *et al.*, 2019). The Hauterivian/Barremian boundary is correlated in the midst of the *Sabaudiella riverorum* Zone (Aguirre-Urreta *et al.*, 2019; Table 3).

The first and last occurrences (FO, LO) of calcareous nannofossils have been integrated with ammonite zones of the Neuquén Basin because they support correlation with the Tethys zones (Aguirre-Urreta *et al.*, 2005, 2007, 2019; Riccardi, 2015); they are also calibrated in the ANDESCS DB (Table 3). However, ranges of some important species are not yet fully extended in the ANDESCS DB because they are reported in single sections. A succession of upper Hauterivian nannofossils, *Lithraphidites bollii*, *C. cuvillieri*, *E. striatus*, and *Nannoconus liguis* (Aguirre-Urreta *et al.*, 2019) is represented in the ANDESCS DB with minor changes in the order (Table 3). Ages of nannofossils in the LOK2016 DB support the correlation of the Pilmatué Member of the Agrio Formation spanning upper Valanginian to lower Hauterivian.

In central Chile the Tithonian-lower Valanginian zones are different (Salazar *et al.*, 2020) (Table 4). At the base of the Tithonian is the *Virgatosphinctes mexicanus / Pseudolissoceras zitteli* Zone, and the upper Tithonian zones are the *Windhauseniceras internispinosum* and *Micracanthoceras microcanthum / Corongoceras alternans* Zone. Base Berriasian is marked by the *Berriasiella jacobi* Zone; middle-upper Berriasian is the *Groebericeras roccardi* Zone. The lower Valanginian zone is the *Thurmanniceras thurmanni / Argentiniceras fasciculatus* Zone.

Paleobiogeography: A brief summary of Early Cretaceous ammonite biogeography frames the different zonal schemes used in the Mediterranean and Andean regions. The biogeographic distribution of Early Cretaceous ammonoids was influenced by a complex of interrelated factors including climate, ocean temperatures and oceanic circulation (Énay, 1972; Cecca, 1998; Westermann, 2000; Page, 2008; Lehmann *et al.*, 2015). Endemism resulted in distinct geographic ammonite assemblages although the calpionellids and calcareous nannofossils were distributed widely (López-Martínez *et al.*, 2017a). During the Berriasian through Hauterivian ages, the Mediterranean-Caucasian Subrealm of the Tethys Realm hosted a biota distinct from the Andean Indo-Pacific Subrealm (Westermann, 2000; Page 2008; Lehmann *et al.*, 2015). However, the Berriasian "*Berriasiella*", *Grobericeras*, *Spiticeras*, and some Olcostephanid ammonites occupied both subrealms (Salazar *et al.*, 2020), although, many genera were endemic to the Andes: *Andiceras, Argentiniceras, Frenguelliceras, Hemispiticeras, Cuyaniceras*, and *Pseudoblanfordia* (Riccardi, 1988; Aguirre-Urreta *et al.*, 2007; Parent *et al.*, 2011; Vennari *et al.*, 2012). During the Valanginian Age Olcostephanids were widely distributed from Mediterranean-Caucasian, Pacific to Andean basins including *Neocomites*, *Kilianella*, *Sarasinella*, and *Thurmanniceras* (Aguirre-Urreta, 1998; Aguirre-Urreta & Rawson, 1999; Rawson, 2007;

Aguirre-Urreta *et al.*, 2008a). Endemism increased in Andean basins during the latest Valanginian when common Neocomitidae genera were *Pseudofavrella, Chacantuceras* and *Decliveites* (Aguirre-Urreta & Rawson, 2003, 2010). During the Hauterivian Age Tethys Indo-Pacific genera in the Andean basins were *Holcoptychites, Favrella, Jeannoticeras*, and *Plesiospitidiscus*. The characteristic early Hauterivan genera differ from the late Hauterivian genera (Lehmann *et al.*, 2015). These genera comprise the basis of Andean Berriasian-Hauterivian biostratigraphy (Aguirre-Urreta & Rawson, 2003, 2010).

Andean Magnetostratigraphy: Polarity chrons are key to correlating Andean biozones with Tethys Mediterranean stages. The Tithonian-Berriasian polarity sequence in the Neuquén Basin is defined in the Vaca Muerta Formation at Arroyo Loncoche (Kietzmann *et al.*, 2018b; Iglesia Llanos & Kietzmann, 2020) and at the Los Catutos section (Kohan Martínez *et al.*, 2018). The Tithonian-Berriasian boundary has been consistently correlated in the middle of polarity chron M19n.2n (Ogg *et al.*, 2016; Wimbledon *et al.*, 2020). In the Neuquén Basin this unit correlates with the lower part of the *Substeueroceras koeneni* Zone in the Vaca Muerta Formation (Kietzmann *et al.*, 2018b). The lower-upper Tithonian boundary has been correlated with polarity chron M20n (Ogg *et al.*, 2016) and at the base of the *Windhauseniceras internispinosum* Zone (Kietzmann *et al.*, 2018b; Kohan Martínez *et al.*, 2018) (Table 3). The new radioisotpic age of 140.3 Ma projects at 112 MUs in the Vaca Muerta Formation, which correlates with polarity chron M19n (Table 3).

Tithonian-Hauterivian Radioisotope Dates: In the past thirteen years numerous new radioisotopic dates spanning the Tithonian-Hauterivian stages have been added to previous ages in GTSS2016 and GTS2020 (Table 2). Prior to that date only five numerical ages had been published and numerical ages in the Geologic Time Scale were estimated by the polarity time scale (Ogg *et al.*, 2012, 2016). However, the new Argentinian dates would significantly alter the Early Cretaceous time scale by 1-4 myr. Most new dates are based on euhedral zircon crystals extracted from ash beds. Such dates are quite precise because selected crystals were apparently deposited penecontemporaneously and were not reworked or displaced down-section or altered (Aguirre-Urreta *et al.*, 2015, 2017, 2019; Lena *et al.*, 2019). Each date was related to a bioevent and its correlative stage (Table 2) (Aguirre-Urreta *et al.*, 2019; Lena *et al.*, 2019).

Radioisotopic U/Pb dates of detrital zircon crystals in the Tordillo Formation underlying the Tithonian Vaca Muerta Formation range in age from 275 Ma to 144 Ma and indicate that the Jurassic Andean arc was the primary sediment source and that older igneous sources contributed minor amounts (Naipauer *et al.*, 2015c). Dates from the basal interval of the Tordillo of 149.5±1.2 Ma and from a higher bed of 143.0±1.0 Ma (Horton *et al.*, 2016; Naipauer *et al.*, 2015a, 2015b) suggest that the Tithonian Stage may be younger than 152.1 Ma as in GTS2016.

Five volcanic tuff beds in the Tithonian-Berriasian Vaca Muerta Formation at the Las Loicas section (Vennari *et al.*, 2014; Lena *et al.*, 2019) are dated by U-Pb zircons or the Bayesian age-depth model. A date of 142.04±0.17 Ma is in the *Crassicolaria* Zone (Table 2). Four dates are associated with uppermost Tithonian nannofossil FADs: 140.6±0.4 Ma, 140.54±0.34 Ma, 140.34 ±0.18 and 140.22±0.13 Ma (Table 2). These dates are interpolated into the ANDESCS DB database by their co-occurrence with ammonites, calpionellids and nannofossils (Table 3).

The base of the uppermost Tithonian-lower Berriasian *Substeueroceras koeneni* Zone in the Las Loicas section underlies an ash bed dated at 140.34±0.08 Ma, which is within polarity Chron M19n. The middle Berriasian *Argentiniceras noduliferum* Zone and the FO of *Nannoconus kamptneri minor* are bracketed by the dates of 140.34±0.08 Ma and 139.96±0.06 Ma. The *Spiticeras damesi* Zone is dated at 139.24±0.05 Ma. The FO of basal Valanginian *C. darderi* and *N. wichmanni* are projected directly above these dates. These ages are significantly younger than calibrated in GTS2016 and in LOK2016 DB (Scott, 2019a). Based on these radioisotopic dates, Vennari *et al.* (2014) and Lena *et al.* (2019) proposed that the numerical age of the base Berriasian should be 141.0 Ma, which is four myr younger than in GTS2016 (Ogg *et al.*, 2016) and about two myr younger than 143.1 Ma in GTS2020.

In the Valanginian-Hauterivian Agrio Formation, zircons from four ash beds date Hauterivian biozones (Fig. 4) (Aguirre-Urreta *et al.*, 2015, 2017, 2019; Kohan Martínez *et al.*, 2017; Rawson *et al.*, 2017). The *Olcostephanus laticosta* Zone in the middle of the Pilmatué Member is dated at 130.39±0.16 Ma (Aguirre-Urreta *et al.*, 2015). The tuff bed in the Agua de la Mula Member about 7 m above the top of the Avilé Member in the *Spitidiscus riccardii* Zone was first dated at 132.5±1.3 Ma by SHRIMP U-Pb on zircons (Aguirre-Urreta *et al.*, 2015) and subsequently a CA-ID TIMS date at 129.09±0.04 Ma. The upper part of the *Paraspiticeras groeberi* Zone was dated at 127.42±0.03 Ma (Aguirre-Urreta *et al.*, 2017) and the *Sabaudiella riverorum* zone that spans the Hauterivian-Barremian boundary was dated by CA-ID-TIMS at 126.97 +/- 0.04 Ma (Aguirre-Urreta *et al.*, 2019).

Numerical ages in the LOK2016 DB are constrained by nine radioisotopic dates (Table 2).

Dates of Valanginian Stage calpionellids and calcareous nannofossils in Mexico, California and Tibet range between 139.85 and 134.0 Ma.

1. The upper lower Berriasian *Calpionella elliptica* Zone in the Lower Tamaulipas Formation in Morelos, Mexico, is dated at 140.512 ±0.031 Ma by U-Pb zircon CA-ID-TIMS from an ash bed (Lena *et al.*, 2019). This date suggests that the base of the Berriasian Stage must be older than proposed by Lena *et al.* (2019).
2. The Berriasian/Valanginian boundary in the Lower Tamaulipas Formation in eastern Mexico is dated at 139.85 Ma by $^{87}Sr/^{86}Sr$ of a limestone 0.4 m above the FO of *Calpionellites darderi* (López-Martínez *et al.*, 2017b).
3. The overlying upper Valanginian *Calpionellites major* Subzone is dated at 134.0±0.5 Ma by U-Pb of zircons from a felsic tuff. Thus, the duration of the Valanginian is at least 5.85 myr compared to 5.1 myr in GTS2020 (Gale *et al.*, 2020).
4. An uppermost Berriasian-lowermost Valanginian calpionellid assemblage in the Pimienta Formation near San Luis Potosí overlies a bentonite bed, from which zircons were dated by U-Pb at 139.1±2 Ma (López-Martínez *et al.*, 2015, Table 1), although, the average age of 20 "best ages" is 141.17 Ma.
5. In the California Coastal Range in the Great Valley Sequence, zircons from two tuff beds 64.6 m apart were dated by U-Pb at 137.1±1.6/-0.6 Ma (Bralower *et al.*, 1990). The lower tuff bed directly underlies the Valanginian assemblage of *Cretarhabdus angustiforatus* and a few meters above are the FOs of *Micrantholithus hoschulzii* and *Rhagodiscus nebulosus*.
6. In southern Tibet the uppermost Tithonian-Berriasian-Valanginian succession was recognized by ammonite and calcareous nannofossil assemblages (Liu *et al.*, 2013; Wan *et al.*, 2011). Ash beds yielded zircons dated from 140.0±1.3 to 141.8±1.2 Ma by SIMS U-Pb.
7. An ash bed dated at 141±1 is bracketed by the FOs of three upper Tithonian-Valanginian calcareous nannofossils.
8. In a separate Tibetan section, an ash bed overlying the *C. oblongata* Zone is dated at 136 Ma (Wan *et al.*, 2011).
9. The age of the base Albian Stage is constrained by a date of 113.1±0.3 Ma by $^{206}Pb/^{238}U$ of zircons from an ash bed in the Gault Formation, Vöhrum, Germany (Selby *et al.*, 2009), which in GTS2020 is 113.2 (Gale *et al.*, 2020).

4. Results

Correlation of Andean zones with Mediterranean Tithonian-Hauterivian Stages: Standard European stage boundaries can be correlated with the Andean sections by means of nannofossils, calpionellids and polarity chrons that are in both the LOK2016 DB and the ANDESCS DB. Stratigraphic positions in the former database are in mega-annums and in the latter database positions are scaled in meters (MUs) of the Chos Malal reference section.

The two data sets were correlated by plotting the LOK2016 DB in MA on the X-axis, and the ANDESCS DB on the Y-axis in MUs (Fig. 5). The black correlation lines (CLS) on the X/Y plots project stage boundaries defined in European reference sections with the Andean standard ammonite zones. On the right side of the plot are the FOs of Andean ammonites and their numerical ages in Ma are derived by projecting to the Mediterranean data by the CLS.

The first correlation hypothesis in the Vaca Muerta Formation (black, bold, dashed CLS) is constrained by tops of polarity chrons and the Agrio Formation is correlated by fossil FADs or LADs (Fig. 5). The plot has three segments at two bends, and the contact between the Quintuco and Mulichinco formations separates segments three and four. The lower segment in the Vaca Muerta Formation is constrained by the tops of polarity chrons M22n through M16n (plus signs). Nannofossil and calpionellid FOs (squares) also constrain the line including the FO of *Calpionellites darderi* (Fig. 5). Several Andean FO bioevents are above and left of the line because they have not been recorded lower in the Vaca Muerta; conversely several FOs to the right of the line (not shown) will be extended older in the LOK2016 DB, which incorporates few Tithonian sections and species. The second CLS segment spans the upper part of the Vaca Muerta and the Quintuco and Mulichinco formations; it is unconstrained by bioevents because none of the fossiliferous sections of the Quintuco and Mulichinco formations are in the ANDES Database, although a few Berriasian and lower Valanginian ammonites are in the Quintuco (Schwarz *et al.*, 2006; Garrido & Parent, 2017). The Mulichinco overlies the *L. riveroi* Zone and underlies the *P. angulatiformis* Zone and in its uppermost intervals *O. atherstoni* and *O. permolestus* are present where the Mulichinco grades into the Agrio (Schwarz *et al.*, 2006).

In the Agrio Formation two correlation interpretations are reasonable. The black CLS A is constrained by nannofossil FOs and LOs, and it will extend fewer LOs than alternate CLSs. At its base is the FO of *Eiffellithus striatus*, which is a well-established upper Valanginian bioevent in both databases and GTS2016 (Bown *et al.*, 1998). The FOs of a number of other nannofossils are left of the CLS and would be projected lower in Andean strata but have yet to documented there. The upper part of the black CLS A is tightly constrained by the LOs of the nannofossils *Tubodiscus verenae*, *Cruciellipsis cuvillieri*, and *Lithraphidites bolli*. To the right of the CLS is a stack of numerous other nannofossils that have longer ranges. To the left side of CLS A is a smaller group of LOs that are younger in the Andes than in sections in the LOK2016 DB. Their range ages will be extended by the Andean data set.

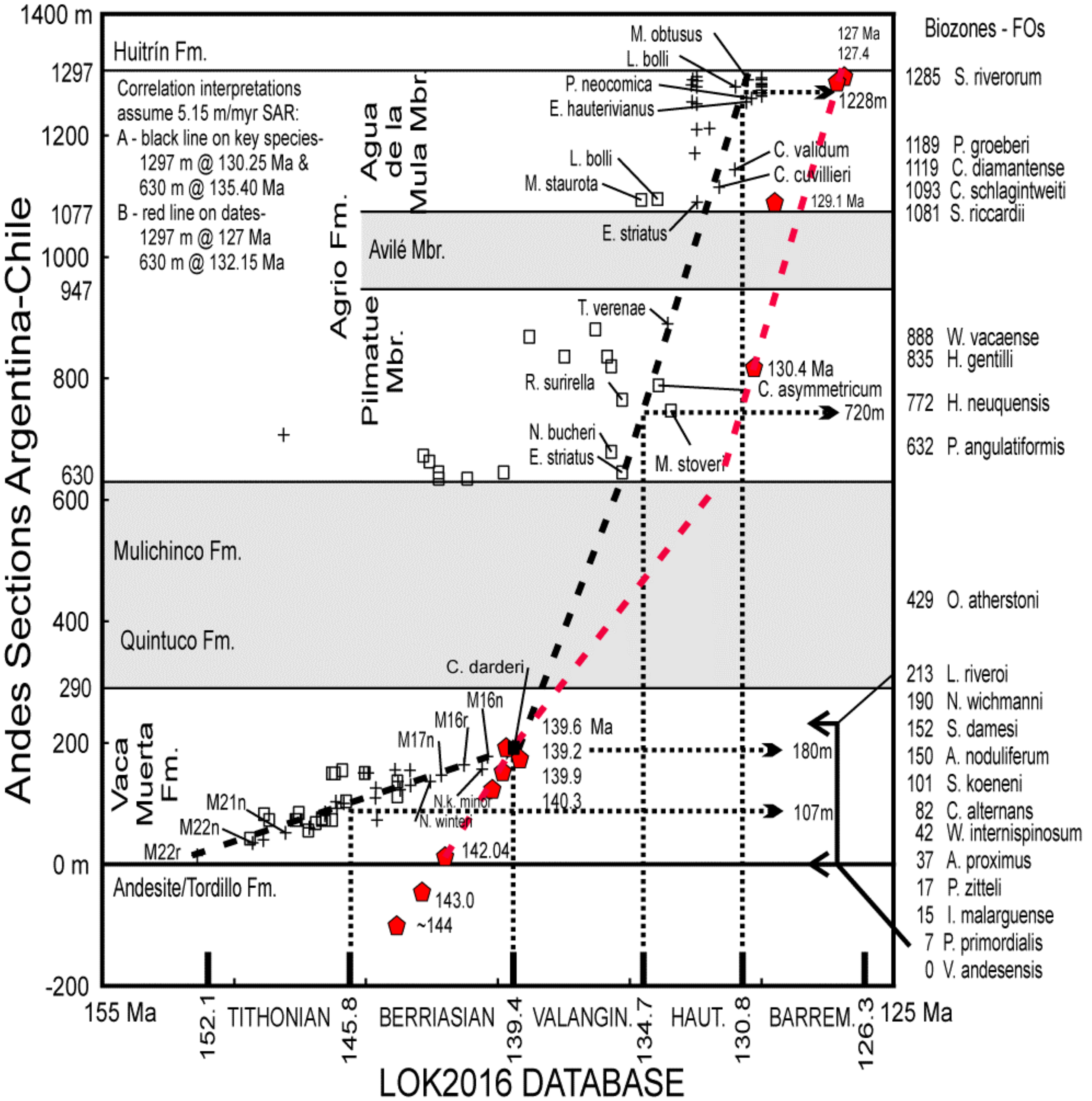

Figure 5: Correlation plot of LOK2016 DB (X-axis) in mega-annums (Ma) with ANDESCS DB (Y-axis) in metric units (MUs). Berriasian, Valanginian, Hauterivian, and Barremian stage boundaries defined at Tethys reference sections. Polygons are radioisotopic dates of Andean ash beds. Black dashed correlation lines are tied to polarity chrons M22n to M16n and calcareous nannofossils. Dotted lines project standard stage boundaries into Andean sections.

The second correlation interpretation places the red CLS through the nine radioisotopic ages (red polygons, Fig. 5). The correlation line in the lower part of the Vaca Muerta Formation would date it much younger than ages of polarity chrons in GTS2016 and GTS2020. Also, the Agrio Formation would be younger than projected by the LOK2016 DB.

The slopes of the CLSs represent sediment accumulation rates (SARs), not sedimentation rates because these rocks have been compacted and lithified. The SAR of the Vaca Muerta Formation increases from 0.050 mm/kyr to 0.344 mm/kyr. The SAR of the combined Mulichinco and Agrio formations is estimated at 0.633 mm/kyr by CLS A and 0.851 mm/kyr. Because the base of the Mulichinco varies from conformable to unconformable across the basin (Schwarz *et al.*, 2006), the duration of the hiatus in Figure 5 is not estimated.

The black CLSs of this stratigraphic experiment correlates base Berriasian at MU 107 above the FO of *S. koeneni* at MU 101. This is consistent with correlations that place base Berriasian within the *S. koeneni* Zone (Leanza *et al.*, 2011; Salazar Soto, 2012; Salazar & Stinnesbeck, 2015; Kietzmann *et al.*, 2018, 2021a). Base Valanginian projects at MU 180 at the base of the *N. wichmanni* Zone and FO of *C. darderi*, which is consistent with projections by Leanza *et al.* (2011) and Kietz-

MANN *et al.* (2018) among others. Base of the Hauterivian Stage is projected at MU 720 below the base of the *Holcoptychites neuquensis* Zone at 772 Mu, which is lower than previous correlations (AGUIRRE-URRETA *et al.*, 2017, 2019). Base of Barremian Stage as defined in the Mediterranean sections, projects into the *S. riverorum* Zone below the unconformable contact between the Agrio and Huitrín formations consistent with previous correlations (AGUIRRE-URRETA *et al.*, 2017).

The base of the Mulichinco Formation, base of the Middle Mendoza Subgroup, is bracketed in the middle part of the Valanginian Stage (KIETZMANN *et al.*, 2020) and may correlate with the 136.4 Ma sea-level event of HAQ (2014) and the intra-Valanginian unconformity in the Texas Gulf Coast (SCOTT, 2019b). The unconformity at base of Avilé Member of the Agrio Formation, base of the Upper Mendoza Subgroup, may correlate with the 132.8 Ma or the 131.8 Ma mid Hauterivian sea-level event (HAQ, 2014).

The X/Y plot of the Andean data with the LOK2016 data correlates Andean biozones with Tethys biozones and interpolates numerical ages for the FOs (Table 4). These correlations generally reproduce those of the Tithonian-Berriasian (RICCARDI, 2015). The calpionellid zonal schemes of RICCARDI differ in some details from that of LAKOVA and PETROVA (2013), so the correlations differ. However, both schemes correlate similarly with polarity chrons. The calcareous nannofossil zones in both regions are based on FAD/LADs and reproduce those of AGUIRRE-URRETA *et al.* (2019).

Stage and Ammonite Zone Durations: Calculating durations of Tithonian and Lower Cretaceous stages and associated ammonite zones by different methods tests numerical ages of stage boundaries (Fig. 6). Cyclostratigraphic astrochronologic calibration of stage durations is an important tool to calibrate numerical ages of stage boundaries. However, the durations vary depending on the stratigraphic sections, the boundary criteria and the methods. The GTS2020 time scale measures the duration of base Berriasian to top Hauterivian at 16.5 myr (Fig. 6.C). New dates from the Neuquén Basin measure the duration of this interval at 14.35 Myr (Fig. 6.D). This stratigraphic experiment estimates the duration of the upper part of the Tithonian Stage into the lower part of the Valanginian Stage in the Vaca Muerta and Quintuco formations to be about 15 myr (Fig. 5).

Cyclostratigraphic astrochronology of the Vaca Muerta Formation calculated the durations of the Tithonian Stage at least **5.67** myr and the Berriasian Stage at **5.27 myr** (Fig. 6.E) (KIETZMANN *et al.*, 2018, 2020) compared with durations of 6.1 and 5.4 myr in GTS2020 (Fig. 6.C; GALE *et al.*, 2020; HESSELBO *et al.*, 2020).

The duration of the Valanginian Stage may have been up to 6 myr duration based on the Sr isotope date of 139.85 Ma and the U-Pb zircon date of 134.0 Ma in eastern Mexico (Table 2). However, radio-astrochronology calibrated the duration at 5.08 myr in French and Spanish reference sections using the FO of *Tirnovella pertransiens* as the base Valanginian (MARTINEZ *et al.*, 2013, 2015). A slightly shorter duration of 4.74 myr was measured in the Angles section, France, where base Valanginian is defined at FO *Calpionellites darderi* and its top at FO of *Acanthodiscus radiatus* (data from BUSNARDO *et al.*, 1979, Fig. 8E). The mid-point duration of this range is **5.3 myr**, which is used here to calculate stage boundary ages (Fig. 6.E).

The duration of the Hauterivian Stage ranges from 5.96 to 5.21 myr. In French reference sections four cyclostratigraphic astrochronologic studies measured the duration from 5.3 myr to 5.93±0.41 myr (MARTINEZ *et al.*, 2015). In the Neuquén Basin at El Portón in the Agrio Formation precise CA-ID TIMS U-Pb radioisotopic dates, biostratigraphy and astrochronology of bedding cycles calculated the duration of the Hauterivian at 5.21±0.08 myr (AGUIRRE-URRETA *et al.*, 2019). Low-frequency eccentricity cycles of the Agrio Formation at Arroyo Loncoche calculated the duration of the Hauterivian at 5.96 myr (KIETZMANN *et al.*, 2020). The mid-point age of 5.585 myr is rounded to **5.6 myr** as Hauterivian duration.

The graphic correlation experiment of the Neuquén Basin data presents two possible interpretations of the Hauterivian duration (Fig. 5). Correlation line A estimates the duration at 5.15 myr, close to the proposed 5.21 myr duration. It is constrained at base of the Agrio Formation by the FO of *Eiffellithus striatus* with an age of 135.30 Ma (Appendix 2). The FAD of *E. striatus* is uppermost Valanginian (GTS2016, OGG *et al.*, 2016). The top of correlation line A at 130 Ma is constrained by a cluster of late Hauterivian nannofossil LADs (BOWN *et al.*, 1998): *Cruciellipsis cuvillieri, Eiffellithus striatus* and *Lithraphidites bollii* (Fig. 5).

Correlation hypothesis B calibrates the duration at 5.18 myr. Correlation line B is constrained by the set of four radioisotopic dates with an age of 132.15 Ma at the base of the Agrio and 126.97 Ma at its top. These durations assume a uniform rate of accumulation of the Avilé Member with no significant hiatus, which assumptions need to be fully evaluated. Longer durations could be represented between these two hypotheses by correlation lines with lower slopes. The range of durations calculated by astrochronology from 5.21 myr to 5.93 myr suggests that the assumptions should also be reevaluated as noted by MARTINEZ *et al.* (2015).

KIETZMANN *et al.* (2018, 2020) estimated the durations of Tithonian-Berriasian ammonite zones in the Vaca Muerta Formation by the number of 405 myr-period depositional cycles. Durations calculated by this method are compared to durations measured between the FADs of each zonal species in LOK2016 DB (Table 5, Appendix 2). Most zonal durations estimated by the graphic method are longer than those measured by cyclostratigraphy because the graphic method relates the zonal ages to ages of polarity chrons in GTS2016. In contrast, zonal durations measured using the Andean radioisotopic dates are much shorter.

Table 5. Comparison of durations of Andean ammonite zones with revisions by new radioisotopic dates.

Zone	Durations kyr			
	KIETZMANN, 2018	LOK 2016DB	Revised Age Ma	Duration
N. wichmanni			139.51	
S. damesi	1.62	2.09	140.09	0.58
A. noduliferum	0.81	1.61	140.14	0.05
S. koeneni	2.43	0.95	140.7	0.56
C. alternans	1.21	2.11	141.28	0.58
W. interspinosum	1.21	1.63	141.52	0.24
A. proximus	0.61	0.65	141.59	0.07
P. zitteli	0.61	1.38	141.74	0.15
V. andesensis	0.81	1.56	141.91	0.17

5. A revised Berriasian-Hauterivian Time Scale

Since 2016 four studies have revised the Berriasian-Hauterivian time scale (Fig. 6.A-D). New radioisotopic dates and cyclostratigraphic astrochronologic durations from the Neuquén Basin revise the ages of these stages. If the age of one stage is dated consistently be several methods, it can anchor ages of other stages by adding or subtracting stage durations. Using this method, the ages of other stage boundaries are proposed (Fig. 6.E).

The base of the Valanginian Stage in Mediterranean sections is consistently defined by the FAD of *"Thurmanniceras" pertransiens* and alternatively by *Calpionellites darderi* (REBOULET *et al.*, 2018) and secondarily by calcareous nannofossil biomarkers. The dates range between 140 Ma and 139 Ma in Argentina, Mexico, California, and Tibet (Table 2). The mid-point date of **139.5 Ma** is used here as the numerical age of the Berriasian/Valanginian boundary. In the Neuquén Basin base Valanginian correlates with the base of the *Neocomites wichmanni* Zone, which is projected to range in age from 139.45 to 139.16 Ma by the graphical plot (Fig. 5).

By adding the astrochronologically derived durations of the Berriasian (5.27 myr) and Tithonian (5.67 myr) to 139.50, a recalibrated age of base Berriasian is 144.77 Ma and Tithonian is 150.44 Ma (Fig. 6.E). New radioisotope dates of the two lowermost Berriasian zones that span Tithonian-Berriasian, *Nannoconnus steinmanni minor* and *Argentiniceras noduliferum*, are younger ranging from 140.7 Ma to 137.9 Ma (Table 2). LENA *et al.* (2019, Fig. 4) estimated the age of this boundary between 141.0 and 140.7 Ma below an ash bed dated at 140.34±0.18 Ma (Table 2). The age of 152.1 Ma at base of the Tithonian Stage (Fig. 6.A; OGG *et al.*, 2016) was supported by astronomical calibration (HUANG, 2018). GTS2020 revised the age to 149.24 Ma (HESSELBO *et al.*, 2020). A new radioisotopic date of 147.112± 0.078 Ma in the Tordillo Formation 1.5 m below the lower but not lowest Tithonian *Virgatosphinctes andesensis* Zone in the Vaca Muerta Formation is consistent with the GTS2020 age (Table 2; LENA *et al.*, 2019, p. 10).

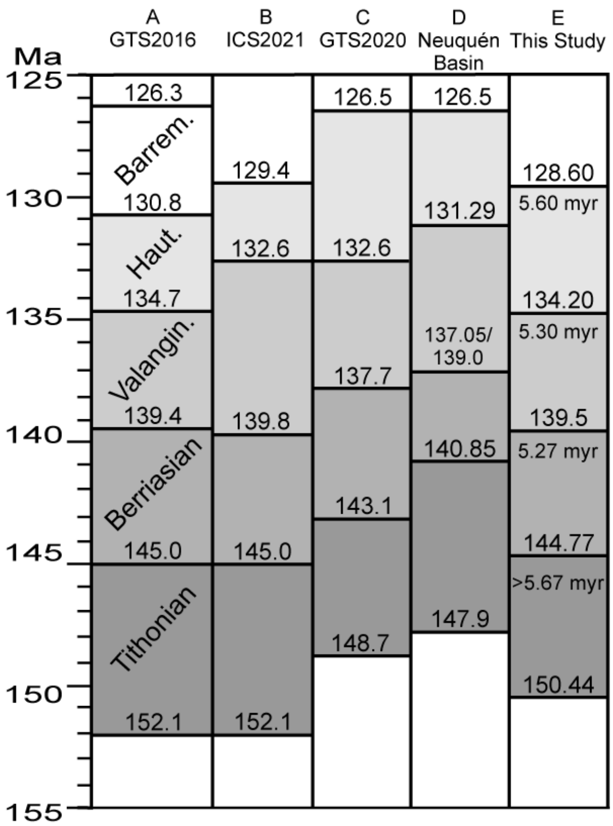

Figure 6: Comparison of five recent time scales of Tithonian to Barremian stages. Column A, OGG *et al.* (2016); B, International Commission on Stratigraphy (COHEN *et al.*, 2021); C, GALE *et al.* (2020); D, composited time scale of MARTINEZ *et al.* (2013, 2015), KIETZMANN *et al.* (2018), AGUIRRE-URRETA *et al.* (2019), and LENA *et al.* (2019); E, alternative time scale based on stage durations anchored on base Valanginian dated at 139.50Ma.

The base of the Hauterivian Stage is recalibrated at 134.20 Ma by subtracting the Valanginian duration of 5.30 myr from 139.50 Ma. However, a range of radioisotopic dates between 132 to 130.5 Ma near the stage base (Table 2) is younger even than the GTS2020 age of 132.6 Ma (Fig. 6.C). In the Neuquén Basin base Hauterivian is correlated with the base of the *Holcoptychites neuquensis* Zone (AGUIRRE-URRETA, 2001); the FO of this taxon is dated at 131.16 Ma (AGUIRRE-URRETA *et al.*, 2019). An alternative age of 131.96 ±1.0 Ma was derived from a radioisotopically dated tuff bed in the Neuquén Basin constrained biostratigraphically (MARTINEZ *et al.*, 2015). The graphic plot to the new radioisotopic date of 130.40 Ma (Fig. 5) would recalibrate the base age at 130.49 Ma. A new date of 130.39±0.16 Ma in the middle of the *N. neuquensis* Zone in the Pilmatúe Member of the Agrio Formation (Table 2) is consistent with these ages. This new data suggests an age of 132 to 131 Ma for base Hauterivian, thus the duration of the Valanginian would be longer than calculated. The incompatibility between Hauterivian ages derived by stage durations and radioisotope dates is yet to be resolved.

The top of the Hauterivian is recalibrated at 128.60 Ma by subtracting the mean duration of 5.60 myr from the recalibrated age of 134.20 Ma (Fig. 6.E). In the Neuquén Basin top Hauterivian correlates approximately within the *Sabaudiella riverorum* Zone at the top of the Agua de la Mula Member of the Agrio Formation. The FO of *S. riverorum* coincides with a new radioisotopic date of 126.97 Ma. MARTINEZ *et al.* (2012, 2015) dated top Hauterivian at 126.02±1.0 Ma by cyclostratigraphy.

6. Conclusions

The graphic correlation experiment of twenty-three sections in the Andean part of the Indo-Pacific Subrealm span middle Tithonian to Hauterivian stages and integrates ranges of 254 species, sequence boundaries, polarity chrons, and radioisotopic ages that compose the ANDESCS DB. This database accurately reproduces the order of the Andean ammonite zones and places them in a relative metric scale of the Chos Malal reference section. This composite of three measured sections represents continuous deposition throughout this time interval in the Neuquén Basin. This achievement demonstrates that the ANDESCS DB is reliable so that correlation with standard reference sections in the Mediterranean-Caucasian Subrealm will produce meaningful results. A larger database of 70 sections and 877 stratigraphic markers primarily in the Mediterranean-Caucasus Subrealm compose the LOK2016 DB and prior to publication of GTS2020 was calibrated to GTS2016. This database contains the standard reference sections of the Berriasian, Valanginian and Barremian stages and the Hauterivian GSSP.

The X/Y plot of the LOK2016 DB to ANDESCS DB projects boundaries of the Berriasian, Hauterivian and Barremian stages as defined in the Mediterranean region into the ANDESCS DB. This stratigraphic experiment confirms the approximate correlation of stages defined by endemic ammonites and cosmopolitan calcareous nannofossils. The FO of *Substeueroceras koeneni* is latest Tithonian. The base of the Valanginian correlates with the FOs of *Neocomites wichmanni* and *Calpionellites darderi*. These two bioevents are younger than three new upper Berriasian dates that average 139.58 Ma, which is consistent with an age of 139.50 Ma at base Valanginian. This age of the base Valanginian defined by *Calpionellites darderi* is confidently confirmed by multiple dates in Argentina, Mexico, Tibet, and California. The base of the Hauterivian projects between the FOs of *Pseudofavrella angulatiformis* and *Holcoptychites neuquensis*. Top of the Hauterivian Stage is projected into the uppermost part of the Agrio Formation in the *Sabaudiella riverorum* Zone.

A revised time scale of the Tithonian to Hauterivian stages is recalibrated by adding or subtracting stage durations from the age of base Valanginian Stage, which is dated consistently by various methods in widely separate sections. Durations of the have been measured by different methods in both subrealms, so they are reliable. The age of the Tithonian base is proposed at 150.40 Ma, base Berriasian Stage at 144.77 Ma, base Valanginian at 139.50 Ma, base Hauterivian at 134.20 Ma, and top Hauterivian at 128.60 Ma.

The new radioisotopic ages in the Neuquén Basin would result in several significant differences if adopted. The ages of most of the biostratigraphic and magnetostratigraphic events would be recalibrated much younger. The duration of the Jurassic would increase by up to 4 myr. The rates of sediment accumulation would increase dramatically. The durations of ammonite zones would be reduced to unreasonable numbers. The precise ages of Tithonian to Barremian stage boundaries will continue to evolve as new data become available from other localities.

Acknowledgements

This stratigraphic correlation experiment was possible only because of superb research by the international community of Cretaceous stratigraphers, biostratigraphers, magnetostratigraphers, and radioisotopic geochemists, who have documented an enormous amount of high quality data during many decades. I am particularly grateful to the late Luc G. BULOT for sharing his original ammonite data from the French sections and encouraging the compilation of the Cretaceous database. The methodology of quantitative stratigraphy by graphic correlation was pioneered by Alan SHAW and the software by Kenneth HOOD. The former Berriasian Working Group (International Subcommission on Cretaceous Stratigraphy) under the leadership of W.A.P. WIMBLEDON has produced a large volume of reliable and essential stratigraphic data spanning the Tithonian-Berriasian stage boundary in a global set of sections (WIMBLEDON, 2017, WIMBLEDON *et al.*, 2020). GRANIER *et al.* (2020) have thoughtfully reviewed the history and issues surrounding definition of the Jurassic-Cretaceous boundary. Helpful reviews by Dr. Beatriz AGUIRRE-URRETA, Dr. Diego A. KIETZMANN, Dr. Ottilia SZIVES, Dr. Jacek GRABOWSKI, Dr. Christian A. SALAZAR SOTO, and an anonymous reviewer materially improved the accuracy of this stratigraphic experiment, but this author is responsible for all interpretations.

This research received no specific grants from funding agencies in the public, commercial, or not-for-profit sectors. It has been self-funded by Precision Stratigraphy Associates.

Bibliographic references

Aguado R., Company M. & Tavera J.M. (2000).- The Berriasian/Valanginian boundary in the Mediterranean region: New data from the Caravaca and Cehegín sections, SE Spain.- *Cretaceous Research*, vol. 21, p. 1-21.

Aguirre-Urreta M.B. (1998).- The ammonites *Karakaschiceras* and *Neohoploceras* (Valanginian Neocomitidae) from the Neuquen Basin, West-Central Argentina.- *Journal of Paleontology*, Cambridge, UK, vol. 72, p. 39-59.

Aguirre-Urreta M.B. (2001).- Marine Upper Jurassic-Lower Cretaceous stratigraphy and biostratigraphy of the Aconcagua-Neuquén Basin, Argentina and Chile.- *Journal of Iberian Geology*, Madrid, vol. 27, p. 71-90.

Aguirre-Urreta M.B., Casadío S., Cichowolski M., Lazo D.G. & Rodriguez D.L. (2008a).- Afinidades paleobiogeográficas de los invertebrados cretácicos de la Cuenca Neuquina.- *Ameghiniana*, Buenos Aires, vol. 45, p. 593-613.

Aguirre-Urreta B., Lescano M., Schmitz M.D., Tunik M., Concheyro A., Rawson P.F. & Ramos V.A. (2015).- Filling the gap: New precise Early Cretaceous radioisotopic ages from the Andes.- *Geological Magazine*, Cambridge (UK), vol. 152, p. 557-564.

Aguirre-Urreta B., Martinez M., Schmitz M., Lescano M., Omarini J., Tunik M., Kuhnert H., Concheyro A., Rawson P.F., Ramos V.A., Reboulet S., Noclin N., Frederichs T., Nickl A.-L. & Pälike H. (2019).- Interhemispheric radio-astrochronological calibration of the time scales from the Andean and the Tethyan areas in the Valanginian-Hauterivian (Early Cretaceous).- *Gondwana Research*, vol. 70, p. 104-132.

Aguirre-Urreta M.B., Mourgues A.F., Rawson P.F., Bulot L.G. & Jaillard E. (2007).- The Lower Cretaceous Chañarcillo and Neuquén Andean basins: Ammonoid biostratigraphy and correlations.- *Geological Journal*, vol. 42, p. 143-173.

Aguirre-Urreta M.B., Pazos P.J., Lazo D.G., Fanning C.M. & Litvak V.D. (2008b).- First U-Pb SHRIMP age of the Hauterivian stage, Neuquén Basin, Argentina.- *Journal of South American Earth Sciences*, vol. 26, p. 91-99.

Aguirre-Urreta M.B. & Rawson P.F. (1999).- Stratigraphic position of *Valanginites*, *Lissonia*, and *Acantholissonia* in the Lower Valanginian (Lower Cretaceous) ammonite sequence of Neuquén Basin, Argentina. *In*: Olóriz F. & Rodríguez-Tovar F.J. (eds.), Advancing research on living and fossil Cephalopods.- Kluwer/Plenum, New York, p. 521-529.

Aguirre-Urreta M.B. & Rawson P.F. (2003).- Lower Cretaceous ammonites from the Neuquén Basin, Argentina: The Hauterivian genus *Holcoptychites*.- *Cretaceous Research*, vol. 24, p. 589-613.

Aguirre-Urreta M.B. & Rawson P.F. (2010).- Lower Cretaceous ammonites from the Neuquén Basin, Argentina: The neocomitids of the *Pseudofavrella angulatiformis* Zone (upper Valanginian).- *Cretaceous Research*, vol. 31, p. 321-343.

Aguirre-Urreta M.B., Rawson P.F., Concheyro G.A., Bown P.R. & Otton E.G. (2005).- Lower Cretaceous (Berriasian-Aptian) biostratigraphy of the Neuquén Basin. *In*: Veiga G., Spalletti L., Howell J.A. & Schwarz E. (eds.), The Neuquén Basin: A case study in sequence stratigraphy and basin dynamics.- *Geological Society, London, Special Publications*, vol. 25, p. 57-81.

Aguirre-Urreta M.B., Schmitz M.D., Lescano M., Tunik M., Rawson P.F., Concheyro A., Buhler M. & Ramos V.A. (2017).- A high precision U-Pb radioisotopic age for the Agrio Formation, Neuquén Basin, Argentina: Implications for the chronology of the Hauterivian Stage.- *Cretaceous Research*, vol. 75, p. 193-204.

Alleman F., Catalano R., Farés F. & Remane J. (1971).- Standard Calpionellid zonation (Upper Tithonian-Valanginian) of the Western Mediterranean Province. *In*: Farininaci A. (ed.), Proceedings of the II Planktonic Conference, Roma, 1970.- Edizioni Tecnoscienza, Rome, p. 1337-1340.

Andreini G., Caracuel J. & Parisi G. (2007).- Calpionellid biostratigraphy of the Upper Tithonian-Upper Valanginian interval in Western Sicily (Italy).- *Swiss Journal of Geosciences*, 100, p. 179-198. DOI: https://doi.org/10.1007/s00015-007-1227-z.

Applegate J.L. & Bergen J.A. (1988).- Cretaceous calcareous nannofossil biostratigraphy of sediments recovered from the Galicia Margin, ODP Leg 103.- *Proceedings of the Ocean Drilling Program, Scientific Results*, College Station - TX, vol. 103, p. 293-348. DOI: https://doi.org/10.2973/odp.proc.sr.103.144.1988

Arkadiev V., Guzhikov A.U., Baraboshkin E., Savelieva Y., Feodorva A., Shurekova O., Egor P. (2018).- Biostratigraphy and magnetostratigraphy of the upper Tithonian-Berriasian of the Crimean Mountains.- *Cretaceous Research*, vol. 87, p. 5-41.

Arnaud H., Arnaud-Vanneau A., Blanc-Alétru M.-C., Adatte T., Argot M., Delanoy G., Thieuloy J.-P., Vermeulen J., Virgone A., Virlouvet B. & Wermeille S. (1998).- Répartition stratigraphique des orbitolinidés de la plate-forme urgonienne subalpine et jurassienne (SE de la France).- *Géologie Alpine*, Grenoble, vol. 74, p. 3-89.

Arnaud-Vanneau A. & Masse J.-P. (1989).- Les foraminifères benthiques des formations carbonatées de l'Hauterivien-Barrémien *pro parte* du Jura vaudois et neuchâtelois (Suisse).- *Mémoires de la Société neuchâteloise des Sciences naturelles*, vol. 11, p. 257-276.

Atasoy S.G. (unpublished, 2017).- Foraminiferal and calpionellid biostratigraphy, microfacies analyses and tectonic implications of the Upper Jurassic - Lower Cretaceous carbonate platform to slope successions in Sivrihisar Region (Eskişehir, NW Turkey).- MSc. Thesis, Middle East Technical University, Ankara, 254 p.

Atasoy S.G., Altiner D., Okay A.I. (2018).- Reconstruction of a Late Jurassic - Early Cretaceous carbonate platform margin with composite biostratigraphy and microfacies analysis (western Sakarya Zone, Turkey): Paleogeographic and tectonic implications.- *Cretaceous Research*, vol. 92, p.66-93.

Benzaggagh M. (2021).- Systematic revision and evolution of the Tithonian family Chitinoidellidae Trejo, 1975.- *Carnets Geol.*, vol. 21, no. 2, p. 27-53. DOI: 10.2110/carnets.2021.2102

Blauser W.H. & McNulty C.L. (1980).- Calpionellids and nannoconids of the Taraises Formation (Early Cretaceous) in Santa Rosa Canyon, Sierra de Santa Rosa, Nuevo Leon, Mexico.- *Gulf Coast Association of Geological Societies*, *Transactions*, Lafayette - LA, vol. 30, p. 263-272.

Bown P.R., Rutledge D.C., Crux J.A. & Gallagher L.T. (1998).- Early Cretaceous. *In*: Bown P.R. (ed.), Calcareous nannofossil biostratigraphy.- British Micropalaeontological Society Publication Series, Chapman & Hall, London, p. 86-131.

Bralower T.J., Ludwig K.R., Obradovich J.D. & Jones D.L. (1990).- Berriasian (Early Cretaceous) radiometric ages from the Grindstone Creek section, Sacramento Valley, California.- *Earth and Planetary Science Letters*, vol. 98, p. 62-73.

Bralower T.J., Monechi S. & Thierstein H.R. (1989). Calcareous nannofossil zonation of the Jurassic-Cretaceous boundary interval and correlation with the geomagnetic polarity timescale.- *Marine Micropaleontology*, vol. 14, p. 153-235.

Buffler R.T., Schlager W. & Pisciotto K.A. (1984).- 1. Introduction and Explanatory Notes.- *Initial Reports DSDP*, College Station - TX, vol. 77, p. 5-22. DOI: 10.2973/dsdp.proc.77.101.1984.

Bujtor L., Krische O. & Gawlick H.-J. (2013).- Late Berriasian ammonite assemblage and biostratigraphy of the Leube quarry near Salzburg (Northern Calcareous Alps, Austria).- *Neues Jahrbuch für Geologie und Paläontologie*, Abhandlungen, Stuttgart, vol. 267, no. 3, p. 273-295.

Bulot L. (unpublished, 1995).- Les formations à ammonites du Crétacé inférieur dans le Sud-Est de la France (Berriasien à Hauterivien) : Biostratigraphie, paléontologie et cycles sédimentaires.- Ph.D. thesis, Muséum National d'Histoire Naturelle, Paris, 398 p.

Bulot L. Arnaud-Vanneau A. & Blanc É. (1992).- Basin type succession: Biostratigraphic tools, stratigraphic gaps and reworked sediments [excursion guide].- First day: Saturday May 9, International Symposium "Platform Margins", 6-8 May, Chichilianne, IAS & ASF, p. 25-40.

Bulot L.G., Thieuloy J.-P., Blanc É. & Klein J. (1993).- Le cadre stratigraphique du Valanginien supérieur et de l'Hauterivien du Sud-Est de la France : Définition des biochronozones et caractérisation de nouveaux biohorizons.- *Géologie Alpine*, Grenoble, vol. 68, p. 13-56.

Busnardo R., Thieuloy J.-P. & Moullade M. (1979).- Hypostratotype Mesogéen de l'étage Valanginien.- *Les stratotypes Francais*, vol. 6, Centre National de la Recherche Scientifique, Paris, 143 p.

Busnardo R., Clavel B., Charollais J. & Schroeder R. (1991).- Hauterivian-Barremian boundary at Mont Aiguille (Vercors, France): Biostratigraphy and sequence stratigraphy.- *Revue de Paléobiologie*, Genève, vol. 10, p. 359-364.

Caracuel J., Monaco P. & Olóriz F. (2000).- Taphonomic tools to evaluate sedimentation rates and stratigraphic completeness in Rosso Ammonitica facies (epioceanic Tethyan Jurassic).- *Rivista Italiana di Paleontologia e Stratigraphia*, Milano, vol. 106, p. 353-368. DOI: https://doi.org/10.13130/2039-4942/6150

Carney J.L. & Pierce R.W. (1995).- Graphic correlation and composite standard databases as tools for the exploration biostratigrapher. *In*: Mann K.O. & Lane H.R. (eds.), Graphic correlation.- *SEPM* (Society for Sedimentary Geology) *Special Publication*, Tulsa - OK, vol. 53, p. 23-43.

Casellato C.E. & Erba E. (2021).- Reliability of calcareous nannofossil events in the Tithonian-early Berriasian time interval: Implications for a revised high resolution zonation.- *Cretaceous Research*, vol. 117, article 104611, 30 p.

Cecca F. (1998).- Early Cretaceous (pre-Aptian) ammonites of the Mediterranean Tethys: Palaeoecology and palaeobiogeography.- *Palæogeography Palæoclimatology Palæoecology*, vol. 138, p. 305-323.

Celestino R., Wohlwend S., Rehakova D. & Weissert H. (2017).- Carbon isotope stratigraphy, biostratigraphy and sedimentology of the Upper Jurassic - Lower Cretaceous Rayda Formation, central Oman Mountains.- *Newsletters on Stratigraphy*, Stuttgart, vol. 50, p. 91-109.

Channell J.E.T., Cecca F. & Erba E. (1995).- Correlations of Hauterivian and Barremian (Early Cretaceous) stage boundaries to polarity chrons.- *Earth & Planetary Science Letters*, vol. 134, p. 125-140.

Channell J.E.T. & Erba E. (1992).- Early Cretaceous polarity chrons CM0 to CM11 recorded in northern Italian sections near Brescia.- *Earth Planetary Science Letters*, vol. 108, p. 161-179.

Clavel B., Busnardo R., Charollais J., Conrad M. & Granier B. (2010).- Répartition biostratigraphique des orbitolinidés dans la biozonation à ammonites (plate-forme urgonienne du Sud-Est de la France) Partie 1: Hauterivien supérieur-Barrémien basal.- *Carnets Geol.*, Madrid, vol. 10, no. A06 (CG2010_A06), 53 p. DOI: 10.4267/2042/33369

Coccioni R. & Premoli-Silva I. (1994).- Planktonic foraminifera from the Lower Cretaceous of Rio Argos sections (southern Spain) and biostratigraphic implications.- *Cretaceous Research*, vol. 15, p. 645-687.

Cohen K.M., Finney S.C., Gibbard P.L. & Fan J.-X. (2021).- The ICS International Chronostratigraphic Chart (originally published 2013, 2021).- *Episodes*, vol. 36, p. 199-204. URL: http://www.stratigraphy.org/ICSchart/ChronostratChart2021-05.pdf

Di Lucia M., Trecalli A., Mutti M. & Parente M. (2012).- Bio-chemostratigraphy of the Barremian-Aptian shallow-water carbonates of the southern Apennines (Italy): Pinpointing the OAE1a in a Tethyan carbonate platform.- *Solid Earth*, vol. 3, p. 1-28.

Edgell H.S. (1971).- Calpionellid stratigraphy and the Jurassic-Cretaceous boundary in southeast Iran. *In*: Colloque de Jurassique, Luxembourg 1967.- *Mémoires du B.R.G.M.,* Orléans, no. 75, p. 213-247.

Énay R. (2020).- The Jurassic/Cretaceous System Boundary is at an impasse. Why not go back to Oppel's 1865 original and historic definition of the Tithonian?.- *Cretaceous Research*, vol. 106, article 104241, 20 p.

Erba E. & Quadrio B. (1987).- Biostratigrafia a nannofossili calcarei calpionellidi e foraminiferi planctonici della Maiolica (Titoniano superiore-Aptiano) nelle Prealpi bresciane (Italia settentrionale).- *Rivista Italiana di Paleontologia e Stratigrafia*, Milano, vol. 93, no. 1, p. 3-108. URL: https://riviste.unimi.it/index.php/RIPS/article/view/13228

Frau C., Bulot L.G., Reháková D., Wimbledon W.A.P. & Ifrim C. (2016).- Revision of the ammonite index species *Berriasella jacobi* Mazenot, 1939 and its consequences for the biostratigraphy of the Berriasian Stage.- *Cretaceous Research*, vol. 66, p. 94-114.

Frau C., Bulot L.G. & Wimbledon W.A.P. (2015).- Upper Tithonian Himalayitidae Spath, 1925 (Perisphinctoidea, Ammonitina) from Le Chouet (Drôme, France): Implications for the systematics.- *Geologica Carpathica*, Bratislava, vol. 66, p. 117-132.

Frau C., Bulot L.,Wimbledon W.A.P. & Ifrim C. (2016).-Systematic palaeontology of the Perisphinctoidea in the Jurassic/Cretaceous boundary interval at Le Chouet (Drôme, France), and its implications for biostratigraphy.- *Acta Geologica Polonica*, Warsaw, vol. 66, p. 175-204.

Gale A.S., Mutterlose J., Battenberg S., Gradstein F.M., Agterberg F.P., Ogg J.G. & Petrizzo M.R. (2020).- Chapter 27. The Cretaceous Period. *In*: Gradstein F.M., Ogg J.G., Schmitz M.D. & Ogg G.M. (eds.), Geologic Time Scale 2020.- Elsevier, Amsterdam, vol. 2, p. 1023-1086.

Galbrun B., Rasplus L. & Le Hégarat G. (1986).- Données nouvelles sur le stratotype du Berriasien : Corrélations entre magnétostratigraphie et biostratigraphie.- *Bulletin de la Société géologique de France*, Paris, vol. 4, p. 575-584.

Garrido A.C. & Parent H. (2017).- Lithofacies and age of the Quintuco Formation (Lower Cretaceous) in the Mallín Quemado area (Sierra de la Vaca Muerta, Neuquén Basin, Argentina). Stratigraphic and depositional implications.- *Boletín del Instituto de Fisiografía y Geología*, Rosario, vol. 87, p. 1-16.

Grabowski J. (2011).- Magnetostratigraphy of the Jurassic/Cretaceous boundary interval in the Western Tethys and its correlations with other regions: A review.- *Volumina Jurassica*, Warsaw, vol. IX, p. 105-128.

Grabowski J., Lodowski D.G., Schnyder J., Sobień K., Chadimova L., Pszczólkowski A., Krzemiński L. & Schnabl P. (2018).- 17. Magnetic stratigraphy, stable isotopes and chemostratigraphy in the upper Berriasian of Rówienka section (Western Tatra Mts., Fatric succession, Poland): Towards a consistent model of late Berriasian paleoenvironmental changes in the Western Tethys.- JK2018 (December 5-7, 2018), Muséum d'Histoire naturelle de Genève, p. 30-33.

Grabowski J. & Pszczólkowski A. (2006).- Magneto- and biostratigraphy of the Tithonian-Berriasian pelagic sediments in the Tatra Mountains (central Western Carpathians, Poland): Sedimentary and rock magnetic changes at the Jurassic/Cretaceous boundary.- *Cretaceous Research*, vol. 27, p. 398-417.

Gradstein F.M., Ogg J.G., Smith A.G., Bleeker W. & Lourens L.J. (2004).- A new Geologic Time Scale with special reference to Precambrian and Neogene.- *Episodes*, Bangalore, vol. 27, p. 83-100.

Granier B., Énay R. & Charollais J. (2020).- Discussion of the paper by Wimbledon *et al.*, 2020b, entitled "The proposal of a GSSP for the Berriasian Stage (Cretaceous System): Part 1" [Volumina Jurassica, XVIII (1)].- *Volumina Jurassica*, Warsaw, vol. XVIII, no. 2, p. 111-124. URL: https://vjs.pgi.gov.pl/article/view/28578/20272

Haq B.U. (2014).- Cretaceous eustasy revisited.- *Global and Planetary Change*, vol. 113, p. 44-58.

Hesselbo S.P., Ogg J.G. & Ruhl M. (2020).- The Jurassic Period, Chap. 26. *In*: Gradstein F.M, Ogg J.G., Schmitz M.D. & Ogg G.M. (eds.), Geologic Time Scale 2020.- Elsevier, Amsterdam, vol. 2, p. 955-1022.

Hinte J.E. van (1976).- A Cretaceous time scale.- *American Association of Petroleum Geologists Bulletin*, vol. 60, p. 269-287.

Hoedemaeker P. (2013).- Genus *Pseudothurmannia* Spath, 1923 and related subgenera *Crioceratites* (*Balearites*) Sarkar, 1954 and C. (*Binelliceras*) Sarkar, 1977 (Lower Cretaceous

Ammonoidea).- *Revue de Paléobiologie*, Genève, vol. 32, no. 1, p. 1-209.

HOEDEMAEKER P., JANSSEN N., CASELLATO C., GARDIN S., REHÁKOVÁ D. & JAMRICHOVÁ M. (2016).- Jurassic/Cretaceous boundary in the Río Argos succession (Caravaca, SE Spain).- *Revue de Paléobiologie*, Genève, vol. 35, p. 111-247.

HOEDEMAEKER P.J. & LEEREVELD H. (1995).- Biostratigraphy and sequence stratigraphy of the Berriasian-lowest Aptian (Lower Cretaceous) of the Rio Argos succession.- *Cretaceous Research*, vol. 16, p. 195-230.

HOOD K.C. (1995).- Evaluating the use of average composite sections and derived correlations in the graphic correlation technique. *In*: MANN K.O. & LANE H.R. (eds.), Graphic correlation.- *SEPM* (Society for Sedimentary Geology) *Special Publication*, Tulsa - OK, vol. 53, p. 83-93.

HORTON B.K., FUENTES F., BOLL A., STARCK D. RAMIREZ S.G. & STOCKLI D.F. (2016).- Andean stratigraphic record of the transition from backarc extension to orogenic shortening: A case study from the northern Neuquén Basin, Argentina.- *Journal of South American Earth Sciences*, vol. 71, p. 17-40.

HOUSA V., KRSA M., MANA O., PRUNERA P., VENHODOVA D., CECCA F., NARDIC G. & PISCITELLO M. (2004).- Combined magnetostratigraphic, palaeomagnetic and calpionellid investigations across Jurassic/Cretaceous boundary strata in the Bosso Valley, Umbria, central Italy.- *Cretaceous Research*, vol. 25, p. 771-785.

HUANG C. (2018).- Chapter 2. Astronomical Time Scale for the Mesozoic.- *Stratigraphy & Timescales*, vol. 3, p. 81-150.

ICE R.G. & MCNULTY CL. (1980).- Foraminifers and calcispheres from the Cuesta del Cura and lower Agua Nueva(?) formations (Cretaceous) in east-central Mexico.- *Association of Geological Societies*, *Transactions*, Lafayette - LA, vol. 30, p. 403-425.

IGLESIA LLANOS M.P. & KIETZMANN D.A. (2020).- Magnetostratigraphy of the Jurassic through Lower Cretaceous in the Neuquén Basin. *In*: KIETZMANN D.A. & FOLGUERA A. (eds.), Opening and Closure of the Neuquén Basin in the Southern Andes.- Springer Earth System Sciences, New York - NY, p. 175-210.

IGLESIA LLANOS M.P., KIETZMANN D.A., MARTINEZ M.K. & PALMA R.M. (2017).- Magnetostratigraphy of the Upper Jurassic-Lower Cretaceous from Argentina: Implications for the J-K boundary in the Neuquén Basin.- *Cretaceous Research*, vol. 70, p. 189-208.

IVANOVA D.K. & KIETZMANN D.A. (2017).- Calcareous dinoflagellate cysts from the Tithonian-Valanginian Vaca Muerta Formation in the southern Mendoza area of the Neuquén Basin, Argentina.- *Journal of South American Earth Sciences*, vol. 77, p. 150-169.

KEDZIERSKI M. & OCHABSKA A. (2012).- Calcareous nannofossil biostratigraphy and sedimentary environment of Valanginian-Hauterivian rhythmites (Silesian Nappe, Polish Carpathians).- *Annales Societatis Geologorum Poloniae*, Kraków, vol. 82, p. 225-237.

KENJO S., REBOULET S., MATTIOLI E. & MA'LOULEH K. (2021).- The Berriasian-Valanginian boundary in the Mediterranean Province of the Tethyan Realm: Ammonite and calcareous nannofossil biostratigraphy of the Vergol section (Montbrun-les-Bains, SE France), candidate for the Valanginian GSSP.- *Cretaceous Research*, vol. 121, article 104738.

KIETZMANN D.A. (2017).- Chitinoidellids from the Early Tithonian-Early Valanginian Vaca Muerta Formation in the northern Neuquén basin, Argentina.- *Journal of South American Earth Science*, vol. 76, p. 152-164.

KIETZMANN D.A., AMBROSIO A.L., SURIANO J., ALONSO M.S., GONZÁLEZ TOMASSINI F., DEPINE G. & REPOL D. (2016).- The Vaca Muerta-Quintuco system (Tithonian-Valanginian) in the Neuquén Basin, Argentina: A view from the outcrops in the Chos Malal fold and thrust belt.- *American Association of Petroleum Geologists Bulletin*, Tulsa - OK, vol. 100, p. 743-771. DOI: 10.1306/02101615121

KIETZMANN D.A., IGLESIA LLANOS M.P. & KOHAN MARTÍNEZ M. (2018).- Ch. 8, Astronomical calibration of the Tithonian-Berriasian in the Neuquén Basin, Argentina: Contribution from the Southern Hemisphere to the Geological Time Scale.- *Stratigraphy & Timescales*, vol. 3, p. 327-351.

KIETZMANN D.A., IGLESIA LLANOS M.P. & KOHAN MARTÍNEZ M. (2020).- Orbital Controls and high-resolution cyclostratigraphy of Late Jurassic-Early Cretaceous in the Neuquén Basin. *In*: KIETZMANN D.A. & FOLGUERA A. (eds.), Opening and closure of the Neuquén Basin in the Southern Andes.- Springer Earth System Sciences, New York, p. 211-235.

KIETZMANN D.A., IGLESIA LLANOS M.P., PALACIO J.P. & STURLESI M.A. (2021a).- Facies analysis and stratigraphy across the Jurassic-Cretaceous boundary in a new basinal Tithonian-Berriasian section of the Vaca Muerta Formation, Las Tapaderas, Southern Mendoza Andes, Argentina.- *Journal of South American Earth Sciences*, vol. 109, article 103267, 22 p.

KIETZMANN D.A., IGLESIA LLANOS M.P., GONZÁLEZ TOMASSINI F., LANUSSE NOGUERA I., VALLEJO D. & REIJENSTEIN H. (2021b).- Upper Jurassic-Lower Cretaceous calpionellid zones in the Neuquén Basin (Southern Andes, Argentina): Correlation with ammonite zones and biostratigraphic synthesis.- *Cretaceous Research*, vol. 127, article 104950, 28 p.

KIETZMANN D.A., MARTÍN-CHIVELET J., PALMA R.M., LÓPEZ-GÓMEZ J., LESCANO M. & CONCHEYRO A. (2011).- Evidence of precessional and eccentricity orbital cycles in a Tithonian source rock: The mid-outer carbonate ramp of the Vaca Muerta Formation, Northern Neuquén Basin, Argentina.- *American Association of Petroleum Geologists Bulletin*, Tulsa - OK, vol. 95, p. 1459-1474.

KIETZMANN D.A., PALMA R.M. & IGLESIA LLANOS M.P. (2015).- Cyclostratigraphy of an orbitally-driven Tithonian-Valanginian carbonate ramp succession, Southern Mendoza, Argentina: Implications for the Jurassic-Cretaceous boundary in the Neuquén Basin.- *Sedimentary Geology*, vol. 315, p. 29-346.

KIETZMANN D. & PAULIN S. (2019).- Cyclostratigraphy of an upper Valanginian - lower Hauterivian mixed siliciclastic-carbonate ramp succession (Pilmatué Member of the Agrio Formation), Loma La Torre Section, Northern Neuquén Basin, Argentina.- *Cretaceous Research*, vol. 98, p. 26-46.

KOHAN MARTÍNEZ M., AGUIRRE-URRETA B.M., MARINA L., JULIETA O., MAISA T. THOMAS F., ANNA-LEAH N. & HEIKO P. (2017).- Radio-astrochronology of the Agrio Formation (Neuquén Basin, Argentina) to reduce the uncertainties of the geological time scale in Early Cretaceous times.- *Geophysical Research Abstracts*, vol. 19, article EGU2017-12075, 1 p. (abstract).

KOHAN MARTÍNEZ M., KIETZMANN D.A. & IGLESIA LLANOS M.P. (2018).- Magnetostratigraphy and cyclostratigraphy of the Tithonian interval from the Vaca Muerta Formation, southern Neuquén Basin, Argentina.- *Journal of South American Earth Science*, vol. 85, p. 209-228.

LAKOVA I. & PETROVA S. (2013).- Towards a standard Tithonian to Valanginian calpionellid zonation of the Tethyan Realm. *Acta Geologica Polonica*, Warsaw, vol. 63, p. 201-221.

LAKOVA I., STOYKOVA K. & IVANOVA D. (1997).- Tithonian to Valanginian bioevents and integrated zonation on calpionellids, calcareous nannofossils and calcareous dinocycts from the Western the Western Balkanides, Bulgaria.- *Mineralia Slovaca*, Dionýz Štúr, vol. 29, p. 301-303.

LAZO D.G., CONCHEYRO A., OTTONE G., GULER M.V. & AGUIRRE-URRETA B. (2009). Bioestratigrapfía integrada de la Formación Agrio en su localidad tipo, Cretácico temprano de Cuenca Neuquina.- *Revista de la Asociación Geológica Argentina*, Buenos Aires, vol. 65, p. 322-341.

LEANZA H.A., SATTLER F., MARTINEZ R.S. & CARBONE O. (2011).- La Formación Vaca Muerta y equivalentes (Jurásico Tardío-Cretácico Temprano) en la Cuenca Neuquina.- Relatorio del XVIII Congreso Geológico Argentino, Neuquén, 2011, p. 113-129.

LE HÉGARAT G. (1973).- Le Berriasien du Sud-Est de la France.- *Documents des Laboratoires de Géologie de la Faculté des Sciences de Lyon*, Villeurbanne, no. 43, 575 p.

LE HÉGARAT G. & REMANE J. (1968).- Tithonique supérieur et Berriasien de l'Ardèche et de l'Hérault. Corrélation des ammonites et des calpionelles.- *Geobios*, Villeurbanne, vol. 1, no. 1, p. 7-70.

LEHMANN J., IFRIM C., BULOT L. & FRAU C. (2015).- Paleobiogeography of Early Cretaceous Ammonoids. *In*: KLUG C., KORN D., DE BAETS K., KRUTA I. & MAPES R.H. (eds.), Ammonoid paleobiology: From macroevolution to paleogeography.- *Topics in Geobiology*, Dordrecht, vol. 44, p. 229-257.

LENA L., LÓPEZ-MARTÍNEZ R., LESCANO M., AGUIRRE-URRETA B., CONCHEYRO A., VENNARI V., NAIPAUER M., SAMANKASSOU E., PIMENTEL M., RAMOS V. & SCHALTEGGER U. (2019a).- High precision U-Pb ages in the early Tithonian to early Berriasian and implications for the numerical age of the Jurassic/Cretaceous boundary.- *Solid Earth*, vol. 10, p. 1-14. DOI: 10.5194/se-10-1-2019

LIU Yong-Qing, JI Qiang, JIANG Xiao-Jun, KUANG Hong-Wei, JI Shu'an, GAO Lian-Feng, ZHANG Zhen-Guo, PENG Nan Yuan, CHONG-XI Wang, XU Ri & XU Huan (2013).- U-Pb Zircon Ages of Early Cretaceous Volcanic Rocks in the Tethyan Himalaya at Yangzuoyong Co Lake, Nagarze, Southern Tibet, and Implications for the Jurassic/Cretaceous Boundary.- *Cretaceous Research*, vol. 40, p. 90-101.

LÓPEZ-MARTÍNEZ R., AGUIRRE-URRETA B., LESCANO M., CONCHEYRO A., VENNARI V. & RAMOS V.A. (2017a).- Tethyan calpionellids in the Neuquén Basin (Argentine Andes), their significance in defining the Jurassic/Cretaceous boundary and pathways for Tethyan-Eastern Pacific connections.- *Journal of South American Earth Sciences*, vol. 78, p. 116-125.

LÓPEZ-MARTÍNEZ R., BARRAGÁN R., BERNAL J.P., REHÁKOVÁ D., GÓMEZ-TUENA A., MARTINI M. & ORTEGA C. (2017b).- Integrated stratigraphy and isotopic ages at the Berriasian-Valanginian boundary at Tlatlauquitepec (Puebla, Mexico).- *Journal of South American Earth Sciences*, vol. 85, p. 209-228.

LÓPEZ-MARTÍNEZ R., BARRAGÁN R., REHÁKOVA D. & COBIELLA-REGUERA J.L. (2013).- Calpionellid distribution and microfacies across the Jurassic/Cretaceous boundary in western Cuba (Sierra de los Órganos).- *Geologica Carpathica*, Bratislava, vol. 64, p. 195-208.

LÓPEZ-MARTÍNEZ R., BARRAGÁN R., REHÁKOVÁ D., MARTINI M. & EGUILUZ DE ANTUÑANO S. (2015).- Calpionellid biostratigraphy, U-Pb geochronology and microfacies of the Upper Jurassic-Lower Cretaceous Pimienta Formation (Tamazunchale, San Luis Potosí, central-eastern Mexico).- *Boletín de la Sociedad Geológica Mexicana*, Mexico City - D.C., vol. 67, p. 75-86.

LOWRIE W. & CHANNELL J.E.T. (1984).- Magnetostratigraphy of the Jurassic-Cretaceous boundary in the Maiolica limestone (Umbria, Italy).- *Geology,* Boulder - CO, vol. 12, p. 44-47.

LUKENENDER A., HALÁSOVA E., KROH A., MAYRHOFER S., PRUNER D., REHÁKOVA D., SCHNABL P., SPROVIERI M. & WAGREICH M. (2010).- High resolution stratigraphy of the Jurassic-Cretaceous boundary interval in the Gresten Klippenbelt (Austria).- *Geologica Carpathica*, Bratislava, vol. 61, p. 365-381.

MAALOUI K. & ZARGOUNI F. (2016).- The lower and middle Berriasian in Central Tunisia: Integrated ammonite and calpionellid biostratigraphy of the Sidi Kralif Formation.- *Acta Geologica Polonica*, Warsaw, vol. 66, p. 43-58.

Maaloui K. & Zargouni F. (2017).- Biostratigraphical study around the Jurassic/Cretaceous boundary in Central Tunisia zonal schemes and correlation.- *Journal of African Earth Sciences*, vol. 125, p. 166-176.

Martinez M., Aguirre-Urreta B.M., Marina L., Julieta O., Maisa T., Thomas F., Anna-Leah N. & Heiko P. (2017).- Radio-astrochronology of the Agrio Formation (Neuquén Basin, Argentina) to reduce the uncertainties of the geological time scale in Early Cretaceous times.- *Geophysical Research Abstracts*, vol. 19, article EGU2017-12075, 1 p. (abstract).

Martinez M., Deconinck J.-F., Pellenard P., Reboulet S. & Riquier L. (2013).- Astrochronology of the Valanginian Stage from reference sections (Vocontian Basin, France) and palaeoenvironmental implications for the Weissert Event.- *Palæogeography Palæoclimatology Palæoecology*, vol. 376, p. 91-102.

Martinez M., Deconinck J-F., Pellenard P., Riquier L., Company M., Reboulet S. & Moiroud M. (2015).- Astrochronology of the Valanginian-Hauterivian stages (Early Cretaceous): Chronological relationships between the Paraná-Etendeka large igneous province and the Weissert and the Faraoni events.- *Global and Planetary Change*, vol. 131, p. 158-17.

Martinez M., Pellenard P., Deconinck J.-F., Monna F., Riquier L., Boulila S., Moiroud M. & Company M. (2012).- An orbital floating time scale of the Hauterivian/Barremian GSSP from a magnetic susceptibility signal (Río Argos, Spain).- *Cretaceous Research*, vol. 36, p. 106-115.

Masure E. (1988).- 25. Berriasian to Aptian dinoflagellate cysts from the Galicia margin, Offshore Spain, Sites 638 and 639, ODP Leg 103.- *Proceedings of the Ocean Drilling Program, Scientific Results*, College Station - TX, vol. 103, p. 433-438.

Mutterlose J., Rawson P.F., Reboulet S., Baudin F, Bulot L., Emmanuel L., Gardin S., Martinez M. & Renard M. (2020).- The Global Boundary Stratotype Section and Point (GSSP) for the base of the Hauterivian Stage (Lower Cretaceous), La Charce, southeast France.- *Episodes*, Beijing, vol. 44, p. 129-150. DOI: 10.18814/epiiugs/2020/020072

Naipauer M., García Morabito E., Marques J.C., Tunik V., Rojas Vera E., Vujovich G.I., Pimentel M.P. & Ramos V.A. (2012).- Intraplate Late Jurassic deformation and exhumation in western central Argentina: Constraints from surface data and U-Pb detrital zircon ages.- *Tectonophysics*, vol. 524-525, p. 59-75.

Naipauer M., Lescano M., Zavala C., Aguirre-Urreta B., Pimente M.M. & Ramos V.A. (2015a).- Estudio multidisciplinario en la Formación Vaca Muerta: Ambiente de sedimentación, bioestratigrafía, edades U-Pb en circones y áreas de proveniencia del Miembro Huncal.- XIV Congresso Geológica Chilean, La Serena, Resumenes Expandidos Electrónicos, p. 1-4.

Naipauer M., Tapi F., Mescu J., Faria M., Pimente M.M. & Ramos V.A. (2015b).- Detrital and volcanic zircon U-Pb ages from southern Mendoza (Argentina): An insight on the source regions in the northern part of the Neuquén Basin.- *Journal of South American Earth Sciences*, vol. 64, p. 434-451.

Naipauer M., Tunik M., Marques J.C., Rojas-Vera E.A., Vujovich G.I., Pimentel M.M. & Ramos V.A. (2015c).- U-Pb detrital zircon ages of Upper Jurassic continental successions: Implications for the provenance and absolute age of the Jurassic-Cretaceous boundary in the Neuquén Basin. *In*: Sepúlveda S.A., Giambiagi L.B., Moreiras S.M., Pinto L., Tunik M., Hoke G.D. & Farías M. (eds.), Geodynamic Processes in the Andes of central Chile and Argentina.- *Geological Society, London*, *Special Publications*, vol. 399, p. 131-154.

Ogg J.G., Agterberg F.P. & Gradstein F.M. (2004).- The Cretaceous Period. *In*: Gradstein F.M., Ogg J.G. & Smith A.G. (eds.), A Geologic Time Scale, 2004.- Cambridge University Press, Cambridge - MA, p. 344-383.

Ogg J.G., Hinnov L.A. & Huang C. (2012).- Cretaceous. *In*: Gradstein F.M, Ogg J.G., Schmitz M.D.& Ogg G.M. (eds.), The Geologic Time Scale 2012.- Elsevier, Amsterdam, p. 793-853.

Ogg J.G., Ogg G.M. & Gradstein F.M. (2016).- A Concise Geologic Time Scale 2016.- Elsevier, Amsterdam, 234 p.

Olóriz F., Villaseñor A.B., Gonzalez-Arreola C. & Westermann G.E.G. (1999).- Ammonite biostratigraphy and correlations in the Upper Jurassic-lowermost Cretaceous La Caja Formation of North-Central Mexico (Sierra de Catorce, San Luis Potosí). *In*: Olóriz F. & Rodríguez-Tovar F.J. (eds.), Advancing research on living and fossil Cephalopods.- Kluwer/Plenum, New York, p. 463-491.

Parent H., Garrido A.C., Scherzinger A., Schweigert G. & Főzy I. (2015).- The Tithonian-Lower Valanginian stratigraphy and ammonite fauna of the Vaca Muerta Formation in Pampa Tril, Neuquén Basin, Argentina.- *Boletín del Instituto de Fisiografía y Geología*, Rosario, vol. 86, p. 1-96.

Parent H., Scherzinger A. & Schweigert G. (2011).- The Tithonian-Berriasian ammonite fauna and stratigraphy of Arroyo Cieneguita, Neuquén-Mendoza Basin, Argentina.- *Boletín del Instituto de Fisiografía y Geología*, Rosario, vol. 79-81, p. 21-94

Parent H., Scherzinger A., Schweigert G. & Garrido A.C. (2017).- Additional Tithonian and Berriasian ammonites from the Vaca Muerta Formation in Pampa Tril, Neuquén Basin, Argentina.- *Volumina Jurassica*, Varsaw, vol. XV, p. 139-154.

Petrova S., Koleva-Rekalova E., Ivanova D. & Lakova I. (2019).- Biostratigraphy and microfacies of the pelagic carbonate formations in

the Yavorets section (Tithonian-Berriasian), Western Balkan Mts, Bulgaria.- *Geologica Balcanica*, Sofia, vol. 48, p. 51-73.
PRUNER P., HOUŠA V.F., OLORIZ F., KOŠAK M.M., KRS M., MAN O., SCHNABL P., VENHODOVÁ D., TAVERA J.M. & MAZUCH M. (2010).- High-resolution magnetostratigraphy and biostratigraphic zonation of the Jurassic/Cretaceous boundary strata in the Puerto Escaño section (southern Spain).- *Cretaceous Research*, vol. 31, p. 192-206.
PSZCZÓLKOWSKI A. & MYCZYNSKI R. (2010).- Tithonian-Early Valanginian evolution of deposition along the proto-Caribbean margin of North America recorded in Guaniguanico successions (western Cuba).- *Journal of South American Earth Science*, vol. 29, p. 225-253.
RAWSON P.F. (2007).- Global relationships of Argentine (Neuquén Basin) Early Cretaceous ammonite faunas.- *Geological Journal*, vol. 42, p. 175-183.
RAWSON P.F., CONCHEYRO A., BUHLER M. & RAMOS V.A. (2017). A high precision U-Pb radioisotopic age for the Agrio Formation, Neuquén Basin, Argentina: Implications for the chronology of the Hauterivian Stage.- *Cretaceous Research*, vol. 75, p. 193-204.
REBOULET S. (2008).- The Global Boundary Stratotype Sections and Points (GSSP) of the Hauterivian: La Charce section (Drôme, France, Vocontian basin). *In*: MATTIOLI E., GARDIN S., GIRAUD F., OLIVERO F., PITTET B. & REBOULET S. (Eds.), Guidebook for the post-congress fieldtrip in the Vocontian Basin, SE France (September 11-13 2008).- Carnets de Géologie, Madrid, Book 2008/01 (CG2008_B01), p. 7-10. DOI: 10.4267/2042/18137
REBOULET S. & ATROPS F. (1999).- Comments and proposals about the Valanginian-Lower Hauterivian ammonite zonation of south-eastern France.- *Eclogae Geologicae Helvetiae*, Basel, vol. 92, no. 2, p. 183-198.
REBOULET S., SZIVES O., AGUIRRE-URRETA B., BARRAGÁN R., COMPANY M., FRAU C., KAKABADZE M.V., KLEIN J., MORENO-BEDMAR J.A., LUKENEDER A., PICTET A., PLOCH I., RAISOSSADAT S.N., VAŠÍČEK Z., BARABOSHKIN E.J. & MITTA V.V. (2018).- Report on the 6th International Meeting of the IUGS Lower Cretaceous Ammonite Working Group, the Kilian Group (Vienna, Austria, 20th August 2017).- *Cretaceous Research*, vol. 91, p. 100-110.
REHAKOVA D., HALÁSOVA E. & LUKENEDER A. (2009).- The Jurassic-Cretaceous boundary in the Gresten Klippenbelt (Nutzhof, Lower Austria): Implications for micro- and nannofacies analysis.- *Annalen des Naturhistorischen Museums in Wien*, vol. 110A, p. 345-381.
REMANE J., FAURE-MURET A., ODIN G.S., CITA M.B., DERCOURT J., BOUYSSE P. & REPETTO F. (2002).- International stratigraphic chart.- International Commission on Stratigraphy, International Union of Geological Sciences, Paris, 1 chart.
RICCARDI A.C. (1988).- The Cretaceous system of southern South America. *In*: KLUG C., KORN D., DE BAETS K., KRUTA I. & MAPES R.H. (eds.), Ammonoid paleobiology: From macroevolution to paleogeography.- *Geological Society of America*, *Memoir*, Boulder - CO, vol. 186, p. 116-143.
RICCARDI A.C. (2015).- Remarks on the Tithonian-Berriasian ammonite biostratigraphy of west central Argentina.- *Volumina Jurassica*, Varsaw, vol. XIII, no. 2, p. 23-52.
SALAZAR SOTO C.A. (unpublished, 2012).- The Jurassic-Cretaceous boundary (Tithonian-Hauterivian) in the Andean Basin of central Chile: Ammonites, bio- and sequence stratigraphy and palaeobiogeography.- Unpublished Dissertation, Rupecht-Karls-Universität, Heidelberg, 388 p.
SALAZAR C. & STINNESBECK W. (2015).- Redefinition, stratigraphy and facies of the Lo Valdes Formation (Upper Jurassic-Lower Cretaceous) in central Chile.- *Boletín del Museo Nacional de Historia Natural*, Santiago, vol. 64, p. 41-68.
SALAZAR C. & STINNESBECK W. (2016).- Tithonian-Berriasian ammonites from the Baños del Flaco Formation, central Chile.- *Journal of Systematic Palaeontology*, vol. 14, no. 2, p. 149-182.
SALAZAR C., STINNESBECK W. & ÁLVAREZ M. (2020).- Ammonite biostratigraphy and bioevents in the Jurassic - Cretaceous boundary of central Chile.- *Cretaceous Research*, vol. 107, article 104282, 18 p.
SCHWARZ E., ÁLVAREZ-TRENTINI G. & VALENZUEL M.E. (2013).- Ciclos mixtos carbonáticos/silicoclásticos en el Miembro Superior de la Formación Mulichinco (Yacimiento Cañadón Amarillo, Cuenca Neuquina Central, Argentina): Implicancias secuenciales y para caracterización de reservorios.- *Latin American Journal of Sedimentology and Basin Analysis*, Buenos Aires, vol. 20, p. 21-49.
SCHWARZ E., SPALLETTI L.A. & HOWELL J.A. (2006).- Sedimentary response to a tectonically induced sea-level fall in a shallow back-arc basin: The Mulichinco Formation (Lower Cretaceous), Neuquén Basin, Argentina.- *Sedimentology*, vol. 53, p. 55-81.
SCHWARZ E., SPALLETTI L.A., VEIGA G.D. & FANNING C.M. (2016).- First U-Pb SHRIMP age for the Pilmatué Member (Agrio Formation) of the Neuquén Basin, Argentina: Implications for the Hauterivian lower boundary Hauterivian lower boundary.- *Cretaceous Research*, vol. 58, p. 223-233.
SCOTT R.W. (1990).- Models and stratigraphy of Mid-Cretaceous reef communities, Gulf of Mexico.- *SEPM (Society for Sedimentary Geology), Concepts in Sedimentology and Paleontology*, Tulsa - OK, vol. 2, 102 p.
SCOTT R.W. (2014).- Cretaceous chronostratigraphic database: Construction and applications.- *Carnets Geol.*, Madrid, vol. 14, no. 2, p. 1-13. DOI: 10.4267/2042/53522

Scott R.W. (2019a).- Jurassic-Cretaceous boundary bioevents and magnetochrons: A stratigraphic experiment.- *Cretaceous Research*, vol. 100, p. 97-104.

Scott R.W. (2019b).- Valanginian Knowles Limestone, East Texas, A potential reservoir.- *Gulf Coast Association of Geological Societies*, Houston - TX, vol. 8, p. 79-88.

Selby D., Mutterlose J. & Condon D.J. (2009).- U-Pb and Re-Os geochronology of the Aptian/Albian and Cenomanian/Turonian stage boundaries: Implications for timescale calibration, osmium isotope seawater composition and Re-Os systematics in organic-rich sediments.- *Chemical Geology*, vol. 265, p. 394-409.

Sheridan R.E. & Gradstein F.M. (1983).- Site 534: Blake-Bahama Basin (Shipboard Scientific Party).- *Initial Reports of the Deep Sea Drilling Project*, College Station - TX, vol. 76, p. 141-340. DOI: 10.2973/dsdp.proc.76.101.1983

Simmons M.D. & Hart M.B. (1987).- The biostratigraphy and microfacies of the Early to mid-Cretaceous carbonates of Wadi Mi'aidin, Central Oman Mountains. *In*: Hart M.B. (ed.), Micropalaeontology of carbonate environments.- Ellis Horwood, Totnes, p. 176-207.

Skupien P. & Doupovcová P. (2019).- Dinoflagellates and calpionellids of the Jurassic-Cretaceous boundary, Outer Western Carpathians (Czech Republic).- *Cretaceous Research*, vol. 99, p. 209-228.

Speranza F., Satolli S., Mattioli E. & Calamita F. (2005).- Magnetic stratigraphy of Kimmeridgian-Aptian sections from Umbria-Marche (Italy): New details on the M polarity sequence.- *Journal of Geophysical Research*, vol. 110, B12109. DOI: https://agupubs.onlinelibrary.wiley.com/doi/epdf/10.1029/2005JB003884.

Szives O. & Főzy I. (2022).- Towards the ammonite zonation of the Jurassic/Cretaceous transition: New data from ammonitico rosso/biancone sections of the Transdanubian Range (Hungary).- *Newsletters on Stratigraphy*, Stuttgart, 42 p. DOI: 10.1127/nos/2022/0679

Vennari V.V., Lescano M., Naipauer M., Aguirre-Urreta B., Concheyro A., Schalteggerb U., Armstrong R., Pimentel M. & Ramos V.A. (2014).- New constraints on the Jurassic-Cretaceous boundary in the High Andes using high-precision U-Pb data.- *Gondwana Research*, vol. 26, p. 374-385.

Vennari V.V. (2016).- Tithonian ammonoids (Cephalopoda, Ammonoidea) from the Vaca Muerta Formation, Neuquén Basin, West-Central Argentina.- *Palaeontographica Abteilung A*, Stuttgart, Band 306, Lieferung 1-6, p. 85-165.

Vennari V.V. & Pujana I. (2017).- Finding of two new radiolarian associations calibrated with ammonoids in the Vaca Muerta Formation (Late Jurassic-Early Cretaceous), Neuquén Basin, Argentina.- *Journal of South American Earth Sciences*, vol. 75, p. 35-50.

Walker J.D., Geissman J.W., Bowring S.A. & Babcock L.E., (compilers, 2018).- Geologic Time Scale v. 5.0.- Geological Society of America, Boulder - CO. URL: https://www.geosociety.org/documents/gsa/timescale/timescl.pdf

Wan Xiaoqiao, Scott R.W., Chen Wen, Gao Lianfeng & Zhang Yiyi (2011a).- Early Cretaceous stratigraphy and SHRIMP U-Pb age constrain the Valanginian-Hauterivian Boundary in Southern Tibet.- *Lethaia*, Oslo, vol. 43, p. 231-244. DOI: 10.1111/j.1502-3931.2010.00238.x.

Wan X., Scott R., Chen W., Gao L. & Yiyi Z. (2011b).- Early Cretaceous stratigraphy and SHRIMP U-Pb age constrain the Valanginian-Hauterivian Boundary in Southern Tibet.- *Lethaia*, Oslo, vol. 44, p. 231-244.

Westermann G.E.G. (2000).- Biochore classification and nomenclature in paleobiogeography: An attempt at order.- *Palæogeography Palæoclimatology Palæoecology*, vol. 158, p. 1-13.

Wimbledon W.A.P., Reháková D., Pszczółkowski A., Cassellato C.E., Halásová E., Frau C., Bulot L.G., Grabowski J., Sobień K., Pruner Schnabl P. & Čížková K. (2013).- A preliminary account of the bio- and magnetostratigraphy of the upper Tithonian-lower Berriasian interval at Le Chouet, Drôme (SE France).- *Geologica Carpathica*, Bratislava, vol. 64, p. 437-460.

Wimbledon W.A.P. (2017).- Developments with fixing a Tithonian/Berriasian (J/K) boundary.- *Volumina Jurassica*, Warsaw, vol. XV, p. 181-186.

Wimbledon W.A.P., Reháková D.A., Svobodová A., Schnabl P., Pruner P., Elbra T., Šifnerová K., Kdýr š., Frau C., Schnyder J. & Galbrun B. (2020).- Fixing a J/K boundary: A comparative account of key Tithonian-Berriasian profiles in the departments of Drôme and Hautes-Alpes, France.- *Geologica Carpathica*, Bratislava, vol. 71, p. 24-46.

Wippich M.G.E. (2003).- Valanginian (Early Cretaceous) ammonite faunas from the western High Atlas, Morocco, and the recognition of western Mediterranean 'standard' zones.- *Cretaceous Research*, vol. 24, p. 357-374.

Appendices

Appendix 1: List of sections and sources of biostratigraphic and lithostratigraphic data in LOK2016DB. Catalog numbers are used by GraphCor software.

Catalog #-Name:	Reference
CRET.16 Standard Reference Section-2016 Geologic Time Scale:	OGG *et al.*, 2012, Figs. 13.4, 27.6, Table 27.2-3, Appendix 2
LOK.1 DSDP 534 Blake Plateau:	SHERIDAN *et al.*, 1983
LOK.2 DSDP 535 Blake Plateau:	BUFFLER *et al.*, 1984
LOK.3 Rio Argos section, Spain, **Barremian Candidate GSSP**:	COCCIONI & PREMOLI-SILVA, 1994; HOEDEMAEKER & LEEREVELD, 1995
LOK.5 Santa Rosa Canyon, Mexico:	BLAUSER & MCNULTY, 1980; ICE & MCNULTY, 1980
LOK.6 Berrias Section, France (Galbrun *et al.*):	GALBRUN *et al.*, 1986, Fig. 2
LOK.6B Berrias Section, France (Le Hegarat):	LE HÉGARAT & REMANE, 1968, Table VII, p. 45; LE HÉGARAT, 1971, Table 7
LOK.7 ODP 638B & C, Offshore Spain:	APPLEGATE & BERGEN, 1988; MASURE, 1988, Figs. 2-3
LOK.8 Bosso Valley, Italy:	HOUSA *et al.*, 2004
LOK.10 Barret-le-Bas Section, France:	BUSNARDO *et al.*, 1979, p. 44, Fig. 13; p. 90, Fig. 28; p. 105, Fig. 30; BULOT, 1995, Figs. 3, 6-7
LOK.11 Angles Section, France:	BUSNARDO *et al.*, 1979
LOK.12 Angles Section (Bulot 1993):	BULOT *et al.*, 1993, Table VI, p. 27, VII, p. 30, Table VIII, p. 35, XII, p. 44, XIV. BULOT, 1995
LOK.13 La Charce Section, France 1995, **Hauterivian GSSP**:	BULOT *et al.*, 1993, Table VI, p. 27, VII, p. 30, Table VIII, p. 35, XII, p. 44, XIV. BULOT, 1995
LOK.13b La Charce Section, France 2008, **Hauterivian GSSP**:	REBOULET, 2008, Figs. 2.1, 3.1
LOK.14 Curnier Section, France:	BULOT *et al.*, 1993, Table III, p. 22
LOK.15 Moriez (St-Firmin) Section, France:	BULOT *et al.*, 1993, Table IV, p. 24
LOK.16 Baumugne Section, France:	BULOT *et al.*, 1993, Table V, p. 25
LOK.17 La Charce Combe Reboul, France:	BULOT *et al.*, 1993; BULOT, 1995, this is a key reference section for 2 Upper Hauterivian zones
LOK.18 Chamaloc-Col du Rousset, France:	BULOT *et al.*, 1992, Fig. 1.7, p. 40; HOEDEMAEKER, 2013
LOK.19 Mont Aiguille I, Vercors, France:	BUSNARDO *et al.*, 1991
LOK.20 Mont Aiguille II, Vercors, France:	BUSNARDO *et al.*, 1991
LOK.21 Miravetes Section, Spain:	AGUADO *et al.*, 2000, Fig. 3
LOK.22 Canada Lengua Section, Spain:	AGUADO *et al.*, 2000, Fig. 4
LOK.23 Canada Lengua-2 Section, Spain, Valanginian Candidate GSSP:	AGUADO *et al.*, 2000, Fig. 5
LOK.24 Barlya Section, Bulgaria:	LAKOVA *et al.*, 1997, Fig. 1
LOK.25 Gyangze Section, Tibet :	WAN *et al.*, 2010.
LOK.26 Fiume Bosso Section, Italy:	LOWRIE & CHANNELL, 1984, magnetostratigraphic data; BRALOWER *et al.*, 1989, Fig. 3, p. 162
LOK.27 Fonte Giordano Section, Italy:	BRALOWER *et al.*, 1989, Fig. 4, p. 163
LOK.28 Puerto Escaño Section, South Spain, base Berriasian:	CARACUEL *et al.*, 2000; PRUNER *et al.*, 2010
LOK.29 Grindstone Creek, California:	BRALOWER *et al.*, 1990
LOK.30 Miravetes-1 Rio Argos, Spain:	AGUADO *et al.*, 2000, Fig. 3
LOK.31 Canada Luenga-2 Rio Argos, Spain:	AGUADO *et al.*, 2000, Fig. 4
LOK.32 Canada Luenga-3 Rio Argos, Spain:	AGUADO *et al.*, 2000, Fig. 5
LOK.34 Tang-E Asbu, Kuh-E Ginau, Iran:	EDGELL, 1967, Fig. 8
LOK.35 Le Chouet, Drome, SE France:	WIMBLEDON *et al.*, 2013; FRAU *et al.*, 2015, Fig. 1, p. 118; FRAU *et al.*, 2016, Fig. 1
LOK.36 Crimea West:	ARKADIEV *et al.*, 2018
LOK.37 Crimea East:	ARKADIEV *et al.*, 2018
LOK.38 Leube Quarry, Salzburg, Austria:	BUJTOR *et al.*, 2013
LOK.39 Guidaloca Section, NW Sicily:	ANDREINI *et al.*, 2007, Figs. 2, 4
LOK.40 Dieni I & II Section, W Sicily:	ANDREINI *et al.*, 2007, Fig. 3
LOK.41 Polaveno Italy:	CHANNELL & ERBA, 1992; CHANNELL *et al.*, 1995, Fig. 12, Table 2
LOK.42 Jebel Rheouis Section, Tunisia:	MAALOUI & ZARGOUNI, 2016
LOK.43 Jebel Meloussi Section, Tunisia:	MAALOUI & ZARGOUNI, 2016
LOK.44 Nara section, Tunisia:	MAALOUI & ZARGOUNI, 2016
LOK.45 Sidi Kralif section, Tunisia:	MAALOUI & ZARGOUNI, 2016
LOK.49 Nutzhof Section 2009, Austria [2009+2010]:	REHAKOVA *et al.*, 2009; LUKENENDER *et al.*, 2010, Figs. 2, 6

LOK.52 Bruzovice Section, West Carpathians:	SKUPIEN & DOUPOVCOVA, 2019
LOK.56 SGT Section, Turkey:	ATASOY, S.G., 2017, ranges from Appendices A-B; ATASOY *et al.*, 2018
LOK.57A Wadi Mi'iadin, Oman 1987:	SIMMONS & HART 1987, Fig. 10.7-8, .10-11.
LOK.57B Wadi Mi'iadin, Oman 1990:	SCOTT, 1990
LOK.57C Wadi Mi'iadin, Oman 2016:	CELESTINO *et al.*, 2016
LOK.60 Tamazunchale, San Luis Potosi, Mexico:	LOPEZ-MARTINEZ *et al.*, 2015, Fig. 8
LOK.61 Poznachowice Dolne, Poland:	KEDZIERSKI & OCHABSKA, 2012, Fig. 3, Table 1
LOK.62 Tre Maroua, Drome, SE France	WIMBLEDON *et al.*, 2020
LOK.63 Rancho San Vicente, SW Cuba:	PSZCZÓŁKOWSKI & MYCZYŃSKI, 2010; LÓPEZ-MARTÍNEZ *et al.*, 2013
LOK.64 Ain Hammouch, Morocco Val-Haut:	WIPPICH, 2003, Fig. 5
LOK.65 65 Torre de Busi section Italy:	ERBA & QUADRIO, 1987; ANDREINI *et al.*, 2007; CASELLATO & ERBA, 2020, Fig. 5
LOK.66 66 Mt. Pernice section Italy:	ERBA & QUADRIO, 1987; CASELLATO & ERBA, 2020, Fig. 6
LOK.69 69 Yavorets section, Bulgaria:	PETROVA *et al.*, 2019, Fig. 3
LOK.70 Vergol section, France, Vocontian Basin, France:	KENJO *et al.*,2021
HA-BACS.1 Catalog File of Hauterivian-Barremian Carbonates:	**HA-BA.1** Pont de Laval, France; **HA-BA. 2** Pas de l'Essaure, France; **HA-BA. 3** Mont Aiguille, France; **HA-BA. 4** Grands Goulets, France; **HA-BA. 5** Combe de Bella Cha, France; **HA-BA. 6** Pic de l'Oeillette, Chartreuse, France; **HA-BA. 7** Chames Vivarais, France; **HA-BA. 8** Arredons Vivarais, France. **Urgo.1** Col de Rousset, SE France, ARNAUD *et al.*, 1998, Fig. 21. **Urgo.2** Gorges du Nant, ARNAUD *et al.*, 1998, Fig. 27. **Urgo.3** Gorges du Frou, Arnaud *et al.*, 1998, Fig. 28. **Urgo.4** Rocher de Cluses, Arnaud *et al.*, 1998, Fig. 29. **MIDK.102** La Russille, Switzerland; **MIDK 103** Vaulion, Switzerland; **MIDK 104** La Sarraz Eclepens, Switzerland; Gorges de l'Orbe, Switzerland: ARNAUD-VANNEAU & MASSE, 1989; **MIDK.103** Vaulion, Switzerland; ARNAUD-VANNEAU & MASSE, 1989; **MIDK.104** La Sarraz Éclepens, Switzerland; **MIDK.105** Gorges de l'Orbe, Switzerland; **MIDK.106** Gellin-Rochejean, Switzerland. **BACI.**1 Mt. Croce Section, Italy; **BACI.2** Mt. Motola Section, Italy; **BACI.3** Mt. Coccovello Section, Italy; **BACI.4** Mt. Raggeto Section, Italy; **BACI.5** Mt. Tobenna Section, Italy: DI LUCIA *et al.*, 2012, Fig. 8.
Tatra.1 Posrednie III Section, Poland; Tatra.2 Posrednie II Section, Poland; Tatra.3 Rowienka Section, Poland:	GRABOWSKI & PSZCZOLKOWSKI, 2006, Figs. 4-6
ANDESCS.1 Andes Sections Argentina-Chile–ANDES DB, see Appendix 3.	

Appendix 2: LOK2016 DB 09/17/2021: Bioevents, Polarity Chrons, Radioisotopic Ages, and Sequences (SB) in Mega-annums calibrated to GTS2016. Asterisks = no data. Negative sign an artifact of orientation of X/Y plot.

Acaenolithus vimineus	-130.7224	-130.2981
Acanthodiscus radiatus	-134.7294	-134.1235
Acanthodiscus rebouli	-134.7887	-134.1235
Achomosphaera neptuni	-139.7813	-130.4596
Acrioceras pulcherrinum	-131.5870	-131.4780
Acrioceras puzosianum	-130.8221	-130.8221
Acrioceras seringuei	-131.3472	-131.3472
Acrioceras tabarelli	-130.8640	-130.8539
Agrio tuff bed 126.97	-130.1558	***
Agrio tuff bed 127.42	-130.2259	***
Agrio tuff bed 129.09	-131.7887	***
Agrio tuff bed 130.40	-133.9840	***
Aldorfia dictyotum	-135.1896	-135.1896
Alvellodinium falsificum	-136.8908	-136.5085
Amphizygus brooksii	-132.8665	-130.6650
Amphizygus infracretacea	-134.9580	-133.5160
Amphorellina lanceolata	-140.4337	***
Amphorula delicata	-140.0724	-138.8577
Amphorula metaelliptica	-142.6067	-137.7134
Ancyloceras vandenheckii	-129.1604	-129.1604
Andes J-K SB 1	-147.7527	***
Andes J-K SB 2	-145.9279	***
Andes J-K SB 3	-142.6842	***
Andes J-K SB 4	-140.5289	***
Andiceras acuticostum	-148.1857	-146.5407
Aprobolocysta eilema	-131.9987	-131.2840
Apteodinium maculatum	-136.2827	-133.9153
Ardesciella rhodanica	-145.8887	-145.8887
Argentiniceras fasciculatum	-143.8925	-141.6715
Argentiniceras noduliferum	-144.4639	-141.9289
Aspidoceras depressus	-139.4232	-139.4232
Aspidoceras euomphalum	-148.2864	-144.9288

Aspidoceras quinchaoi	-146.7752	-146.3036
Aspidoceras rogoznicensis	-145.9821	-144.0502
Assipetra infracretacea	-144.8638	-132.4596
Assipetra terebrodentarius	-130.3153	-130.2755
Aulacosphinctes proximus	-148.6696	-143.7945
Aulacosphinctes sulcatus	-147.8308	-146.3750
Avramidiscus kiliani	-130.7834	-130.4925
Axopodorhabdus dietzmannii	-139.0080	-130.0161
Balearites balearis	-131.3690	-131.0289
Baronnites hirsutus	-137.5468	-137.1511
Barremites spp.	-131.1221	-125.8838
Base Albian	-113.1400	***
Base Aptian	-126.3000	***
Base Barremian	-130.8600	***
Base Berriasian	-145.7000	145.0000
Base Hauterivian	-134.7000	***
Base Valanginian	-139.4000	***
Batioladinium gochtii	-136.8908	-134.8651
Batioladinium varigranosa	-137.7466	-135.1885
Berriasella bebrovensis	-142.6661	-140.2646
Berriasella callisto	-141.5873	-139.4634
Berriasella chomeracensis	-145.7500	-144.0591
Berriasella jacobi	-145.7583	-143.7890
Berriasella malbosi	-144.6594	-140.2568
Berriasella paramacillenta	-144.9717	-143.8667
Berriasella picteti	-142.6421	-139.2625
Berriasella privasensis	-143.8669	-142.0898
Berriasella subcallisto	-145.7340	-143.6672
Berriasella subprivasensis	-144.1210	-144.1210
Berriasella tithonica	-146.3000	-145.8000
Biorbifera johnewingii	-142.8262	-135.4659
Biscutum constans	-145.9889	-130.0000
Blanfordiceras vetustum	-145.7957	-143.9674
Bochianites neocomiensis	-138.8470	-134.6804
Bochianites oosteri	-134.7000	-134.6256
Borzaiella atava	-142.1924	-141.0966
Borzaiella slovenica	-148.9733	-146.4902
Boughdiriella chouetensis	-146.1110	-145.8887
Bourkidinium granulatum	-133.4430	-130.9993
Braarudosphaera bigelowii	-140.0507	-134.3880
Braarudosphaera discula	-134.9864	-133.5160
Braarudosphaera regularis	-134.1125	-132.2382
Breistrofferella castellanensis	-134.7282	-134.0627
Breistrofferella varappensis	-134.6804	-134.4245
Buchia pacifica	-137.6250	-135.5000
Buchia uncitoides	-139.0000	-138.0750
Bukrylithus ambiguus	-139.0080	-130.0161
Burckhardticeras peroni	-147.8308	-147.8308
Busnardoiceras busnardoi	-146.0433	-145.8887
Busnardoites campylotoxum	-138.5141	-135.6475
Busnardoites desori	-136.8564	-135.6475
Busnardoites subcampylotoxum	-136.795	-136.795
Caddasphaera halosa	-138.0278	-134.8203
Cadosina fusca	-146.8745	-141.4428
Cadosina fusca cieszynica	-145.2419	-145.2419
Cadosina semiradiata	-149.3071	-143.8031
Calcicalathina oblongata	-139.5554	-130.5848
Calcicalathina praeoblongata	-141.3878	-138.5064
Callaiosphaeridium asymmetricum	-134.153	-130.00
Calpionella alpina	-146.9167	-134.0660
Calpionella elliptalpina	-146.4940	-145.0320
Calpionella elliptica	-144.9150	-139.2050
Calpionella grandalpina	-146.7081	-143.2117
Calpionella minuta	-142.1674	***
Calpionellites caravacaensis	-139.4586	-138.4756
Calpionellites coronata	-139.3957	-136.5576
Calpionellites darderi	-139.4672	-133.5600
Calpionellites major	-139.3957	-133.5600
Calpionellopsis oblonga	-143.3071	-133.5600
Calpionellopsis simplex	-144.4744	-133.5600
Canninginopsis colliveri	-134.0444	-132.7406
Carbon peak Valanginian OAEb	-138.963	-138.769
Carbon peak Valanginian OAEc	-136.381	***
Carbon peak Valanginian OAEd	-134.1475	***
Carpistomiosphaera borzai	-150.8000	-149.1181
Carpistomiosphaera tithonica	-149.1700	-148.8213
Carpistomiosphaera valanginiana	-139.160	-138.830
Cassiculosphaeridia reticulat	-134.1811	-132.5330
Catutosphinctes americanensis	-148.380	-146.817
Catutosphinctes guenenokenensis	-150.87	-149.51
Catutosphinctes inflatus	-146.4850	-145.6913
Catutosphinctes proximus	-148.5300	-146.4675
Cerbia tabulata	-132.7406	-132.5330
Chacantuceras ornatum	-135.1895	-134.9810
Cheloniceras spp.	-125.6695	-125.6695
Chiastozygus bilamellus	-137.2383	-134.2975
Chiastozygus litterarius	-133.5523	-132.5309
Chiastozygus platyrhethus	-133.5035	-132.5414
Chiastozygus striatus	-135.0461	-130.5160
Chiastozygus tenuis	-136.8009	-133.5160
Chigaroceras loteroense	-146.7041	-144.3597
Chitinoidella boneti	-147.7338	-145.4263
Chitinoidella dobeni	-147.8319	-147.0225
Chitinoidella elongata	-147.5023	-147.0316
Chitinoidella hegarati	-147.5443	-146.7081
Chitinoidella slovenica	-147.8308	-146.2811
Chlamydophorella huguoniotii	-135.695	-133.805
Chlamydophorella membranoidea	-133.738	-133.76
Chlamydophorella nyei	-135.2687	-130.000
Choicensisphinctes burckhardti	-150.68	-149.227
Choicensisphinctes choicensis	-150.150	-148.304
Choicensisphinctes erinoides	-150.221	-147.295
Choicensisphinctes platyconus	-150.873	-149.748
Choicensisphinctes striolatus	-145.378	-143.203
Choicensisphinctes windhauseni	-149.244	-148.639
Cieneguiticeras falculatum	-149.670	-147.1275

Cieneguiticeras perlaevis	-149.9339	-148.6956
Circulodinium distinctum	-142.2500	-130.0000
Clavihedbergella eocretacea	-130.2629	-125.608
Clavihedbergella semielongata	-130.263	-125.608
Clavithurmannia foraticostata	-140.076	-139.782
Clepsilithus maculosus	-135.0204	-130.2356
Colchidites sp.	-127.1700	-126.0369
Colomisphaera carpathica	-147.4556	-141.6868
Colomisphaera cieszynica	-147.8319	-143.8745
Colomisphaera conferta	-139.8093	-138.6887
Colomisphaera fortis	-147.5243	-143.6067
Colomisphaera helicosphaera	-139.255	-138.7358
Colomisphaera lapidosa	-147.4556	-139.3957
Colomisphaera lucida	-145.1938	-143.8944
Colomisphaera nagyi	-150.8000	-147.0225
Colomisphaera pieniniensis	-150.8000	-147.0225
Colomisphaera radiata	-147.4556	-147.4556
Colomisphaera tenuis	-148.1071	-143.3798
Colomisphaera volgeri	-139.1604	-138.6887
Cometodinium whitei	-138.6217	-130.1032
Cometodinium? whitei	-135.9912	-132.7406
Comittosphaera sublapidosa	-147.4556	-146.4450
Conusphaera maledicto	-150.0800	***
Conusphaera mexicana	-149.6262	-130.0000
Conusphaera mexicana minor	-149.636	-140.6229
Corollithion acutum	-136.7605	-132.5927
Corollithion ellipticum	-139.0080	-132.4596
Corollithion geometricum	-134.3456	-130.5618
Corollithion signum	-135.3959	-135.3959
Corongoceras alternans	-146.4757	-145.9821
Corongoceras evolutum	-146.4386	-146.2102
Corongoceras involutum	-146.4014	-146.2968
Corongoceras koellikeri	-145.2441	-143.5279
Corongoceras koeni	-146.4014	-146.1786
Corongoceras lotenoense	-147.5985	-145.9506
Corongoceras mendozanum	-147.1025	-144.0502
Corongoceras multimum	-146.4386	-146.4386
Corongoceras praecursor	-148.5164	-146.8825
Corongoceras steinmanni	-145.7957	-145.7957
Coronifera oceanica	-132.6670	-130.0000
Crassicollaria brevis	-146.6856	-144.4639
Crassicollaria colomi	-146.4554	-144.5822
Crassicollaria intermedia	-147.0800	-144.9200
Crassicollaria massutiniana	-147.6800	-143.8944
Crassicollaria parvula	-147.6800	-139.8093
Crassiculosphaeridia reticulata	-130.573	-130.000
Cretarhabdus angustiforatus	-141.900	-135.500
Cretarhabdus conicus	-142.8262	-130.0000
Cretarhabdus crenulatus	-142.0705	-134.3880
Cretarhabdus loriei	-135.6338	-132.5414
Cretarhabdus octofenestratus	-145.004	-140.979
Cretarhabdus striatus	-134.8215	-130.4350
Cretarhabdus surirellus	-146.3025	-130.1558

Cribellopsis elongata	-131.4775	-130.5234
Cribellopsis neoelongata	-131.0552	-130.4745
Cribellopsis schroederi	-130.8380	-130.7193
Cribellopsis thieuloyi	-130.8380	-130.7193
Cribroperidinum sepimentum	-133.002	-130.000
Cribrosphaerella ehrenbergii	-135.3959	-135.3959
Crioceratites andinum	-131.5133	-131.4798
Crioceratites basseae	-131.3690	-131.3690
Crioceratites diamantense	-131.5196	-131.4798
Crioceratites duvalii	-132.3500	-131.8057
Crioceratites fabreae	-131.3254	-131.2818
Crioceratites gr. *quenstedti*	-133.4112	-132.1908
Crioceratites loryi	-134.2881	-133.8625
Crioceratites majorisensis	-131.6088	-131.4344
Crioceratites matsumotoi	-132.0532	-131.9672
Crioceratites nolani	-134.4682	-131.2448
Crioceratites perditum	-131.5053	-131.4239
Crioceratites remanei	-131.3690	-131.3690
Crioceratites schlagintweiti	-131.7270	-131.7110
Criohimantoceras gigas	-136.0119	-134.9787
Criosarasinella furcillata	-135.4300	-135.0247
Criosarasinella heterocostata	-135.430	-135.193
Criosarasinella mandovi	-135.2400	-134.9506
Cruasiceras cruasense	-132.2300	-132.1683
Crucibiscutum nequenensis	-131.7509	-131.2963
Crucibiscutum salebrosum	-134.9864	-133.5160
Cruciellipsis chiasta	-140.0507	-134.5708
Cruciellipsis cuvillieri	-147.0599	-131.5509
Cruciplacolithus furtivus	-132.8665	-131.4172
Cruciplacolithus salebrosus	-140.5103	-135.6505
Ctenidodinium elegantulum	-135.4659	-134.6907
Ctenidodinium scissum	-135.8210	-135.8210
Cuyaniceras raripartitum	-141.7864	-140.9119
Cuyaniceras transgrediens	-143.5279	-139.4232
Cyclagelosphaera deflandrei	-146.8181	-130.7779
Cyclagelosphaera margerelii	-148.6707	-130.0000
Cyclagelosphaera tubulata	-131.5944	-131.5944
Cyclonephelium distinctum	-134.4564	-132.7406
Cyclonephelium hystrix	-139.7813	-133.6636
Cymatiosphaera delicatula	-134.2732	-133.5532
Cymososphaeridium validum	-136.3043	-131.0296
Dalmasiceras biplanum	-144.9607	-144.9607
Dalmasiceras crassicostatum	-145.4730	-145.4730
Dalmasiceras dalmasi	-142.8000	-142.6902
Dalmasiceras djanelidzei	-144.8350	-144.8350
Dalmasiceras punctatum	-142.8000	-141.8496
Dalmasiceras subloevis	-145.2603	-144.8780
Dapsilidinium warrenii	-139.5724	-130.3853
Decliveites agrioensis	-134.4865	-134.3429
Decliveites crassicostatum	-134.7178	-134.7178
Deshayesites oglanlensis	-126.3000	-126.3000
Deshayesites weissi	-126.0369	-125.8991
Diadorhombus rectus	-139.0080	-131.7612

Diazomatolithus lehmanii	-146.6772	-130.0000
Dicanthum hollisteri	-142.8262	-130.0000
Dichotomites petschi	-136.2850	-135.9287
Dichotomites vergunnorum	-135.4482	-135.3385
Diloma placinum	-133.6829	-133.6118
Dingodinium albertii	-137.3749	-133.3539
Dingodinium cerviculum	-138.9044	-130.0000
Dingodinium europaeum	-129.0379	-127.2312
Discorhabdus biradiatus	-133.7892	-133.6447
Discorhabdus ignotus	-142.8098	-130.0000
Discorhabdus rotatorius	-142.5769	-133.5160
Discorsia nanna	-133.8054	-133.8054
Djurjuriceras catutosense	-146.4084	-146.3036
Dobeniella bermudezi	-147.5489	-146.9398
Dobeniella cubensis	-147.5489	-146.9398
Druggidium apicopaucicum	-138.4730	-131.9987
Druggidium deflandrei	-135.6038	-127.1240
Druggidium rhabdoreticulatum	-136.8969	-128.9920
Durangites acanthicus	-146.3000	-145.8000
Durangites astillerensis	-146.3000	-145.8000
Durangites vulgaris	-146.3000	-145.8000
Eiffellithus primus	-148.0991	-137.0000
Eiffellithus striatus	-135.3000	-131.7509
Eiffellithus windi	-139.2677	-132.5450
Elenaelia cularensis	-145.7340	-145.6760
Eleniceras nikolovi	-134.7718	-134.4611
Eleniceras tchechitevi	-135.4683	-134.6804
Eleniceras transsylvanicum	-134.9075	-134.7650
Emericiceras emerici	-130.8640	-130.7513
Endoscrinium campanula	-142.2500	-130.0000
Endoscrinium glabra	-136.5227	-136.5085
Eopalorbitolina charollaisi	-130.8100	-130.7437
Eopalorbitolina pertenuis	-130.8221	-130.7437
Eprolithus floralis	-131.2166	-131.0969
Erdenella paquieri	-141.6455	-138.6995
Erdenella zianidia	-141.7535	-141.0331
Escharisphaeridia pocockii	-142.8262	-142.8262
Ethmorhabdus gallicus	-145.9784	-133.5160
Ethmorhabdus hauterivianus	-139.7364	-130.4350
Euptychoceras meyrati	-133.4112	-132.1908
Euvirgalithacoceras malarguense	-150.3983	-148.6394
Exiguisphaera phragma	-137.7466	-135.2687
Falsurgonina pileola	-131.4775	-130.7193
Falsurgonina vanneauae	-131.5768	-130.4745
Fauriella boissieri	-141.6945	-139.3891
Fauriella donzei	-140.0000	-139.8813
Fauriella gallica	-142.6902	-140.8890
Fauriella kiliani	-140.0965	-138.1346
Fauriella rarefurcata	-143.2876	-139.9524
Faviconus multicolumnatus	-150.7160	-144.4940
Flabellites oblonga	-133.5933	-132.6252
Foucheria modesta	-140.0724	-136.6659
Frenguelliceras magister	-143.1385	-141.6715
Fromea amphora	-135.0502	-135.0502
Gaarderella granulifera	-130.3600	-130.0161
Glob'oides algeriana	-126.4917	-126.4028
Glob'oides aptiense	-127.1700	-126.7106
Glob'oides blowi	-127.9355	-125.6082
Glob'oides gottisi	-135.9654	-125.6082
Glob'oides maridalensis	-125.6082	-122.5459
Globochaete alpina	-144.6595	***
Globuligerina hoterivica	-138.3380	-125.6695
Gonyaulacysta helicoidea	-145.7073	-130.0000
Gonyaulacysta kostromiensis	-136.5085	-133.1871
Grantarhabdus meddii	-139.0080	-132.4492
Groebericeras bifrons	-143.8400	-141.9926
Groebericeras rocardi	-143.1393	-143.1007
Gubkinella graysonensis	-135.1336	-125.6695
Haploceras staszycii	-149.6700	-149.2267
Haplophylloceras strigile	-144.6797	***
Haqius circumradiatus	-142.9085	-130.0000
Hayesites atlanticus	-135.0461	-133.6447
Hayesites radiatus	-133.9498	-130.0711
Hedb aptiana	-130.2629	-125.6082
Hedb aptica	-138.3380	-125.6082
Hedb delrioensis	-135.5587	-125.6082
Hedb excelsa	-125.6695	-125.6695
Hedb kuznetsovae	-130.2629	-125.6695
Hedb sigali	-138.3380	-125.6695
Hedb similis	-130.4925	-125.6082
Heinzia provincialis	-129.1604	-129.1604
Heinzia sartousi	-127.4149	-127.3078
Helenea chiastia	-148.6707	-130.0000
Heterosphaeridium? galliciae	-135.9912	-132.7406
Hexalithus geometricus	-146.7013	-144.6900
Hexalithus magharensis	-140.8365	-140.8365
Hexalithus noelae	-148.7000	-143.3986
Himalayites treubi	-142.9481	-142.9481
Himantoceras trinodosum	-136.0119	-134.6937
Holcodiscus caillaudianus	-130.0791	-129.6351
Holcophylloceras calypso	-144.8463	-137.1906
Holcoptychites agrioensis	-134.0638	-134.0638
Holcoptychites magdalensae	-134.3031	-134.1356
Holcoptychites neuquensis	-134.2861	***
Hoplytocrioceris gentilli	-133.7847	-133.6252
Hoplytocrioceris giovinei	-133.8644	-133.8405
Hypophylloceras courchonense	-135.5761	-135.3385
Hypophylloceras perlobatum	-137.7457	-136.6546
Hystrichodinium furcatum	-136.8969	-133.1871
Hystrichodinium pulchrum	-138.8068	-131.1072
Hystrichodinium voigtii	-142.2500	-130.3853
Indansites malarguensis	-150.3983	-149.9233
Inoceramus everesti	-144.0392	***
Jeanthieuloyites quinquestriatus	-135.4447	-134.6433
Karakaschiceras attenuatum	-137.0024	-136.0532
Karakaschiceras biasalense	-138.0339	-136.4899

Karakaschiceras heteroptychum	-136.7607	-136.7734
Karakaschiceras neumayri	-137.0780	-136.8407
Karakaschiceras pronecostatum	-136.7125	-135.3691
Kilianella busnardoi	-141.9457	-141.7535
Kilianella gr.*chamalocensis*	-141.3182	-138.9727
Kilianella lucensis	-139.7691	-136.2014
Kilianella pexiptycha	-139.9406	-138.9333
Kilianella retrocostata	-140.0965	-137.6375
Kilianella roubaudi	-139.0340	-136.2014
Kilianella roubaudiana	-139.1867	-137.0405
Kilianella superba	-137.0660	-137.0405
Kiokansium polypes	-137.7466	-130.0000
Kleithriasphaeridium corrugatum	-137.3749	-137.3749
Kleithriasphaeridium eoinodes	-133.7790	-132.5487
Kleithriasphaeridium fasciatum	-137.3302	-132.5487
Kleithriasphaeridium simplicispinum	-137.2264	-136.5227
Krantziceras azulense	-145.3783	-145.3783
Krantziceras compressum	-141.9926	-141.9289
Krantziceras disputabile	-147.1025	-147.1025
Krantziceras planulatum	-142.5022	-142.3111
Kutekiceras pseudocolubrinus	-147.8308	-147.8308
Laeviaptychus crassissimus	-149.9176	-147.9057
Laeviaptychus latus	-147.9692	-146.5505
Leopoldia buxtorfi	-134.4345	-134.0750
Leopoldia leopoldina	-134.5275	-134.4087
Leptoceras studeri	-141.1600	-138.6778
Leupoldina cabri	-125.6082	-125.6082
Leupoldina pustulans	-130.2629	-125.6082
Leymeriella schrammeni anterior	-113.1000	-113.1000
Lissonia riveroi	-139.2741	-138.5129
Lithastrinus septentrionalis	-132.8665	-130.0000
Lithoceras picunleufuense	-150.8733	-149.7480
Lithraphidites bollii	-133.9498	-130.2356
Lithraphidites carniolensis	-147.7160	-130.0000
Lorenziella hungarica	-143.9394	-137.2302
Lorenziella plicata	-145.3436	-133.8360
Luppovella superba	-137.5627	-136.9573
Lyticoceras nodosoplicatum	-133.5537	-133.3875
Lyticoceras subfimbriatum	-134.0600	-134.0600
Lytoceras juileti	-137.7457	-136.3597
Lytoceras montanum	-144.9609	-144.9609
Lytohoplites burckhardti	-146.3387	-146.2804
Lytohoplites rauloi	-146.4386	-145.3387
Lytohoplites vareloe	-146.2968	-145.6480
Lytohoplites zambranoi	-146.4757	-145.6480
Magnetochron CM0R	-126.3000	-126.0000
Magnetochron CM10	-133.9313	-133.6694
Magnetochron CM10N	-135.3408	-134.3082
Magnetochron CM1R	***	-127.5912
Magnetochron CM2	***	-128.0208
Magnetochron CM3R	-130.8011	-128.6813
Magnetochron CM5R	-131.7071	-131.4307
Magnetochron CM6R	-131.8776	-131.7973

Magnetochron M6	***	-132.0222
Magnetochron M7	***	-132.1807
Magnetochron CM7R	-132.3155	-131.9912
Magnetochron CM8R	-132.7334	-132.5194
Magnetochron M8	***	-133.0312
Magnetochron CM9R	-133.4655	-133.0008
Magnetochron M9	***	-133.6578
Magnetochron M11r	***	-136.0997
Magnetochron M12n	***	-136.9000
Magnetochron M12r	***	-137.7535
Magnetochron M13n	***	-138.3000
Magnetochron M13r	***	-138.4059
Magnetochron M14n	***	-138.6000
Magnetochron M14r	***	-139.2348
Magnetochron M15n	***	-139.4462
Magnetochron M15r	***	-139.9000
Magnetochron M16n	***	-140.4000
Magnetochron M16r	***	-141.2865
Magnetochron M17n	***	-142.1538
Magnetochron M17r	***	-142.5645
Magnetochron M18n	***	-143.3173
Magnetochron M18r	***	-143.7134
Magnetochron M19n	***	-144.6496
Magnetochron M19n.1n	***	-145.0000
Magnetochron M19n.1r	***	-145.1333
Magnetochron M19n.2n	***	-145.3000
Magnetochron M19r	***	-145.8432
Magnetochron M20n	***	-146.1054
Magnetochron M20n.1n	***	-146.1689
Magnetochron M20n.1r	***	-146.3727
Magnetochron M20n.2n	***	-146.5132
Magnetochron M20r	***	-147.1557
Magnetochron M21n	***	-147.5443
Magnetochron M21r	-149.2386	-148.4143
Magnetochron M22A	***	-150.5000
Magnetochron M22n	***	-148.7717
Magnetochron M22r	***	-150.0481
Malbosiceras malbosi	-144.0857	-143.7945
Manivitella pemmatoidea	-146.1787	-130.0000
Markalius circumradiatus	-142.5769	-134.3880
Markalius inversus	-130.6982	-130.6982
Marker bed 134.0 U-Pbf	***	-134.0660
Marker bed 138.45	-138.0000	-136.0000
Marker bed 139.85 Sr	-139.8500	-139.8500
Marker bed 305	-136.9518	***
Marker bed 321	-136.5449	***
Marker bed A 137.1	-138.0625	-138.0525
Marker bed Ap SB SL 1	-126.5805	-126.5805
Marker bed B 137.1	-136.4375	-136.4275
Marker bed Ba1	-130.8446	***
Marker bed Ba2	-130.7936	***
Marker bed Faraoni bed	-131.0776	-131.0539
Marker bed Ha6	-131.5340	***

Marker bed Ha7	-131.1679	***
Marker bed SbB3	-131.4278	***
Marker bed Tuff 136	-133.1500	***
Mazatepites arredondense	-149.6700	-147.8187
Mazenoticeras paramimounum	-142.2667	-140.8890
Mazenoticeras tarini	-145.7823	-145.6760
Megacrioceras doublieri	-131.4126	-131.4126
Meiourogonyaulax pertusa pertusa	-137.1198	-131.9987
Meiourogonyaulax stoveri	-134.4863	-127.0475
Micracanthoceras lamberti	-147.1504	-146.5470
Micracanthoceras microcanthum	-147.5538	-145.5449
Micracanthoceras spinulosum	-146.2157	-143.9568
Micracanthoceras vetustum	-144.5726	-144.0502
Micrantholithus hoschulzii	-142.2385	-130.1000
Micrantholithus obtusus	-141.1637	-130.1399
Micrantholithus speetonensis	-142.8851	-138.6887
Microhedbergella renilaevis	-113.1400	-113.1400
Microstaurus chiastius	-148.8920	-135.5000
Microstaurus quadratus	-146.0433	-133.5160
Micula infracretacea	-141.1637	-134.3880
Montseciella alguerensis	-131.0252	-130.7279
Montseciella glanensis	-131.4458	-130.7279
Moravisphinctes fischeri	-146.5267	-146.1400
Moravisphinctes moravicus	-147.5538	-146.3750
Muderongia brachialis	-131.7188	-131.7188
Muderongia extensiva	-136.0875	-136.0163
Muderongia perforata	-135.2687	-134.0444
Muderongia simplex	-142.6012	-134.2183
Muderongia simplex microperforata	-137.7466	***
Muderongia staurota	-134.5668	-128.5939
Nannoconus bermudezii	-143.3213	-130.0000
Nannoconus boletus	-132.7014	-132.7014
Nannoconus bonetii	-133.6187	-133.6187
Nannoconus broennimannii	-145.2244	-133.3458
Nannoconus bucheri	-135.6983	-130.0000
Nannoconus circularis	-135.0293	-130.2356
Nannoconus colomii	-145.8403	-130.0000
Nannoconus compressus	-148.0278	-145.3562
Nannoconus cornutus	-145.9014	-133.2976
Nannoconus dolomiticus	-144.6766	-141.0086
Nannoconus elongatus	-135.6983	-130.6982
Nannoconus erbae	-146.6348	-143.9735
Nannoconus globulus	-146.2516	-130.0000
Nannoconus globulus globulus	-145.7047	-130.1399
Nannoconus globulus minor	-147.0800	-133.2344
Nannoconus infans	-148.1960	-141.0538
Nannoconus kamptneri	-144.3913	-130.1399
Nannoconus kamptneri minor	-145.0573	-140.5965
Nannoconus ligius	-131.2963	-130.2259
Nannoconus puer	-147.7160	***
Nannoconus quadratus	-143.9989	-138.8302
Nannoconus steinmannii	-145.2957	-127.7118

Nannoconus steinmannii minor	-145.9020	-134.4311
Nannoconus truitti	-141.0538	-130.4589
Nannoconus wassallii	-134.9132	-126.3093
Nannoconus wintereri	-146.3026	-143.3310
Neocomiceramus curacoensis	-131.6698	-131.1772
Neocomites callidiscus	-134.9787	-134.9075
Neocomites crassicostatum	-141.5930	-141.4653
Neocomites flucticulus	-134.8125	-134.4087
Neocomites neocomiensiformis	-138.5501	-135.1636
Neocomites neocomiensis	-139.4961	-135.2914
Neocomites pachydicranus	-135.4300	-134.0600
Neocomites peregrinus	-136.4329	-135.9287
Neocomites platycostatus	-136.9518	-135.2871
Neocomites polygonius	-135.0975	-135.0975
Neocomites premolicus	-139.3702	-137.7446
Neocomites subquadratus	-138.5865	-136.7086
Neocomites subtenuis	-137.1650	-135.2914
Neocomites teschenensis	-137.1927	-135.8337
Neocomites wichmanni	-139.4472	-139.1555
Neocosmoceras malbosiforme	-139.4232	-139.3429
Neocosmoceras sayni	-143.8189	-143.1007
Neohoploceras arnoldi	-137.0780	-136.8407
Neohoploceras depereti	-136.7125	-136.1425
Neohoploceras provinciale	-137.3214	-135.5331
Neohoploceras submartini	-136.9518	-136.4901
Neolisoceras salinarium	-137.8633	-135.9640
Neolissoceras aberrans	-137.4128	-137.4128
Neolissoceras grasianum	-141.6945	-131.8057
Occisucysta tentorium	-138.5607	-130.2437
Octopodorhabdus decussatus	-137.1751	-135.6505
Octopodorhabdus polytretus	-132.4927	-131.3415
Octopodorhabdus reinhardtii	-134.2539	-133.4788
Odontochitina operculata	-133.0018	-127.0475
Olcostephanus atherstoni	-137.2291	-136.8407
Olcostephanus balestrai	-136.1859	-135.2162
Olcostephanus densicostatus	-135.4116	-134.0627
Olcostephanus drumensis	-140.2899	-137.4281
Olcostephanus guebhardi	-137.0660	-135.8612
Olcostephanus hispanicus	-134.6758	-134.6758
Olcostephanus jeannoti	-134.3124	-133.4523
Olcostephanus josephinus	-137.5468	-137.1511
Olcostephanus laticosta	-133.9681	-133.9202
Olcostephanus nicklesi	-136.0119	-135.3385
Olcostephanus sayni	-133.9547	-133.7912
Olcostephanus stephanophorous	-137.6945	-135.7266
Olcostephanus tenuituberculatus	-138.5141	-133.2827
Olcostephanus thieuloyi	-135.3706	-135.2471
Olcostephanus variegatus	-133.5775	-133.4587
Oligosphaeridium complex	-137.4847	-130.0000
Oligosphaeridium dividuum	-134.6907	-133.4430
Oligosphaeridium pulcherrimum	-135.8581	-130.2078
Oligosphaeridium verrucosum	-132.5487	***
Oloriziceras magnum	-147.7615	-147.6231

Oloriziceras salariensis	-147.7615	-147.6231
Oosterella cultrata	-135.3113	-134.4682
Oosterella cultrataeformis	-135.5013	-134.4245
Oosterella fascigera	-136.4038	-135.8337
Oosterella garciae	-135.9202	-134.9787
Oosterella stevenini	-135.8575	-135.3113
Orbitolinopsis cuvillieri	-130.8282	-130.7437
Orbitolinopsis debelmasi	-130.8315	-130.7193
Orbitolinopsis flandrini	-130.7071	-130.6993
Orbitolinopsis subkiliani	-130.7071	-130.5260
Paleodictyoconus actinostoma	-130.8282	-130.7437
Paleodictyoconus beckerae	-131.5967	-130.9483
Paleodictyoconus cuvillieri	-131.6762	-130.4745
Paracoskinolina arcuata	-131.5768	-130.7437
Paracoskinolina hispanica	-130.8539	-130.4745
Paracoskinolina jourdanensis	-131.4079	-130.4745
Paracoskinolina maynci	-131.5570	-130.4745
Paracoskinolina praereicheli	-130.8315	-130.7361
Paracoskinolina querolensis	-131.4458	-130.5357
Paracoskinolina reicheli	-130.8446	-130.7437
Paradontoceras calistoides	-146.3225	-144.1928
Paraspiticeras groeberi	-130.9613	-130.2259
Paraspiticeras precrassispinum	-131.5216	-131.5216
Parastomiosphaera malmica	-149.3071	-146.9757
Parathurmannia sarasini	-131.1211	-131.0581
Paraulacosphinctes senoides	-146.5267	-146.1400
Paraulacosphinctes transitorius	-147.5538	-146.1274
Pareodinia ceratophora	-144.7305	-135.1885
Parhabdolithus achlyostaurion	-140.1490	-137.2383
Parhabdolithus asper	-145.1543	-134.3880
Parhabdolithus embergeri	-148.0337	-134.3880
Parhabdolithus infinitus	-136.9295	-130.0000
Parhabdolithus judithae	-138.8304	-137.3639
Parhabdolithus splendens	-142.2385	-134.3880
Parhabdolithus swinnertonii	-137.2383	-132.9078
Pasottia andina	-149.6700	-148.8710
Percivalia fenestrata	-140.8846	-130.2356
Percivalia nebulosa	-141.5873	-138.9182
Phoberocysta neocomica	-145.7073	-130.3853
Phoberocysta tabulata	-137.8081	-137.8081
Phylloceras tethys	-137.8994	-134.9912
Phyllopachyceras winckleri	-134.7170	-134.6987
Pickelhaube furtiva	-144.0957	-133.5160
Piriferella paucicalcarea	-131.5967	-130.4745
Platylenticeras cardioceroides	-137.5468	-137.4281
Platylenticeras occidentale	-138.1799	-137.3094
Plesiospitidiscus ligatus	-132.0230	-130.9333
Plesiospitidiscus subdifficilis	-131.2234	-131.0135
Podorhabdus dietzmanni	-138.1799	-134.6804
Polycostella beckmannii	-149.3960	-144.3560
Polycostella senaria	-148.8680	-131.4000
Polygonifera evittii	-144.7305	-144.7305
Polypodorhabus madingleyensis	-145.5646	-132.4950
Praecalpionellites murgeanui	-139.9667	-138.4912
Praedictyorbitolina busnardoi	-131.6762	-131.6762
Praedictyorbitolina carthusiana	-131.4775	-130.5260
Praedictyorbitolina claveli	-131.6762	-130.7437
Praetintinnopsella andrusovi	-147.2500	-145.4263
Praturlonella danilovae	-131.4079	-130.4745
Prediscosphaera columnata	-113.1000	-113.1000
Protacanthodiscus andreaei	-146.1400	-145.8887
Protacanthodiscus berriasensis	-145.7500	-144.6359
Protacanthodiscus heterocosmus	-145.7500	-144.6359
Protacrioceras ornatum	-131.4344	-131.3908
Protacrioceras puzosianum	-133.5537	-133.5300
Protancyloceras punicum	-140.0000	-139.9209
Protetragonites quadrisulcatus	-139.2250	-135.3385
Protoellipsodinium seghire	-134.0444	-133.6636
Protoellipsodinium touile	-134.5384	-133.4430
Pseudhimalayites subpretiosus	-148.3400	-147.8187
Pseudinvoluticeras douvillei	-150.3033	-148.0435
Pseudinvoluticeras primordialis	-150.5670	-149.9339
Pseudoacanthodiscus hexagonus	-145.8887	-145.8887
Pseudoceratium anaphrissum	-128.9001	-127.2006
Pseudoceratium pelliferum	-142.6067	-127.2312
Pseudocyclammina lituus	-138.8436	-138.5807
Pseudofavrella angulatiformis	-135.4160	-135.3982
Pseudofavrella australe	-135.1485	-135.1485
Pseudofavrella garatei	-135.4160	-135.3892
Pseudolissoceras zitteli	-149.9233	-147.2950
Pseudomoutoniceras annulare	-131.8486	-131.8486
Pseudosaynella termieri	-125.6695	-125.6695
Pseudosubplanites euxinus	-144.9717	-143.9896
Pseudosubplanites lorioli	-145.0197	-143.3660
Pseudosubplanites ponticus	-145.3079	-144.2326
Pseudothurmannia angulicostata	-131.2138	-130.9150
Pseudothurmannia catulloi	-131.1457	-130.8447
Pseudothurmannia ohmi	-131.1915	-130.8141
Pseudothurmannia picteti	-131.5833	-131.0050
Pseudothurmannia pseudomalbosi	-131.4967	-131.1491
Pterolytoceras exoticum	-144.3114	-144.3114
Pterospermella aureolata	-138.1600	-133.1871
Pterospermella australiensis	-137.7146	-137.5051
Ptychophylloceras diphyllum	-136.8009	-135.3385
Ptychophylloceras semisulcatum	-143.9243	-131.8057
Raimondiceras alexandrense	-141.3556	-141.3556
Reinhardtites elegans	-135.0461	-133.4800
Reinhardtites fenestratus	-141.5000	-130.0000
Remaniella borzai	-144.2732	-138.8622
Remaniella cadischiana	-145.0677	-138.4756
Remaniella catalanoi	-144.7714	-139.6111
Remaniella colomi	-144.5900	-141.7265
Remaniella dadayi	-139.4672	-137.2662
Remaniella duranddelgai	-144.9500	-136.3200
Remaniella ferasini	-145.2167	-143.1667
Remaniella filipescui	-143.3071	-136.6650

Remaniella murgeanui	-139.8458	-137.2662
Retecapsa angustiforata	-145.2134	-130.0000
Retecapsa levis	-130.3715	-130.2500
Retecapsa neocomiana	-143.0732	-133.2059
Retecapsa octofenestratus	-143.8907	-130.2356
Retecapsa surirella	-139.6485	-130.1558
Rhabdolekiskus parallelus	-132.8665	-130.3715
Rhabdolithus rectus	-139.7230	-135.0540
Rhagodiscus angustus	-133.9498	-133.9498
Rhagodiscus asper	-148.0337	-130.0000
Rhagodiscus eboracensis	-134.5589	-134.5589
Rhagodiscus nebulosus	-140.7146	-136.0000
Rhagodiscus reightonensis	-135.2495	-133.4800
Rhagodiscus splendens	-142.9579	-130.0000
Rhynchodiniopsis aptiana	-133.6636	-132.5487
Rhynchodiniopsis fimbriata	-137.7466	***
Rodighieroites rutimeyeri	-136.3800	-136.1425
Rotelapillus laffittei	-144.9670	-130.0000
Rotelapillus radians	-143.5726	-143.5726
Rucinolithus irregularis	-130.7224	-130.1995
Rucinolithus terebrodentarius	-132.6331	-130.7224
Rucinolithus wisei	-141.4818	-134.8773
Sabaudiella riverorum	-130.1957	-130.1957
Salpingoporella genevensis	-131.4458	-130.4745
Sarasinella biformis	-136.9518	-136.5449
Sarasinella eucyrta	-139.0444	-137.4384
Sarasinella hirticula	-136.1425	-135.7165
Sarasinella longi	-137.8546	-137.7274
Sarasinella trezanensis	-138.7673	-137.4384
Sarasinella uhligi	-137.5366	-137.5366
Saynella clypeiformis	-133.5867	-133.4587
Saynoceras verrucosum	-136.9525	-135.2914
Scriniodinium attadalense	-135.1873	-130.0000
Sirmiodinium grossii	-134.7146	-134.7146
Sollasites horticus	-141.1526	-132.4596
Sollasites lowei	-130.5160	-130.5160
Sornayites gp. simionescui	-131.5833	-131.1877
Speetonia colligata	-141.5541	-131.3415
Spiniferites dentatus	-132.6670	-130.0000
Spiniferites ramosus	-137.4847	-130.0000
Spiniferites ramosus multibrevis	-138.2895	-133.4430
Spiticeras acutum	-145.8110	-143.2667
Spiticeras damesi	-142.1348	-139.3786
Spiticeras fraternum	-143.8400	-139.4232
Spiticeras gr. multiforme	-141.6945	-140.0091
Spiticeras pricei	-142.6245	-142.6245
Spiticeras pseudogroteanum	-145.4730	-144.9703
Spiticeras spitiense	-143.1259	-142.4513
Spiticeras tripartitum	-144.1585	-141.4983
Spitidiscus fasciger	-133.7912	-132.4590
Spitidiscus gr. lorioli	-134.5757	-134.0627
Spitidiscus gr. pavlowi	-133.9575	-133.5062
Spitidiscus hugii	-130.8141	-130.5385

Spitidiscus kilapiae	-131.8159	-131.8159
Spitidiscus riccardii	-131.8227	-131.7819
Staurolithites crux	-139.3556	-130.4350
Staurolithites mutterlosei	-138.7112	-132.4500
Stenosemellopsis hispanica	-139.5829	-138.7121
Stephanolithion laffittei	-140.1019	-132.4596
Stomiosphaera acculeata	-145.7712	-145.7712
Stomiosphaera echinata	-146.1865	-138.6887
Stomiosphaera proxima	-146.6375	-141.8957
Stomiosphaera wanneri	-143.8625	-138.8302
Stradneria crenulata	-143.3366	-130.0000
Sturiella oblonga	-141.1871	-141.1871
Subaspinoceras mulsanti	-131.3908	-131.3908
Suboosterella heliaca	-133.6962	-133.6962
Subpulchellia nicklesi	-130.5538	-130.1863
Subsaynella mimica	-132.1538	-132.1102
Subsaynella sayni	-132.2424	-131.8014
Substeueroceras calistoide	-146.2968	-144.0198
Substeueroceras ellipsostomum	-147.3397	-146.7469
Substeueroceras koeneni	-145.8110	-142.9481
Substeueroceras striolatissimum	-147.2261	-143.1007
Substreblites callomoni	-141.1798	-141.1798
Substreblites zonarius	-136.8009	-136.5815
Subthurmannia boissieri	-141.3556	-139.1912
Subthurmannia clareti	-142.8583	-142.8583
Subthurmannia floquinensis	-144.1311	-143.7469
Subthurmannia occitanica	-143.3864	-141.2972
Subthurmannia patruliusi	-142.8102	-142.0657
Subthurmannia subalpina	-143.9390	-143.6000
Subtilisphaera perlucida	-132.8252	-127.0475
Subtilisphaera senegalensis	-130.5538	-127.0475
Subtilisphaera terrula	-133.0018	-130.0000
Systematophora areolata	-139.7813	-137.6920
Systematophora fasciculigera	-136.5093	-136.5093
Systematophora palmula	-142.1618	-135.5812
Systematophora silybum	-137.1198	-133.4430
Tanyosphaeridium boletus	-138.8068	-130.2437
Tanyosphaeridium magneticum	-140.0724	-127.2312
Tanyosphaeridium salpinx	-143.6494	-130.0000
Tanyosphaeridium variecalamus	-132.8252	-130.0000
Taveraidiscus intermedius	-130.8609	-130.5522
Taveridiscus oosteri	-130.8600	-130.6916
Tegumentum stradneri	-135.9912	-130.2156
Teschenites callidiscus	-134.9787	-134.7782
Teschenites castellanensiformis	-134.7377	-134.5275
Teschenites flucticulus	-134.8125	-134.0898
Teschenites neocomiensiformis	-135.9202	-134.6758
Teschenites pachydicranus	-135.4482	-134.0898
Teschenites subflucticulus	-135.0247	-134.7406
Teschenites subpachydicranus	-134.9224	-134.7310
Tetrapodorhabdus coptensis	-139.0080	-130.2156
Tetrapodorhabdus decorus	-139.0080	-135.2414
Thurmanniceras gratianopolitense	-139.4667	-138.5064

Thurmanniceras otopeta	-140.2899	-138.3606
Thurmanniceras perisphinctoides	-139.9483	-139.8458
Thurmanniceras pertransiens	-139.4356	-137.9424
Thurmanniceras salientum	-139.9739	-139.9483
Thurmanniceras thurmanni	-142.6296	-137.9309
Tintinnopsella carpathica	-147.0565	-133.5600
Tintinnopsella dacica	-138.5053	***
Tintinnopsella doliphormis	-145.1938	-142.1260
Tintinnopsella longa	-144.1758	-133.5600
Tintinnopsella remanei	-147.6200	-144.4639
Tintinnopsella subacuta	-140.4337	-139.2093
Tirnovella alpillensis	-141.5873	-139.2418
Tirnovella occitanica	-145.7340	-145.6760
Tirnovella pertransiens	-139.4000	-137.7731
Tirnovella romani	-139.7667	-139.7640
Top Mulichino Fm	-137.3348	-135.3357
Toulisphinctes rafaeli	-148.3400	-147.1025
Toxaster retusus	-131.6265	-131.1899
Toxaster seynensis	-131.2138	-130.5724
Tranolithus gabalus	-139.0080	-130.0138
Tranolithus salillium	-138.8495	-134.1125
Trichodinium castanea	-136.6366	-133.7586
Tubodiscus jurapelagicus	-141.3878	-130.7939
Tubodiscus verenae	-140.7182	-133.3460
Andean tuff beds		
Tuff bed 139.24	-142.0638	***
Tuff bed 139.55	-141.6066	***
Tuff bed 139.96	-143.5496	***
Tuff bed 140.34	-144.6925	***
Tuff bed 142.04	-147.2261	***
Turnovella kayseri	-144.5726	-144.3114
Umbria granulosa	-147.4496	-139.1604
Umbria granulosa minor	-147.8161	***
Urgonina alpillensis	-131.4775	-130.4745
Vagalapilla compacta	-140.0507	-135.0643
Vagalapilla stradneri	-144.5798	-130.0000
Valanginites bachelardi	-138.3092	-135.2914
Valanginites nucleus	-136.9518	-135.4237
Valserina broennimanni	-131.2138	-130.5260
Valserina primitiva	-131.4775	-130.8539
Valserina turbinata	-130.7437	-130.5234
Varlheideites peregrinus	-136.3800	-135.0957
Vekshinella angusta	-133.7586	-130.9746
Vekshinella stradneri	-138.8495	-133.3458
Viluceras permolestus	-135.4249	-135.4249
Virgatosphinctes andesensis	-151.0000	-148.2974
Virgatosphinctes mendozanum	-149.7544	-148.2974
Virgatosphinctes scythicus	-149.3303	-148.9848
Wallodinium cylindrica	-138.8068	-130.0000
Wallodinium krutzschii	-142.2500	-130.0000
Wallodinium lunua	-134.1410	-133.1769
Watznaueria barnesae	-148.6707	-130.0000
Watznaueria biporta	-148.6707	-130.0161
Watznaueria britannica	-148.6707	-130.0000
Watznaueria communis	-148.6707	-130.0000
Watznaueria fossacincta	-148.6707	-130.1000
Watznaueria manivitiae	-148.6707	-131.1926
Watznaueria oblonga	-134.7194	-130.1032
Watznaueria ovata	-148.3400	-130.1558
Watznaueria supraretacea	-133.6164	-130.0390
Weavericeras vacaense	-133.3620	-132.9153
Windhauseniceras internispinosum	-148.3400	-146.3036
Windhauseniceras windhauseni	-147.6203	-147.6203
Wollemanniceras keilhacki anterior	-113.1000	-113.1000
Wollemanniceras keilhacki keilhacki	-113.1000	-113.1000
Zeugrhabdotus diplogrammus	-138.4768	-130.2117
Zeugrhabdotus embergeri	-150.3728	-130.0000
Zeugrhabdotus erectus	-146.5460	-130.1558
Zeugrhabdotus fluxus	-146.5460	-144.7867
Zeugrhabdotus pseudoangustus	-139.0080	-132.5414
Zeugrhabdotus trivectis	-134.9864	-133.5160
Zygodiscus bicrescenticus	-134.9580	-133.6510
Zygodiscus diplogrammus	-137.7970	-130.0000
Zygodiscus elegans	-141.0456	-130.0000
Zygodiscus erectus	-146.5460	-131.1695

Appendix 3: Sections and data (including taxa) that compose ANDESCS DB. Appendix 3. Andes.# are GraphCor catalog IDs. Preceding * means item not used.

Datum	Taxa/ morph	base (m)	top (m)
Andes.1 Lo Valdés, Chile [33°52'25.7"S 70°02'54.6"W]: Salazar Soto, 2012, Base Valanginian at 275 m @ FO *T. thurmanni*. Type section of Lo Valdés Formation 0-539 m; Tithonian-Berriasian boundary at base of sill 75 m.			
Argentiniceras fasciculatum	/am	280	320
Aulacosphinctes proximus	/am	125	200
Berriasella jacobi	/am	105	200
Corongoceras alternans	/am	10	50
Corongoceras evolutum	/am	15	45
Corongoceras involutum	/am	20	20
Corongoceras koeni	/am	20	50
Corongoceras koellikeri	/am	115	115
Corongoceras lotenoense	/am	15	45
Corongoceras multimum	/am	15	15
Corongoceras mendozanum	/am	20	20
Crioceratites andinum	/am	525	525
Crioceratites diamantense	/am	525	530
Crioceratites perditum	/am	526	526
Cuyaniceras transgrediens	/am	270	270
Frenguelliceras magister	/am	280	345
Groebericeras rocardi	/am	245	245
Lytohoplites vareloe	/am	35	65
Lytohoplites vouloi	/am	15	45
Lytohoplites zambranoi	/am	10	70

Malbosiceras malbosi	/am	180	200
Micracanthoceras microcanthum	/am	20	45
Micracanthoceras spinulosum	/am	45	160
Spiticeras acutum	/am	205	205
Spiticeras spitiense	/am	285	285
Spiticeras tripartitum	/am	175	315
Substeueroceras calistoide	/am	35	65
Substeueroceras koeneni	/am	100	245
Thurmanniceras thurmanni	/am	280	320
Andes.2 Cajón del Morado, Chile [33°48'06.1"S 70°04'12.4"W]: Salazar Soto, 2012. Lo Valdés Formation 0-580 m; Tithonian-Berriasian boundary at ~160-165 m; Base Valanginian at 290 m FO *T. thurmanni*; base Hauterivian between 370-540 at FO *C. diamantense*.			
Argentiniceras fasciculatum	/am	290	345
Aspidoceras rogoznicensis	/am	75	75
Aulacosphinctes proximus	/am	173	305
Berriasella jacobi	/am	300	300
Chigaroceras loteroense	/am	115	173
Corongoceras alternans	/am	45	75
Corongoceras involutum	/am	26	26
Corongoceras koellikeri	/am	165	165
Crioceratites andinum	/am	540	540
Crioceratites diamantense	/am	540	540
Crioceratites perditum	/am	550	550
Frenguelliceras magister	/am	270	345
Groebericeras rocardi	/am	270	273
Lytohoplites vareloe	/am	26	100
Lytohoplites vouloi	/am	26	115
Lytohoplites zambranoi	/am	100	100
Micracanthoceras microcanthum	/am	105	105
Micracanthoceras spinulosum	/am	300	305
Neocosmoceras sayni	/am	271	273
Pseudofavrella angulatiformis	/am	290	300
Spiticeras pricei	/am	290	290
Spiticeras spitiense	/am	271	300
Spiticeras tripartitum	/am	240	355
Substeueroceras calistoide	/am	26	300
Substeueroceras koeneni	/am	225	255
Substeueroceras striolatissimum	/am	273	273
Thurmanniceras thurmanni	/am	290	370
Andes.3 Cruz de Piedra, Chile [34°13'50.5"S 69°56'33.0"W]: Salazar Soto, 2012. Lo Valdés Formation 0-150 m; Base of section @ contact of Lo Valdes Fm.; Tithonian-Berriasian contact ~85-95m.			
Aspidoceras rogoznicensis	/am	120	120
Aulacosphinctes proximus	/am	90	120
Berriasella jacobi	/am	90	130
Corongoceras koellikeri	/am	140	140
Corongoceras mendozanum	/am	50	120
Cuyaniceras transgrediens	/am	140	150
Micracanthoceras microcanthum	/am	50	50
Micracanthoceras spinulosum	/am	50	90
Micracanthoceras vetustum	/am	100	120
Pterolytoceras exoticum	/am	110	110
Spiticeras acutum	/am	150	150
Substeueroceras calistoide	/am	50	110
Substeueroceras koeneni *Occurrence at 70 is too low	/am	90	130
Substeueroceras striolatissimum	/am	100	150
Turnovella kayseri	/am	100	110
Andes.4 Rio Maitenes, Chile [35°00'25.6"S 70°23'18.2"W]: Salazar Soto, 2012. Lo Valdés Formation 0-535 m. Tithonian-Berriasian boundary at 400 m.			
Aulacosphinctes proximus	/am	165	200
Catutosphinctes cf. *americanensis*	/am	180	180
Choicensisphinctes windhauseni	/am	130	165
Corongoceras alternans	/am	360	360
Corongoceras evolutum	/am	360	360
Euvirgalithacoceras malarguense	/am	130	165
Micracanthoceras microcanthum	/am	360	360
Micracanthoceras spinulosum	/am	360	360
Pseudolissoceras cf. *zitteli*	/am	165	165
Substeueroceras koeneni	/am	430	430
Virgatosphinctes scythicus *= *V. mexicanus*	/am	125	145
Windhauseniceras internispinosum	/am	190	205
Andes.5 Las Loicas, Argentina [35°46'59.9"S 70°09'W]: Vennari *et al.*, 2014. CA-ID-TIMS age 139.6+/-0.09/0.18 Ma" at about 58 m. Vennari, 2016. Vaca Muerta Fm. overlies Tordillo Fm., Figs. 4, 20. Lena *et al.*, 2019, Fig. 2; dated U-Pb zircons in 4 ash beds by CA-ID-TIMS 206Pb/238U: beds LL3-139.238+/-0.0.49Ma, LL9-139.956+/-0.063Ma, LL10-140.338+/-0.083Ma, LL13-142.039+/-0.058Ma. Lopez-Martinez *et al.*, 2017a, Fig.1.			
*Lena *et al.*, 2019, Fig. 2			
Tuff bed 139.24	/mb	-54	***
Tuff bed 139.96	/mb	-41	***
Tuff bed 140.34	/mb	-31	***
Tuff bed 142.04	/mb	-2	***
*Vennari, 2016			
Argentiniceras cf. *fasciculatum*	/am	-38	-38
Argentiniceras noduliferum	/am	-53	-66?
Berriasella subprivasensis	/am	-36	-36
Blanfordiceras sp. vetustum	/am	-35	-35
Cuyaniceras transgrediens	/am	-58?	-68
Paradontoceras calistoides	/am	-23	-25
Spiticeras acutum	/am	-25	-25
Substeueroceras ellipsostomum	/am	-0?	-2
Substeueroceras striolatissimum	/am	-2	-2
Euvirgalithacoceras malarguense	/am	-3	4.5
Indansites malarguensis	/am	-3	-4.5

Pseudinvoluticeras primoridalis	/am	-3	-4.5
Pseudolissoceras zitteli	/am	-7	-10
*Lopez-Martinez *et al.*, 2017a, Fig. 1			
Argentiniceras noduliferum	/am	-33	-54
**Berriasella* sp.	/am	-25	-25
Berriasella subprivasensis	/am	-36	-36
Blanfordiceras sp. *vetustum*	/am	-35	-35
Cuyaniceras transgrediens	/am	-58	-68
Lytohoplites burckhardti	/am	-17	-18
**Neocosmoceras* sp.	/am	-60	-60
Paradontoceras calistoides	/am	-23	-25
Spiticeras acutum	/am	-25	-25
Substeueroceras ellipsostomum	/am	-1	-10
Substeueroceras koeneni	/am	-25	-25
Substeueroceras striolatissimum	/am	-2	-2
Calpionella alpina	/ca	-14	-41
Crassicollaria brevis	/ca	-15.5	-33
Crassicollaria colomi	/ca	-15	-15
Crassicollaria parvula	/ca	-15	-15
Crassicollaria massutiniana	/ca	-15	-36
Tintinnopsella carpathica	/ca	-32	-33
Tintinnopsella remanei	/ca	-15	-33
*Vennari *et al.*, 2014, Fig. 3:			
Biscutum constans	/nn	-23	-44
Cyclagelosphaera deflandrei	/nn	-32.5	32.5
Cyclagelosphaera margerelii	/nn	0	-48
Diazomatolithus lehmanii	/nn	-15	-15
Eiffellithus primus	/nn	-17	-36
Manivitella pemmatoidea	/nn	32.5	-35.5
Nannoconus cornutus	/nn	-24.5	-35.5
Nannoconus kamptneri minor	/nn	-33	-37
Nannoconus steinmannii minor	/nn	-35.5	-35.5
Nannoconus wintereri	/nn	-32.5	-35.5
Polycostella senaria	/nn	-20	-37
Rhagodiscus asper	/nn	-26	-38
Umbria granulosa	/nn	-15	-36
Watznaueria barnesae	/nn	0	-58
Watznaueria biporta	/nn	0	-47.5
Watznaueria britannica	/nn	-2	-48
Watznaueria fossacincta	/nn	0	-66
Watznaueria manivitiae	/nn	-15	-34
Watznaueria ovata	/nn	0	-32
Zeugrhabdotus embergeri	/nn	-17.5	-48
Zeugrhabdotus erectus	/nn	-15	-34
Watznaueria barnesae	/nn	0	-58
Andes.6 Pampa Tril, Argentina [37°13'59.9"S 69°49'00.1"W]: Parent *et al.*, 2015. Vaca Muerta Fm., Tithonian-lower Valanginian, Figs. 2, 5, 421.6 m thick; Overlies Tordillo Fm., underlies Quintuco Fm.			
Argentiniceras noduliferum	/am	155	155
Aspidoceras depressus ID as cf.	/am	183	183
Aulacosphinctes proximus ID as *Catutosphinctes ?*	/am	39	42
Blanfordiceras vetustum	/am	101	123
Catutosphinctes guenenokenensis	/am	2	6

Catutosphinctes inflatus	/am	82	102
Catutosphinctes proximus	/am	39	42
Choicensisphinctes burckhardti	/am	5	28
Choicensisphinctes erinoides	/am	17	28
Choicensisphinctes platyconus	/am	2	6
Choicensisphinctes striolatus	/am	105	135
Cieneguiticeras falculatum	/am	21	28
Cieneguiticeras cf. *perlaevis*	/am	17	21
Corongoceras mendozanum	/am	63?	101
Corongoceras steinmanni	/am	101	101
Cuyaniceras transgrediens	/am	183	183
Groebericeras bifrons	/am	154	154
Haploceras staszycii	/am	21	28
Himalayites cf. *treubi*	/am	139	139
Krantziceras azulense	/am	105	105
Krantziceras compressum	/am	154	155
Krantziceras disputabile	/am	63	63
Krantziceras planulatum	/am	146	149
Lissonia riveroi	/am	231	285
Lithoceras picunleufuense	/am	2	6
Lytoceras montanum	/am	109	109
Mazatepites arredondense	/am	21	21
Neocosmoceras malbosiforme	/am	183	192
Neocomites wichmanni	/am	211	213
Paradontoceras calistoides	/am	87	109
Pasottia andina	/am	21	28
Pseudhimalayites subpretiosus	/am	42	42
Pseudolissoceras zitteli	/am	17	28
Raimondiceras alexandrense	/am	164	164
Spiticeras fraternum	/am	183	183
Substeueroceras koeneni	/am	137	139
Subthurmannia boissieri	/am	164	209
Toulisphinctes cf. *rafaeli*	/am	42	63
Windhauseniceras internispinosum	/am	42	43
Andes.7 El Portón, Argentina [37°11'52.1"S 69°41'03.1"W]: Aguirre-Urreta *et al.*, 2017, Fig. 3; Aguirre-Urreta *et al.*, 2019, Figs. 3-4.			
Top Mulichino	/mb	0	0
Agrio tuff bed 126.97	/mb	-660	***
Agrio tuff bed 130.40	/mb	-180	***
Assipetra terebrodentarius	/nn	-640	-645
Biscutum constans	/nn	-527	-527
Bukrylithus ambiguus	/nn	-580	-580
Clepsilithus maculosus	/nn	-470	-650
Cretarhabdus conicus	/nn	-43	-580
Cretarhabdus striatus	/nn	-75	-625
Cretarhabdus surirellus ID in *Retacapsa*	/nn	-135	-660
Crucibiscutum nequenensis	/nn	-460	-517
Cruciellipsis cuvillieri	/nn	-55	-465
Cyclagelosphaera deflandrei	/nn	-502	-582
Cyclagelosphaera margerelii	/nn	-5	-650
Diazomatolithus lehmanii	/nn	-127	-470
Eiffellithus striatus	/nn	-15	-460
Eiffellithus windi	/nn	-15	-175
Eprolithus floralis	/nn	-527	-542
Ethmorhabdus hauterivianus	/nn	-517	-625
Helenea chiastia	/nn	-165	-625

Lithraphidites bollii	/nn	-465	-650
Lithraphidites carniolensis	/nn	-185	-655
Manivitella pemmatoidea	/nn	-125	-617
Markalius inversus	/nn	-592	-592
Micrantholithus hoschulzii	/nn	-5	-667
Micrantholithus obtusus	/nn	-5	-662
Nannoconus bucheri	/nn	-185	-655
Nannoconus circularis	/nn	-95	-650
Nannoconus elongatus	/nn	-190	-592
Nannoconus globulus globulus	/nn	-43	-662
Nannoconus globulus minor	/nn	-43	-274
Nannoconus kamptneri	/nn	-43	-662
Nannoconus ligius	/nn	-517	-622
Nannoconus steinmannii	/nn	-147	-662
Nannoconus truitti	/nn	-260	-622
Percivalia fenestrata	/nn	-205	-650
Retecapsa angustiforata	/nn	-185	-640
Retecapsa octofenestratus	/nn	-475	-650
Retecapsa surirella	/nn	-135	-660
Rhagodiscus asper	/nn	-33	-655
Staurolithites crux	/nn	-140	-625
Tubodiscus jurapelagicus	/nn	-267	-580
Tubodiscus verenae	/nn	-260	-260
Watznaueria barnesae	/nn	-5	-662
Watznaueria biporta	/nn	-15	-662
Watznaueria fossacincta	/nn	-5	-667
Watznaueria manivitiae	/nn	-502	-530
Watznaueria ovata	/nn	-490	-660
Zeugrhabdotus embergeri	/nn	-5	-635
Zeugrhabdotus erectus	/nn	-157	-660
Zeugrhabdotus diplogrammus	/nn	-160	-653
Chacantuceras ornatum	/am	-35	-50
Crioceratites andinum	/am	-493	-494
Crioceratites diamantense	/am	-489	-494
Crioceratites perditum	/am	-498	-501
Crioceratites schlagintweiti	/am	-463	-465
Decliveites agrioensis	/am	-117	-135
Decliveites crassicostatum	/am	-88	-88
Holcoptychites agrioensis	/am	-170	-178
Holcoptychites magdalensae	/am	-140	-161
Hoplytocrioceris gentilli	/am	-205	-225
Hoplytocrioceris giovinei	/am	-195	-198
Olcostephanus laticosta	/am	-182	-188
Paraspiticeras groeberi	/am	-459	-618
Pseudofavrella australe	/am	-34	-34
Pseudofavrella garatei	/am	-2	-5
Sabaudiella riverorum	/am	-655	-655
Viluceras permolestus	/am	-1	-1
Weavericeras vacaense	/am	-258	-314
Andes.7b El Portón, Argentina [37°11'52.1"S 69°41'03.1"W]: Aguirre-Urreta *et al.*, 2019. Pilmatue Mbr. 0-317 m; Avilé Mbr. Agua de la Mula Mbr. 447-700 m.			
Marker tuff bed 126.97	/mb	-660	***
Marker tuff bed 130.40	/mb	-170	***
Assipetra terebrodentarius	/nn	-640	-645
Biscutum constans	/nn	-527	-527
Bukrylithus ambiguus	/nn	-580	-580
Clepsilithus maculosus	/nn	-470	-650
Cretarhabdus conicus	/nn	-43	-580
Cretarhabdus striatus	/nn	-75	-625
Cretarhabdus surirellus ID as *Retacapsa*	/nn	-135	-660
Crucibiscutum nequenensis	/nn	-460	-517
Cruciellipsis cuvillieri	/nn	-55	-465
Cyclagelosphaera deflandrei	/nn	-502	-582
Cyclagelosphaera margerelii	/nn	-5	-650
Diazomatolithus lehmanii	/nn	-127	-470
Eiffellithus striatus	/nn	-15	-460
Eiffellithus windi	/nn	-15	-175
Eprolithus floralis	/nn	-527	-542
Ethmorhabdus hauterivianus	/nn	-517	-625
Helenea chiastia	/nn	-165	-625
Lithraphidites bollii	/nn	-465	-650
Lithraphidites carniolensis	/nn	-185	-655
Manivitella pemmatoidea	/nn	-125	-617
Markalius inversus	/nn	-592	-592
Micrantholithus hoschulzii	/nn	-5	-667
Micrantholithus obtusus	/nn	-5	-662
Nannoconus bucheri	/nn	-185	-655
Nannoconus circularis	/nn	-95	-650
Nannoconus elongatus	/nn	-190	-592
Nannoconus globulus globulus	/nn	-43	-662
Nannoconus globulus minor	/nn	-43	-274
Nannoconus kamptneri	/nn	-43	-662
Nannoconus lignus	/nn	-517	-622
Nannoconus steinmannii	/nn	-147	-662
Nannoconus truitti	/nn	-260	-622
Percivalia fenestrata	/nn	-205	-650
Retecapsa angustiforata	/nn	-185	-640
Retecapsa octofenestratus	/nn	-475	-650
Retecapsa surirella	/nn	-135	-660
Rhagodiscus asper	/nn	-33	-655
Staurolithites crux	/nn	-140	-625
Tubodiscus jurapelagicus	/nn	-267	-580
Tubodiscus verenae	/nn	-260	-260
Watznaueria barnesae	/NN	-5	-662
Watznaueria biporta	/NN	-15	-662
Watznaueria fossacincta	/NN	-5	-667
Watznaueria manivitiae	/NN	-502	-530
Watznaueria ovata	/NN	-490	-660
Zeugrhabdotus embergeri	/NN	-5	-635
Zeugrhabdotus erectus	/NN	-157	-660
Zeugrhabdotus diplogrammus	/nn	-160	-653
Chacantuceras ornatum	/am	-35	-50
Crioceratites andinum	/am	-493	-494
Crioceratites diamantense	/am	-489	-494
Crioceratites perditum	/am	-498	-501
Crioceratites schlagintweiti	/am	-463	-465
Decliveites agrioensis	/am	-117	-135
Decliveites crassicostatum	/am	-88	-88
Holcoptychites agrioensis	/am	-170	-178
Holcoptychites magdalensae	/am	-140	-161
Hoplytocrioceris gentilli	/am	-205	-225
Hoplytocrioceris giovinei	/am	-195	-198
Olcostephanus laticosta	/am	-182	-188
Paraspiticeras groeberi	/am	-459	-618
Pseudofavrella australe	/am	-34	-34
Pseudofavrella garatei	/am	-2	-5
Sabaudiella riverorum	/am	-655	-655
Viluceras permolestus	/am	-1	-1

Weavericeras vacaense	/am	-258	-314
Andes.8 Real de las Coloradas, Argentina [34°01'59.9"S 69°43'59.9"W]: VENNARI, 2016. Vaca Muerta Fm. overlies Tordillo Fm. Revises PARENT's taxonomy(2011).			
Choicensisphinctes choicensis = *C. platyconus* PARENT	/am	8	10
Choicensisphinctes platyconus	/am	1	10
Cieneguiticeras perlaevis	/am	8	18
Pseudinvoluticeras douvillei = *C. lotenoensis* PARENT	/am	9	12
Pseudinvoluticeras primoridalis = *C. platyconus* PARENT	/am	1	8
Pseudolissoceras zitteli	/am	10	18
Virgatosphinctes andesensis	/am	10	12
Virgatosphinctes mendozanum	/am	10	12
Andes.9 Cerro Domuyo, Argentina [36°40'59.9"S 70°25'59.9"W]: VENNARI, 2016. Vaca Muerta Fm. overlies Tordillo Fm. Revises PARENT's taxonomy (2011).			
Choicensisphinctes choicensis = *C. platyconus* PARENT	/am	3	5
Choicensisphinctes platyconus	/am	3	5
Choicensisphinctes erinoides	/am	26	40
Pseudinvoluticeras douvillei	/am	3	3
Pseudolissoceras zitteli	/am	26	40
Virgatosphinctes andesensis	/am	0	0
Andes.10 Mina San Eduardo Composite Section, Argentina [~37°32'25.1"S 70°22'00.1"W]:AGUIRRE-URRETA *et al.*, 2015, Fig. 2; 0-505 m Agrio Fm. Agua de la Mula Mbr. overlies Avilé Mbr., underlies Huitrín Fm. Inoceramid from LAZO, 2006.			
Agrio tuff bed 127.42	/mb	-470	***
Agrio tuff bed 129.09	/mb	-10	***
Crioceratites diamantense	/am	-90	***
Crioceratites schlagintweiti	/am	-40	***
Paraspiticeras groeberi	/am	-410	-470
Sabaudiella riverorum	/am	-480	***
Spitidiscus kilapiae	/am	-2	-2
Spitidiscus riccardii	/am	0	-12
Clepsilithus maculosus	/nn	-15	-410
Cruciellipsis cuvillieri	/nn	-27	-80
Lithraphidites bollii	/nn	-65	-440
Nannoconus ligius	/nn	-365	-470
Neocomiceramus curacoensis	/bi	-45	-190
Andes.11 Arroyo Truquico, Neuquén, Argentina [37°26'06.0"S 70°37'53.4"W]: AGUIRRE-URRETA., 1998, Fig. 2. Lower member Agrio Fm. overlies Mulichino Fm. at 0 m;			
Top Mulichino	/mb	18	18
Karakaschiceras attenuatus	/am	40	70
Karakaschiceras neumayri	/am	35	35
Neohoploceras arnoldi	/am	35	40
Olcostephanus atherstoni	/am	25	35
Pseudofavrella angulatiformis	/am	145	145
Pseudofavrella garatei	/am	145	145

Andes.12 Cerro La Parva, Neuquén, Argentina [37°15'46.1"S 70°30'47.9"W]: AGUIRRE-URRETA, 1998, Fig. 2. Lower member Agrio Fm. overlyies Mulichino Fm., Valanginian.			
Top Mulichino	/mb	-10	-10
Karakaschiceras attenuatus	/am	30	73
Karakaschiceras neumayri	/am	20	22
Neohoploceras arnoldi	/am	20	22
Olcostephanus atherstoni	/am	5	22
Pseudofavrella angulatiformis	/am	115	115
Andes.13 Arroyo Loncoche, Argentina [35°31'40.4"S 69°39'07.9"W]: KIETZMANN *et al.*, 2018, Figs. 3, 6; IGLESIA LLANOS *et al.*, 2017.			
Andes J-K SB 4	/MB	270	***
Andes J-K SB 3	/MB	215	***
Andes J-K SB 2	/MB	149	***
Andes J-K SB 1	/MB	75	***
Andiceras acuticostum ID cf.	/am	65	70
Argentiniceras noduliferum	/am	220	225
Aulacosphinctes proximus	/am	60	70
Blanfordiceras vetustum ID cf.	/am	150	153
Catutosphinctes americanensis	/am	105	105
Choicensisphinctes cf. *erinoides*	/am	18	35
Corongoceras lotenoense	/am	140	145
Corongoceras cf. *mendozanum*	/am	135	135
Cuyaniceras raripartitum	/am	225	230
Cuyaniceras transgrediens	/am	240	255
Laeviaptychus crassissimus	/am	25	50
Laeviaptychus latus	/am	70	117
Micracanthoceras lamberti	/am	90	90
Pseudinvoluticeras sp. *primoridalis*	/am	10	12
Pseudolissoceras zitteli	/am	25	60
Spiticeras damesi	/am	220	275
Substeueroceras koeneni	/am	183	185
Virgatosphinctes andesensis	/am	0	5
Windhauseniceras internispinosum	/am	75	90
Data from KIETZMANN *et al.*, 2011, Fig. 3			
Eiffellithus primus	/nn	67	***
Polycostella beckmannii	/nn	62	***
Polycostella senaria	/nn	121	***
Umbria granulosa	/nn	82	***
Data from IGLESIA LLANOS *et al.*, 2017			
Magnetochron M15r	/MA	***	
Magnetochron M16n	/MA	***	260
Magnetochron M16r	/MA	***	240
Magnetochron M17n	/MA	***	215
Magnetochron M17r	/MA	***	200
Magnetochron M18n	/MA	***	190
Magnetochron M18r	/MA	***	180
Magnetochron M19n	/MA	***	160
*Magnetochron M19n.1r	/MA	***	
*Magnetochron M19n.2n	/MA	***	
Magnetochron M19r	/MA	***	147

Magnetochron M20n	/MA	***	135
Magnetochron M20n.1r	/MA	***	125
Magnetochron M20n.2n	/MA	***	118
*Magnetochron M20r	/MA	***	
Magnetochron M21n	/MA	***	75
Magnetochron M21r	/MA	***	58
Andes.14 Cuesta del Chihuido, Argentina [35°45'39.6"S 69°42'35.3"W]: *KIETZMANN *et al.*, 2018, Fig. 3; IGLESIA LLANOS *et al.*, 2017. Vaca Muerta Fm., Tithonian-Berriasian. Reported section thickness 185 m. *KIETZMANN *et al.*, 2021a [35°44'49.6"S 69°34'37.2"W]			
Andes J-K SB 4	/MB	195	*
Andes J-K SB 3	/MB	164	*
Andes J-K SB 2	/MB	113	*
Andes J-K SB 1	/MB	58	*
Argentiniceras bituberculatum cf.?	/am	165	168
Aulacosphinctes proximus	/am	72	75
Blanfordiceras vetustum	/am	114	117
Choicensisphinctes erinoides cf.?	/am	32	72
Corongoceras mendozanum cf.?	/am	80	110
Laeviaptychus crassissimus	/am	10	58
Laeviaptychus latus	/am	65	80
Neocomites wichmanni cf.?	/am	200	200
Pseudinvoluticeras primordialis sp.?	/am	17	32
Pseudolissoceras zitteli	/am	30	45
Spiticeras damesi cf.?	/am	170	175
Substeueroceras koeneni sp.?	/am	120	152
**Virgatosphinctes andesensis* sp.? * defines base of *V. andesensis* Zone	/am	0	32
Virgatosphinctes mendozanum	/am	0	32
Windhauseniceras internispinosum	/am	60	78
Windhauseniceras windhauseni	/am	60	75
*KIETZMAN *et al.,* 2021a			
Borzaiella slovenica	/dn	50	61
Chitinoidella boneti	/dn	59	87
Chitinoidella hegarati	/dn	59	59
Calpionella alpina	/ca	110	155
Calpionella elliptalpina	/ca	118	121
Calpionella elliptica	/ca	155	155
Calpionella grandalpina	/ca	89	128
Calpionellites darderi	/ca	200	200
Calpionellopsis oblonga	/ca	190	200
Calpionellopsis simplex	/ca	160	200
Crassicollaria brevis	/ca	110	119
Crassicollaria massutiniana	/ca	89	100
Crassicollaria parvula	/ca	114	128
Lorenziella hungarica	/ca	160	200
Tintinnopsella carpathica	/ca	72	175
Tintinnopsella doliphormis	/ca	195	200
Tintinnopsella longa	/ca	155	185
Tintinnopsella remanei	/ca	72	89
Andes.15 Bardas Blancas, Argentina [35°52'40.8"S 69°54'32.0"W]: KIETZMANN *et al.*, 2018, Fig. 3. Vaca Muerta Fm.			
Andes J-K SB 4	/MB	235	***
Andes J-K SB 3	/MB	180	***
Andes J-K SB 2	/MB	110	***
Andes J-K SB 1	/MB	50	***
Andiceras cf. *acuticostum*	/am	80	80
Berriasella sp.	/am	108	119
Chigaroceras loteroense	/am	72	72
Choicensisphinctes choicensis	/am	5	20
Cuyaniceras raripartitum	/am	205	205
Laeviaptychus crassissimus	/am	26	30
Lissonia riveroi	/am	270	270
Neocomites cf. *wichmanni*	/am	240	242
Spiticeras acutum	/am	160	160
Substeueroceras koeneni	/am	113	158
Substeueroceras striolatissimum	/am	100	100
Virgatosphinctes andesensis	/am	18	18
Virgatosphinctes mendozanum	/am	3	3
Windhauseniceras internispinosum	/am	50	70
Andes.16 Arroyo Rahue, Argentina [35°59'56.8"S 69°56'35.9"W]: KIETZMANN *et al.*, 2018, Fig. 3. Vaca Muerta Fm.			
Andes J-K SB 4	/MB	205	***
Andes J-K SB 3	/MB	158	***
Andes J-K SB 2	/MB	91	***
Andes J-K SB 1	/MB	25	***
Argentiniceras noduliferum	/am	160	160
Blanfordiceras vetustum	/am	100	100
Corongoceras lotenoense	/am	45	50
?Neocomites crassicostatum	/am	180	183
Laeviaptychus latus	/am	20	30
Micracanthoceras lamberti	/am	60	60
Pseudinvoluticeras douvillei	/am	10	10
Pseudolissoceras zitteli	/am	7	15
Spiticeras damesi	/am	190	195
Substeueroceras cf. striolatissimum	/am	92	105
Virgatosphinctes andesensis	/am	4	4
Virgatosphinctes mendozanum	/am	4	4
Windhauseniceras internispinosum	/am	25	30
Windhauseniceras windhauseni	/am	20	20
Andes.17 Los Catutos, Argentina [38°49'12.0"S 70°10'12.0"W]: LÓPEZ-MARTÍNEZ *et al.*, 2017b, Fig. 6. Vaca Muerta Fm., Los Catutos Mbr. overlies Tordillo Fm.			
Aspidoceras aff. *euomphalum*	/am	81	81
Aspidoceras quinchaoi	/am	77	95
Aulacosphinctes proximus	/am	32	52
Choicensisphinctes erinoides	/am	3	16
Choicensisphinctes choicensis	/am	3	6
Corongoceras cf. *praecursor*	/am	35	35
Djurjuriceras catutosense	/am	91	95
Pseudinvoluticeras douvillei	/am	0	6
Pseudinvoluticeras primoridalis	/am	0	6
Pseudolissoceras zitteli	/am	18	22
Toulisphinctes rafaeli	/am	57	60
*ID as *Catutosphinctes*	/am		

Windhauseniceras internispinosum	/am	61	95
Magnetochron M20n.2n	/ma	*	87
Magnetochron M20r	/ma	*	61
Magnetochron M21n	/ma	*	51
Magnetochron M21r	/ma	*	37
Magnetochron M22n	/ma	*	30
Magnetochron M22r	/ma	*	5
Andes.18a Bajada Viejo, Neuquén Basin, Argentina [38°22'S 70°W]: Lazo *et al.*, 2009, Fig. 2a. The Agrio Formation age @ 235m 136.4 Ma by biostratigraphic correlation. Valanginian-Hauterivian Stage boundary at 235 m at FAD *Holcoptychites neuquensis*.			
Top Mulichino	/mb	0	0
Clepsilithus maculosus	/nn	70	***
Eiffellithus striatus	/nn	8	***
Nannoconus bucheri	/nn	68	***
Nannoconus circularis	/nn	68	***
Chacantuceras ornatum	/am	32	***
Holcoptychites agrioensis	/am	315	***
Holcoptychites neuquensis	/am	235	***
Hoplytocrioceris gentilli	/am	412	***
Hoplytocrioceris giovinei	/am	408	***
Neocomites crassicostatum	/am	79	***
Neocomites wichmanni	/am	79	***
Olcostephanus laticosta	/am	388	***
Pseudofavrella angulatiformis	/am	3	***
Weavericeras vacaense	/am	446	***
Andes.18b Bajada del Agrio, Neuquén Basin, Argentina [38°22'S 70°W]: Lazo *et al.*, 2009, Fig. 2b. The Agrio Formation ages @ 5m 133.8 Ma & @ 470m = 130.0 Ma by biostratigraphic correlation. Hauterivian-Barremian Stage boundary at 470 m in *Paraspiticeras groeberi* Zone.			
Top Avilé Member	/mb	0	0
Clepsilithus maculosus	/nn	***	432
Eiffellithus striatus	/nn	8	***
Nannoconus bucheri	/nn	***	390
Neocomiceramus curacoensis	/bi	138	***
Crioceratites andinum	/am	78	***
Crioceratites diamantense	/am	78	***
Paraspiticeras groeberi	/am	417	***
Spitidiscus riccardii	/am	5	***
Andes.19 Arroyo Cieneguita, Neuquén Basin, Argentina [35°33'S 69°24'W]: Parent *et al.*, 2011. Vaca Muerta Fm., Tithonian-lower Valanginian, Fig. 2, 143 m thick. Overlies Upper Jurassic Tordillo Fm. sandstone.			
Aspidoceras cf. *euomphalum*	/am	28	100
Blanfordiceras vetustum	/am	95	110
Catutosphinctes guenenokenensis	am	0	7
Catutosphinctes inflatus	/am	89	10
Catutosphinctes proximus	/am	28	71
Choicensisphinctes platyconus	/am	0	3
Choicensisphinctes striolatus	/am	110	111
Cieneguiticeras falculatum	/am	28	49
Cieneguiticeras cf. *perlaevis*	/am	0	21
Corongoceras mendozanum	/am	89	100
Cuyaniceras transgrediens	/am	123	130
Groebericeras bifrons	/am	117	123
Lithoceras picunleufuense	/am	0	3
Mazatepites arredondense	/am	21	36
Paradontoceras calistoides	/am	95	111
Pasottia andina	/am	11	18
Pseudhimalayites subpretiosus	/am	28	36
Pseudolissoceras zitteli	/am	11	21
Spiticeras fraternum	/am	117	130
Substeueroceras koeneni	/am	110	111
Toulisphinctes rafaeli ID as cf.	/am	28	49
Windhauseniceras internispinosum	/am	49	71
Andes.22 Composite Chos Malal Section, Argentina [37°28'08.4"S 69°58'46.6"W]: Composed of **Andes 6 Pampa Tril, Argentina**, Parent *et al.*, 2015. Vaca Muerta Fm., Tithonian-lower Valanginian, Figs. 2, 5, 421.6 m thick; Overlies Upper Jurassic Tordillo Fm. sandstone and underlies lower Valanginian Quintuco Fm. claystone. **Puerta Curaco section**, Schwarz *et al.*, 2006, Fig. 11, Mulichinco Fm. 340m, base on Vaca Muerta, top at Agrio; add 630 m to all below: **Andes.7 El Porton Section, Argentina** [37°11'52.1"S 69°41'03.1"W]: Aguirre-Urreta *et al.*, 2017, Fig. 3; Aguirre-Urreta *et al.*, 2019, Figs. 3-4. Radiometric date @ 660m 126.97+/-0.04 Ma = 1290 Radiometric date @ 180m 130.39+/-0.16 Ma = 810 Mulichinco Fm. overlain by Agrio Fm., Pilmatue Mbr. base at 0m; Avile Mbr. continental deposits 317-437 m; Hauterivian Stage duration 5.21+/-0.08 myr from 131.29 to 126.08+/-0.19 Ma. **Andes.22b, Puerta Curaco, Argentina** [37°22'26.0"S 69°56'17.2"W]: Kietzman *et al.*, 2021a (37°22'26.2"S 69°56'17.2"W); ss *V. andesensis* to *S. damesi* zones. *Kietzmann *et al.*, 2018.			
*Zones on chart Fig. 6.			
**Neocomites wichmanni*	/am	265	360
**Spiticeras damesi*	/am	160	265
**Argenticeras noduliferum*	/am	140	160
**Substeueroceras koeneni*	/am	85	140
**Corongoceras alternans*	/am	65	85
**Windhauseniceras internispinosum*	/am	40	65
**Aulacosphinctes proximus*	/am	30	40
**Pseudolissoceras zitteli*	/am	10	30
**Virgatosphinctes andesensis*	/am	0	10
*Kietzmann *et al.*, 2021a, Fig.			

6.			
Borzaiella slovenica	/dn	20	92
Chitinoidella boneti	/ca	40	45
Calpionella alpina	/ca	92	265
Calpionella elliptalpina	/ca	92	92
Calpionella elliptica	/ca	195	265
Calpionella grandalpina	/ca	80	120
Calpionellites darderi	/ca	310	310
Calpionellopsis oblonga	/ca	225	360
Calpionellopsis simplex	/ca	165	300
Crassicollaria brevis	/ca	165	165
Crassicollaria massutiniana	/ca	60	15
Crassicollaria parvula	/ca	70	70
Lorenziella hungarica	/ca	195	290
Tintinnopsella carpathica	/ca	55	360
Tintinnopsella remanei	/ca	55	80
Andes.23 Las Tapaderas, Argentina [estimated: 35°24'S 70°18'W]: *KIETZMANN *et al.*, 2021b, Fig. 3. base conformable above Tordillo Fm.; top overlain by Pleistocene volcanics			
Aulacosphinctes proximus	/am	0	2
Corongoceras alternans	/am	35	38
Corongoceras lotenoense ID ?	/am	8	8
Corongoceras praecursor	/am	20	20
Substeueroceras koeneni	/am	61	61
Chitinoidella boneti	/ca	8	42
Calpionella alpina	/ca	35	64
Calpionella elliptica	/ca	64	64
Calpionella grandalpina	/ca	25	25
Crassicollaria brevis	/ca	35	40
**Crassicollaria colomi* ID ? too high	/ca	59	61
Crassicollaria massutiniana	/ca		
Crassicollaria parvula	/ca	35	61
Lorenziella hungarica	/ca		
Tintinnopsella carpathica	/ca	16	64
Tintinnopsella doliphormis	/ca		
Tintinnopsella longa	/ca		
Tintinnopsella remanei	/ca	16	16
Cadosina fusca	/dn	61	64
Colomisphaera fortis	/dn	25	64
Colomisphaera tenuis	/dn	2	64
Stomiosphaera echinata	/dn	36	61
Stomiosphaera proxima	/dn	40	64
Stomiosphaera wanneri	/dn	61	64